Potential New Therapies for Sarcomas: Testing the Efficacy of proteasome inhibitors Bortezomib and Ixazomib against Ewing Sarcoma

Submitted by Carmelo Cerra

Bachelor of Biomedical Science/Bachelor of Medicinal Chemistry

This thesis is submitted in total fulfilment of the requirements for a Master of Science degree

Department of Biochemistry and Genetics

College of Science, Health and Engineering

La Trobe Institute for Molecular Science

La Trobe University Victoria, Australia

February 2021

Table of Contents

Statement of Authorship

Except where reference is made in the text of the thesis, this thesis contains no material published elsewhere or extracted in whole or in part from a thesis accepted for the award of any other degree or diploma. No other person's work has been used without due acknowledgement in the main text of the thesis. This thesis has not been submitted for the award of any degree or diploma in any other tertiary institution.

All research procedures reported in this thesis were approved by the animal ethics committee AEC 17-76.

This work was supported by an Australian Government Research Training Program Scholarship.

Carmelo Cerra

19 February 2021

Acknowledgements

Firstly, I would like to start by thanking my ever-supportive supervisor Chris. I really appreciate all your constant help and guidance in the last few years. Even during the stressful COVID-19 lockdown the fact that we were still able to remain in contact and have Zoom meetings really helped with the planning of experiments for my return to the lab. There were times when I would send you emails at all hours of the night with plans and ideas that you were always happy to assist with which I am very thankful for.

I have to also say thank you to Michael (a PhD student in my lab), you have been the most influential student in my entire course from helping me with experiments during my first year when I did not even know how to maintain cells in TC, to providing guidance whenever I asked in my mouse experiments. I will miss our early starts and long days in the animal house together when we would go crazy by the end of those days. I also need to say thank you to Mark for also being someone I could ask for assistance as well as giving me lots of advice about my future studies and career. I will never forget my first day that I was volunteering in the lab and you helped me gain many of the skills I have today. Even now at your new job at RMIT we keep in contact and you are always willing to provide guidance and help me which I am grateful for. Also, to Tanmay, thanks for helping me so much with mouse work and wet lab work during my first year in the Hawkins lab. Next to my buddy Matilda, thanks for always being there to listen to me complain when my experiments were not working properly and always giving me assistance from when I first started back in the lab. I appreciate all your support throughout my course and making sure that I kept to deadlines for my thesis. Also, to my dodgy friend Yanhao, we had countless hours of laughs in the lab and you will always be the best at western blots out of anyone that I have ever seen. I will miss our pre-COVID chips and ribs lunches and I will not forget

to pray to Andy the sheep. Also thankyou to everyone else in the Hawkins lab Steph, Seirian and Megan for all your help and support throughout my course.

I would also like to acknowledge Lucy Coupland and Dr Mark Hulett who provided me with all the sarcoma cells used in this project. I would also like to thank all the animal technicians in SPF that were always so helpful and nice to me when I was completing my mouse experiments.

Most importantly, I need to thank my amazing family. Mum, dad, and Anthony there is no way I could have ever completed one day of this degree without your support. I would at times come home tired and down when things were not working as planned in the lab, but you guys always made me feel better instantaneously. Also, to my nonna and nonno who still to this day do not really understand what I do but always care and support me always which I am very thankful for and always ask how I am going with university. A special mention to my partner Mary, you have been so kind and helpful throughout my course and are always willing to listen and make me feel better. I really appreciate your support especially through my thesis writing as well as being so interested about what I do, I am so thankful.

Abbreviations

Ac-DEVD-AFC	Ac-Asp-Glu-Val-Asp-7-amino-4-trifluoromethylcoumarin
ANOVA	Analysis of variance
BCA assay	Bicinchoninic acid assay
BCL-2	B-cell lymphoma 2
BH3	B-cell lymphoma 2 Homology 3
CI	Combination index
FACS	Fluorescence-activated cell sorting
FCS	Foetal Calf Serum
FDA	Food and Drug Administration
H & E	Hematoxylin and Eosin
IAPs	Inhibitors of apoptosis
IVIS	In Vivo Imaging System
MTT	3-(4,5-dimethylthiazol-2-yl)-2,5-diphenyltetrazolium bromide
NK cells	Natural killer cells
PI	Propidium Iodide
qPCR	Quantitative polymerase chain reaction
SEM	Standard error of the mean
SMAC	Second Mitochondrial-derived activator of caspases
Suc-LLVY-AMC	Succinyl-Leu-Leu-Val-Tyr-7-amino-4-methylcoumarin
WHO	World Health Organisation

Abstract

Ewing sarcoma is the second most common sarcoma in adolescents, which originates in skeletal (axial and non-axial) and extraskeletal sites (soft tissue). Skeletal Ewing sarcoma metastasises most frequently to the lungs or bones, whereas the extraskeletal disease spreads commonly to lymph nodes or bones. Current treatments have increased 5-year survival rates for patients with the localised disease to 70%, although the outcomes for patients with metastatic disease remains low. A newer class of drugs, proteasome inhibitors (such as bortezomib, ixazomib, and carfilzomib) which have recently become FDA approved in the treatment of multiple myeloma, are promising new drug candidates. Bortezomib has undergone unsuccessful clinical trials against Ewing sarcoma and other solid tumour types. However, recent studies provide hope for the efficacy of the newer class proteasome inhibitors ixazomib and carfilzomib against solid tumours.

This project determined that proteasome inhibitors were more effective at reducing the viability of mammalian Ewing cell lines than current chemotherapies, cisplatin, and doxorubicin. Novel extraskeletal Ewing xenograft models were established, by introducing human A673 cells into the muscle or the circulation of BALB/c nude mice. Subsequent experiments revealed that bortezomib and ixazomib significantly increased the survival of mice bearing intramuscular Ewing sarcoma xenografts, although this efficacy was insufficient for clinical relevance. Intravenous inoculation with A673 cells resulted in metastasis at multiple sites.

Patients with metastatic Ewing sarcoma have 5-year survival rates of below 30%, highlighting the importance of developing more effective treatments in this field. Currently published Ewing sarcoma metastatic mouse models report metastatic spread to the lungs with little focus on other sites such as muscle, bone, liver, and brain tissue as seen in the clinical setting. The Ewing sarcoma mouse models developed in this project could be used to test drug efficacy to improve clinical outcomes and better understand the metastatic disease.

Chapter 1: Introduction

1.1 Sarcomas overview

Sarcomas are a rare group of bone and soft tissue cancers which are of mesodermal origin (Toro et al., 2006). They usually originate in soft tissue, cartilage or bone and are classified based on their histology and chromosomal translocations (Fletcher et al., 2003). Overall, soft tissue sarcomas are most prevalent with 4.3 to 6.1 diagnoses per 100,000 people per year, whilst bone sarcomas afflict 1.5 to 2.6 people per 100,000 per year (Trautmann et al., 2015). Although, in totality sarcomas represent 1% of all adult malignancies they are far more prevalent in children as they account for over 10% of all paediatric cancers (Fletcher et al., 2013). Osteosarcoma and Ewing sarcoma are the two most common sarcomas in the 0-24 age group whereas leiomyosarcomas are most common in patients over the age of 65 (Stiller et al., 2013) (Figure 1).

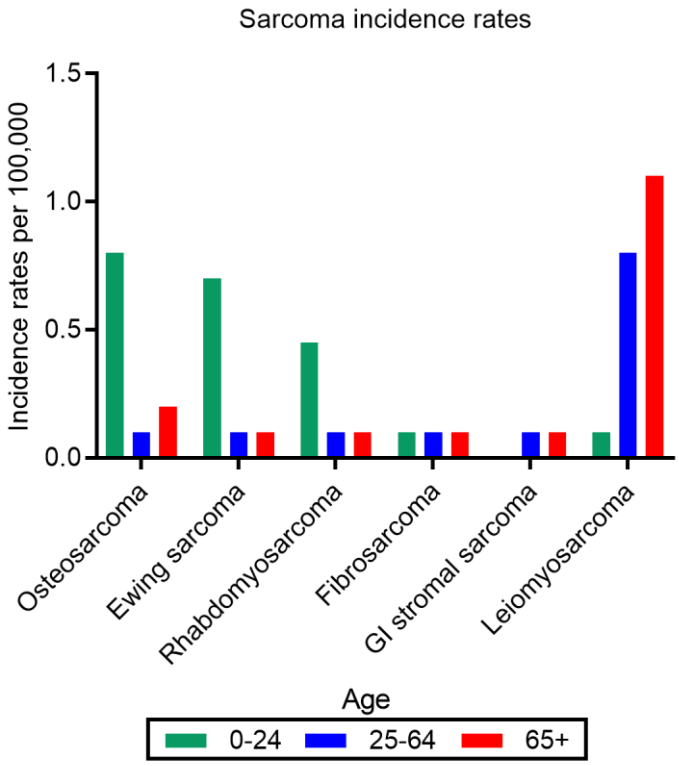

Figure 1: **Incidence rates per 100,000 for sarcomas by age.** Relative incidence rates for various sarcomas based on age group in Europe. Graph generated from published data (Stiller et al., 2013).

On average, current 5-year survival rates for patients diagnosed with a soft tissue sarcoma are 58%, compared to 62% for bone sarcomas (Stiller et al., 2013). Across all sarcoma subtypes, the 5-year survival rate is at around 60-70%, which dramatically decreases for patients with the metastatic disease (Figure 2).

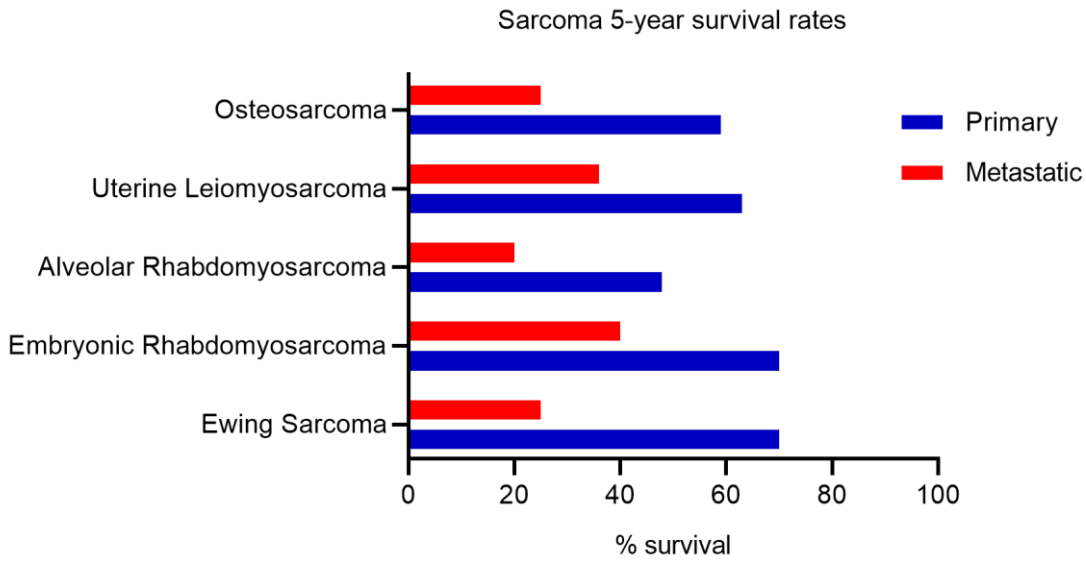

Figure 2: **5-year survival rates for primary and metastatic sarcomas.** This graph shows the 5-year survival rates for osteosarcoma, leiomyosarcoma, rhabdomyosarcoma and Ewing sarcoma for both the primary and metastatic disease, graph generated from published data (Peng et al., 2014; Stiller et al., 2013).

1.2 Sarcomas

1.2.1 Ewing sarcoma

Ewing sarcoma is a 'round cell sarcoma' which was first identified by James Ewing in 1921, when treating a 14 year old girl with a fractured ulna (Ewing, 1972). It is the second most common sarcoma in children and young adults, behind osteosarcoma (Stiller et al., 2013). This sarcoma commonly develops in extraosseous sites (Applebaum et al., 2011) as well as in the femur, tibia and humerus bones, with metastasis in 30% of cases to the lungs, surrounding bone and soft tissue (Cotterill et al., 2000; Rodríguez-Galindo et al., 2007; Womer et al., 2012). When diagnosed primarily in the axial and non-axial skeleton it is classified as skeletal Ewing sarcoma (Worch et al., 2018). In these cases, metastatic

spread most commonly is to the lungs or bones (Worch et al., 2018). Patients diagnosed with extraskeletal Ewing sarcoma present most frequently with the localised disease in the soft tissue surrounding bones (Huh et al., 2015). These tumours spread most prevalently to lymph nodes, bones or lungs (Huh et al., 2015). Although extraskeletal Ewing sarcoma metastasises most commonly to these sites, a significant minority of patients with this disease have metastasis elsewhere such as abdominal organs, the peritoneum, the brain (Huh et al., 2015) as well as cardiac muscle (Murad et al., 2019; Petrovic et al., 2016). Older patients with Ewing sarcoma were shown to have a lower probability of presenting with metastatic disease at diagnosis, whilst pelvic tumours were most likely to metastasise in older patients compared to cranial, limb and spinal tumours (Shi et al., 2020). From the SEER database, 2269 patients were diagnosed with Ewing sarcoma from 1983-2015, two thirds were male whilst 70.1% of total cases were below 20 years of age (Shi et al., 2020). The SEER database (Surveillance, Epidemiology and End Results database) in that study was composed of 18 different cancer registries, accounting for about a third of the total US population from 1983-2015 (Shi et al., 2020).

Around 80% of Ewing cases feature a translocation joining the EWSR1 gene (Ewing sarcoma breakpoint region 1) on chromosome 22 to FLI1 (Friend leukemia virus integration site 1) on chromosome 11, which enhances its metastatic potential (Chaturvedi et al., 2014). The protein encoded by the EWS-FLI1 fusion gene has been shown to function as a transcriptional activator upregulating the oncogene c-myc (Bailly et al., 1994) and more recently as a transcriptional repressor by inhibiting the expression of tumour suppressor genes, which drives tumour development (Sankar et al., 2013a). Knocking down the expression of EWS-FLI1 caused an increase in cell adhesion and reduced motility, which indicated that this translocation plays a role in tumour invasiveness and metastasis (Chaturvedi et al., 2014). Therefore, therapeutically targeting the EWS-FLI1 oncogenic transcription factor is a promising field of research. Consequently, efficacy has

been identified in mouse models in which mRNA expression of EWS-FLI1 was disrupted using transcriptional repressor drug and cells treated with these agents had reduced replication rates and were sensitive to apoptosis (Jacques et al., 2016).

Current chemotherapy treatments for Ewing sarcoma include vincristine, doxorubicin and cyclophosphamide with cycles of ifosfamide and etoposide, which have increased 5-year survival rates for the primary disease from below 40% to 70% (Womer et al., 2012). Prior to chemotherapies, low survival rates reflected the use of treatments that only combated the localised disease through surgery and radiation (Nesbit, 1976). Fifty-percent of relapses occur within 17 months of remission most frequently with patients presenting with metastasis to bones and lungs (Heinemann et al., 2018). Overall 5-year survival rates drop to 10% for patients developing distant recurrent Ewing sarcoma within two years of remission, compared to 24% survival rates for local relapses (Barker et al., 2005; Leavey et al., 2008; Stahl et al., 2011). Along with front-line chemotherapies, recurrent Ewing sarcoma treatments also involve platinating agents such as cisplatin or carboplatin (van Maldegem et al., 2015). Patients with pulmonary metastasis are treated via lung irradiation, as well as the same chemotherapies as the primary disease but unfortunately these are less effective against metastases; patients with the metastatic disease have 5-year survival rates around 30% (Hamilton et al., 2017; Khanna et al., 2017). The most common mouse models for studying Ewing sarcoma biology and treatment involve subcutaneous implantations in the flanks of nude mice (Sankar et al., 2013b). Other models entail establishing primary Ewing sarcoma by implanting Ewing cells into the tibia to study the effects that the tumour has on the bone and surrounding tissues (Chaturvedi et al., 2014).

1.2.2 Rhabdomyosarcoma

Rhabdomyosarcoma is the most common paediatric soft tissue sarcoma, presenting commonly in the head and neck region and is associated with skeletal muscle (Ognjanovic et al., 2009). The most common subtypes are embryonal rhabdomyosarcoma with an annual incidence rate of 4.5 per million people in the US, compared to alveolar rhabdomyosarcoma with 2.6 per million (Ognjanovic et al., 2009). Although less common, the alveolar subtype is more fatal and is associated with a chromosomal translocation in the PAX3 or PAX7 gene on chromosome 2 with FOXO1 on chromosome 13 (Barr et al., 1993; Skapek et al., 2013). This translocation has been shown to enhance the functionality of the RASSF4 gene which is involved in enhancing cell proliferation as well as inhibiting tumour suppresser genes (Crose et al., 2014). Not all alveolar rhabdomyosarcomas present as PAX-gene fusion positive; tumours that lack the fusion protein have a greater mutational burden (number of somatic non-synonymous mutations per tumour genome) (Shern et al., 2014). The most common somatic mutations presenting in rhabdomyosarcoma tumours include NRAS, KRAS and PIK3CA which are involved in the receptor tyrosine kinase pathway predominantly found in embryonal rhabdomyosarcoma tumours (Shern et al., 2014). Other genes vital for cell cycle such as an E3 ubiquitin ligase, FBXW7 were found to be mutated at arginine residues although only found in PAX-gene fusion negative alveolar subtypes (Shern et al., 2014).

The current rhabdomyosarcoma treatments of vincristine, actinomycin D and cyclophosphamide have improved overall 5-year survival rates to around 70%, with minimal impact on the metastatic disease since the 1970s (Crist et al., 1990; Ognjanovic et al., 2009). Although, these same chemotherapy agents only increased 5-year survival rates for alveolar rhabdomyosarcoma from 40% in the 1970s to 48% in the 2000s (Ognjanovic et al., 2009).

Pleomorphic and spindle cell rhabdomyosarcomas are other subtypes which are distinguishable based on their cell morphology and are usually diagnosed via histological analysis of a patient's biopsy (Ingley et al., 2020). Relatively recently, spindle cell rhabdomyosarcoma was clinically distinguished from embryonal rhabdomyosarcoma by the World Health Organisation (Bridge et al., 2013). Since then a genetic point mutation in adult spindle cell rhabdomyosarcomas in the myogenic transcription factor *MYOD1* Leu122Arg has been uncovered to distinguish between subtypes (Szuhai et al., 2014). Although not all pleomorphic rhabdomyosarcomas possess this mutation, patients whose tumours had the mutation had significantly poorer overall survival rates (Kohsaka et al., 2014). Currently, around 35% of rhabdomyosarcoma patients develop metastases, most commonly in surrounding bones, the lungs or less commonly the lymph nodes (Kim et al., 2017).

1.2.3 Leiomyosarcoma

Leiomyosarcomas represent 24% of all soft tissue sarcomas making them the most common smooth muscle sarcoma (Duman et al., 2012; Toro et al., 2006). The most prevalent site of the primary tumour is the uterus (uterine leiomyosarcoma) representing 2% of all uterine cancers (Toro et al., 2006). Other sites of this sarcoma include the abdomen, thorax/trunk, gastrointestinal viscera as well as the genitourinary viscera (Agaram et al., 2016; Gladdy et al., 2013). Leiomyosarcomas can also be classified on their level of smooth muscle cell differentiation based on their histology (Demicco et al., 2015). In one study, primary leiomyosarcomas were well differentiated in 53% of patients compared to 26% in the metastatic disease (Demicco et al., 2015). Metastasis occurs in 81% of patients, most frequently to the lungs or the peritoneum and surrounding bones (Tirumani et al., 2014). Current screening methods of MRI and CT imaging have not been reliable in detecting differences between malignant and non-malignant leiomyosarcomas, with biopsies only

verifying malignancies in around 50% of cases (Ricci et al., 2017; Skorstad et al., 2016). Proteins such as Stathmin 1 (STMN1) which are involved with destabilising microtubules, are used as biomarkers in the detection of primary uterine leiomyosarcoma and have been shown to be expressed in all leiomyosarcoma cases (Allen et al., 2015). Leiomyosarcoma can also feature frameshift, missense and in-frame deletion *TP53* mutations and, less commonly, deletions of the *RB1* gene (Agaram et al., 2016).

Frontline therapies usually involve surgical resection of the tumour and complete removal of the uterus in uterine leiomyosarcoma cases (Juhasz-Böss et al., 2018; Ricci et al., 2017). Although less effective, radiotherapy and chemotherapies such as gemcitabine and docetaxel or doxorubicin and ifosfamide are used (Ricci et al., 2017; Seddon et al., 2017), with the most important predictor of survival being the stage of disease diagnosis (Foley et al., 2015). Patients with stage I disease had an overall 5-year survival rate of 55.2% compared to 21.7% if diagnosed with distant metastasis and stage IV leiomyosarcoma (Zivanovic et al., 2012). A major hurdle in the treatment of leiomyosarcoma has involved overcoming multi-drug resistance. This resistance to chemotherapies is believed to be due to the overexpression of drug efflux transporters on the membrane of the sarcoma cells, such as ATP binding transporter P-glycoprotein 1 (Hua et al., 2005; Hung et al., 2014). Biomarkers involved in regular smooth muscle differentiation such as desmin correlated with improved overall leiomyosarcoma patient survival and, less differentiated tumour tissue correlated with poorer overall survival rates (Demicco et al., 2015).

1.3 Sarcoma mouse models

The development of immunocompetent and immunocompromised sarcoma mouse models has provided a means of evaluating potential new drug candidates against sarcomas. A soft tissue Ewing sarcoma mouse model was established via intramuscular A673 cell injections

in muscles surrounding the tibia which also caused intratibial metastasis (Odri et al., 2010). Also, Ewing sarcoma Patient-Derived Xenografts have been shown to grow in the flanks of immunodeficient mice, as a means for retaining tumour architecture (Ordóñez et al., 2015). KHOS, a human osteosarcoma cell line (Duan et al., 2017) and JJ012, a chondrosarcoma cell line (Liu et al., 2015) have been successfully incorporated into an acellular Matrigel based-matrix providing a scaffold for tumorigenesis. This approach resulted in successful primary sarcoma mouse models in CB-17 SCID mice achieved via subcutaneous implantation of one million cells into the flanks of those immunocompromised mice (Liu et al., 2015).

Genetically engineered mouse models which develop spontaneous sarcomas, and hence have greater clinical relevance than implantation models, have been established for osteosarcoma but unfortunately not to date for Ewing sarcoma. An osteoblast Cre-lox deletion of tumour suppressors p53 and RB-1 in mice mimicked the fibroblastic osteosarcoma phenotype in patients (Berman et al., 2008; Walkley et al., 2008). As a result of this deletion the mice spontaneously developed osteosarcomas in the lower jaws, ribs and hind legs with >39% of mice developing lung metastasis (Walkley et al., 2008). Knockdown of p53 using shRNA led to the development of an osteoblastic model with osteosarcomas spontaneously developing in the mice's long bones with metastasis primarily to the lungs (Mutsaers et al., 2013). Although successful in osteosarcoma, potential Ewing sarcoma spontaneous models via the expression of the EWS-FLI1 transgene have yet to be established. Expression of this transgene using various promoters in osteoblasts, neuronal tissue and ubiquitously all resulted in embryonic lethality or defects in murine development (Minas et al., 2017).

Established metastatic Ewing sarcoma mouse models have involved the implantation of cells into gastrocnemius muscles then, after a defined period of growth, the primary

tumours were surgically removed to allow the mice to survive long enough for lung metastasis to grow (Hong et al., 2015; Lagares-Tena et al., 2016). These BALB/c nude mice developed lung tumours, although 20% were required to be culled prior to endpoint analysis due to tumour relapses post-surgery to tissues that were not resected (Lagares-Tena et al., 2016). Other techniques used to develop metastatic Ewing sarcoma mouse models have involved injecting immunodeficient mice intravenously with 2 x 10^6 A673 Ewing sarcoma cells (Lagares-Tena et al., 2016; Richter et al., 2009; Sáinz-Jaspeado et al., 2010), which led to detectable lung metastasis determined after endpoint analysis.

The efficiency of this "experimental" metastasis was found to be enhanced in other cancer types by transiently depleting natural killer (NK) cells prior to the intravenous implantation of cancer cells (Coupland et al., 2013; Harris et al., 2020c). Twenty-eight days post tail-vein injection of luciferase-expressing osteosarcoma cells into mice, the sarcoma cells became detectable in the lungs via bioluminescent imaging in most of the immunodeficient mice whose NK cells had been depleted (Harris et al., 2020c). At the same time these cells were not detected in any of the animals with unaltered NK cell levels (Harris et al., 2020c). In a patient setting, a correlation has been shown between the number of circulating NK cells and the progression of metastasis in patients suffering from gastrointestinal sarcoma (Delahaye et al., 2011). It was identified that patients with high densities of NK cell infiltration were less likely to present with metastases at diagnosis compared to patients whose tumours contained fewer NK cells (Delahaye et al., 2011). This was also seen in prostate cancer patients with high densities of $CD56^+$ natural killer cells demonstrating lower seminal vesicle invasion (which is associated with increased risk of lymph node metastasis in prostate cancer patients) (Gannon et al., 2009). These data demonstrate an apparent role of NK cells in the prevention of tumour metastasis and the utility of their temporary depletion in the development of a cancer metastatic model.

1.4 Therapies

Although treating sarcoma patients with chemotherapies has improved survival rates, these therapies have probably peaked their survival rates. Thus, further clinical success may require new therapies with novel modes of action, possibly working in combination with current treatments. This study examined the potential of four classes of molecularly targeted therapies.

1.4.1 BH3 mimetics

The ability of cancer cells to avoid apoptotic mechanisms remains an ongoing challenge in the treatment of many cancers. The B cell CLL/lymphoma 2 or BCL-2 family of proteins is a pro-survival group of proteins which play a role in the evasion of apoptosis (Dai et al., 2016; Vaux et al., 1988). A new class of drugs called BH3 mimetics act by mimicking BH3 pro-apoptotic proteins, which inhibit pro-survival BCL-2 proteins as a means of enhancing cancer cell death (Merino et al., 2018). Venetoclax (ABT-199) has been FDA-approved in the treatment of relapsed or refractory chronic lymphocytic leukemia (Stilgenbauer et al., 2016). A second generation BH3 mimetic navitoclax (ABT-263), is an orally bioavailable BCL-2 and BCL-$_{XL}$ inhibitor that in early studies was able to demonstrate complete tumour regression in xenograft mouse models implanted with small-cell lung cancer and chronic lymphocytic leukemia cells (Tse et al., 2008). To date, navitoclax has been evaluated in numerous clinical trials (Rudin et al., 2012; Wilson et al., 2010), none of which involved sarcomas. In one phase I study of solid tumour types, navitoclax was well tolerated by patients whilst its efficacy towards small-cell lung cancer was promising enough to be analysed further in a phase II clinical trial (Gandhi et al., 2011).

Recent work undertaken using BH3-mimetics and sarcomas have involved ABT-737 (a BCL-2 and BCL-$_{XL}$ inhibitor) and A-1331852 (a BCL-$_{XL}$ inhibitor) which synergistically

enhanced the effect of Dinaciclib, a CDK inhibitor, against sarcomas *in vitro* (Rello-Varona et al., 2019). In combination these therapies were able to enhance the degree of apoptosis in DW982 and SK-LMS-1 sarcoma cells (Rello-Varona et al., 2019). Issues encountered in an *in vivo* setting were that the BH3-mimetics used along with Dinaciclib caused major liver toxicity in the mice (Rello-Varona et al., 2019). Via doxycycline inducible EWS-FLI1 expression, BH3 mimetics were identified as potential novel treatments against Ewing sarcoma cells with low and high EWS-FLI1 expression levels (Tsafou et al., 2018). EWS-FLI1 low Ewing cells were found to be most sensitive to navitoclax and EWS-FLI-1 high Ewing sarcoma cells responded best to obatoclax (a Bcl-2 inhibitor) out of the 3,325 compounds screened (Tsafou et al., 2018).

1.4.2 SMAC mimetics

SMAC (second mitochondria-derived activator of caspases) mimetics also engage cell death pathways in cancer cells. They function by inhibiting the Inhibitor of Apoptosis (IAP) proteins XIAP, cIAP1 and cIAP2 (Fulda, 2017). The role of cIAP1/2 is to polyubiquitinate RIPK1, which prevents the formation of the "Ripoptosome" resulting in the evasion of cell death (Silke & Meier, 2013). XIAP (X-linked inhibitor of apoptosis protein), is a tight binding inhibitor of the pro-apoptotic caspases-3, -7 and -9 (Eckelman & Salvesen, 2006). SMAC is an endogenous antagonist of XIAP (Du et al., 2000), cIAP1 and cIAP2 (Yang & Du, 2004) which results in "Ripoptosome" activation, inducing both apoptosis and necroptosis (Silke & Meier, 2013). Through the NF-κB pathway, SMAC mimetics can induce TNFR-1 (Tumour necrosis factor receptor 1) induced cell death via TNFα production (Vince et al., 2007). The SMAC mimetic LCL-161 has been used in clinical trials on patients with advanced solid tumours such as colon, lung and pancreatic cancers (Infante et al., 2014). In a phase I study the drug was able to substantially induce the degradation of cIAPs at doses which were generally tolerated by patients (Infante et al.,

2014). In another phase I clinical trial with solid tumours and lymphomas, the SMAC mimetic birinapant was shown to reduce cIAP activity by 75% whilst stabilising the disease for colorectal and liposarcoma patients (Amaravadi et al., 2015).

LCL-161 in combination with doxorubicin was published to reduce primary osteosarcoma growth in nude mice as well as delaying the detection of lung metastasis (Shekhar et al., 2019). Interestingly, SMAC mimetics GDC-0152 and LCL-161 were less effective *in vitro* without TNFα than they were against osteosarcoma intramuscular mouse models (Shekhar et al., 2019).

1.4.3 HDAC inhibitors

Cancer proliferation is not only dependent on the evasion of apoptosis but also involves epigenetic processes such as DNA histone modifications and DNA methylation. Histone deacetylases are a family of enzymes which cleave an acetyl group from an ε-N-acetyl lysine amino acid causing deacetylation of both histone (Edrissi et al., 2013) and non-histone proteins (Soriano et al., 2013). At homeostasis there is a balance between the activity of histone acetylases and deacetylases, but in a tumourigenic state there is an increase in the activity of deacetylases (Parbin et al., 2014). The removal of acetyl groups by deacetylases increases gene transcription, as a mouse lacking HDAC-1 had a deregulation in 7% of its genes (Zupkovitz et al., 2006). The HDAC inhibitors which suppress this pathway include vorinostat, which is FDA-approved for the treatment of cutaneous T-cell lymphoma (Mann et al., 2007) and Panobinostat, which was FDA-approved for multiple myeloma in 2015 (Moore, 2016).

HDAC-1 and HDAC-2 inhibitor romidepsin was more effective at reducing the cell viability *in vitro* of Ewing sarcoma cells than current clinical treatments of doxorubicin, vincristine and cyclophosphamide (Welch et al., 2019). The most significant synergistic

combinations identified *in vitro* involved romidepsin with vincristine against Ewing sarcoma cells (Welch et al., 2019). The HDAC-1 inhibitor MS-275 was shown to enhance reactive oxygen species accumulation in Ewing sarcoma and osteosarcoma cells which led to major reductions in cell viability (El-Naggar et al., 2019). More significantly, this drug was able to prevent the invasion of CHLA-10 Ewing sarcoma tumours in immunocompromised mice (El-Naggar et al., 2019)

1.5 The proteasome and proteasome inhibitors

1.5.1 The proteasome

The proteasome is an ATP-dependant protease which degrades ubiquitin tagged proteins to maintain intracellular homeostasis (Budenholzer et al., 2017). The human 26S proteasome is composed of a 20S core particle for protein degradation as well as two 19S regulatory subunits involved in exposing tagged proteins to the core (Budenholzer et al., 2017; Groll et al., 1997; Schweitzer et al., 2016). There are three subunits of the 20S core particle which are involved in proteolytic activities: the β1 (caspase-like), β2 (trypsin-like) and β5 (chymotrypsin-like) subunits, of which the β5 subunit is responsible for the majority of 26S associated protein degradation (Kisselev et al., 2006). The Rpn10 receptor on the 26S proteasome is the main subunit involved in ubiquitin substrate recognition (Matyskiela et al., 2013).

Proteasome activity is elevated in cancer cells as the protein production rate is higher in these rapidly proliferating cells, which then causes the concentration of misfolded proteins to increase, so proteasome activity increases accordingly to deal with this (Bianchi et al., 2009; Kambhampati & Wiita, 2020). Multiple myeloma cell lines that contained proteasomes which were only just keeping up with the volume of misfolded proteins (misfolded proteins versus capacity) were more sensitive to proteasome inhibition than

those with reduced proteasome capacity workload (Bianchi et al., 2009). At the same time, multiple myeloma cell lines with higher proteasome activity also contained more than double the cell division rates and hence protein synthesis rates were also increased (Cenci et al., 2012). This supported the explanation that proteasome activity increased to account for more misfolded proteins as a result of increased protein synthesis rates in rapidly proliferating cells (Cenci et al., 2012). Chen & Madura identified heterogeneity in the increase in proteasome activity amongst human primary breast cancer samples, with some specimens demonstrating less than a 2-fold increases in activity compared to the control tissue whilst others were elevated up to 35-fold (Chen & Madura, 2005). Although only using a small sample size, benign tumours did not have elevated levels of proteasome activity compared to controls, supporting the idea that proteasome activity is specifically upregulated in neoplastic cells (Chen & Madura, 2005). Furthermore, chemotherapy resistant tumour lines were shown to be more sensitive to proteasome inhibition than normal human fibroblasts demonstrating a specificity for rapidly proliferating cancer cells (Tsvetkov et al., 2018). Proteasome inhibition of these tumour lines caused cancer cell arrest and apoptosis compared to normal human fibroblasts, which remained viable post treatment (Tsvetkov et al., 2018). Consequently, inhibition of the 26S proteasome has provided potential new therapies in the treatment of cancers.

1.5.2 Proteasome inhibitors

In 2003, bortezomib (PS-341) became the first FDA-approved proteasome inhibitor, for the treatment of multiple myeloma (Soave et al., 2017). It is a reversible peptide boronic acid inhibitor with high affinity for the β5 subunit of the 20S proteasome, and lower affinity for the β1 and β2 subunits (Altun et al., 2005; Soave et al., 2017). In a murine setting, bortezomib can inhibit the proteasome in the liver, kidney and heart by up to 90% one hour post treatment, with recoveries in the 20S activity by at least 60% by 24 hours (Mlynarczuk-

Bialy et al., 2014). Bortezomib prevents the proteolytic breakdown of the NF-κB inhibitor IκB (Hideshima et al., 2001) which is important for cell survival and overexpressed in various tumours (Faria et al., 2017; Teng et al., 2020). Compared to chemotherapy sensitive human multiple myeloma cells, those resistant to chemotherapy contained higher levels of NF-κB and consequently were more sensitive to bortezomib treatment (Ma et al., 2003). In another study, multiple myeloma cells with reduced proteasome expression and an increase in workload were more sensitive to bortezomib-induced apoptosis and cell death (Bianchi et al., 2009). This demonstrated that an increase in protein synthesis and therefore stresses on cancer cells highlights their reliance on proteasome activity for survival and how bortezomib is able to cause apoptosis via this mechanism (Bianchi et al., 2009). While bortezomib is effective in treating multiple myeloma, it has subjected patients to side effects such as peripheral neuropathy and nephrotoxicity (Reece et al., 2011), and its prolonged use has led to drug resistance (Moreau et al., 2011). This led to the synthesis of the newer class proteasome inhibitors such as carfilzomib and ixazomib.

The second generation inhibitor carfilzomib (PR-171) is a tetrapeptide-epoxyketone which forms an irreversible covalent bond specifically with the β5 subunit of the proteasome (chymotrypsin-like activity) (Demo et al., 2007). It showed a more sustained response than bortezomib in early preclinical studies (Demo et al., 2007) as well as being more effective than bortezomib at increasing survival in patients with multiple myeloma (Dimopoulos et al., 2019). Extremely high concentrations of over 1 μM were required in order to observed minor interactions of carfilzomib with the β1 and β2 subunits of the proteasome, demonstrating its enhanced β5 specificity compared to bortezomib (Kuhn et al., 2007). Carfilzomib inhibited proteasome activity in adrenal, heart, liver and whole blood samples in rodents to a similar extent to bortezomib, although the inhibition persists for longer due to carfilzomib's irreversibility (Demo et al., 2007). Due to its irreversible nature, carfilzomib displayed a sustained and widespread pharmacodynamic response in rodents

whilst its plasma half-life was only 15 minutes (Demo et al., 2007). In human blood cells, carfilzomib demonstrated a dose dependant inhibition of the chymotrypsin-like activity by up to 75% one hour post treatment compared to pre-treated samples, with ultimate reduction in activity approaching 90% with subsequent treatments (O'Connor et al., 2009). In 2013 carfilzomib became FDA-approved for treating resistant or relapsed multiple myeloma (Herndon et al., 2013). Similarities were seen in efficacy of carfilzomib compared to bortezomib in a phase III trial against multiple myeloma, though carfilzomib was more likely to cause adverse side effects such as hyperglycaemia, dyspnoea and thromboembolic events (Kumar et al., 2020) Current common side-effects presenting in patients treated with carfilzomib are fatigue, nausea and diarrhoea, with minor respiratory symptoms of coughing and dyspnea (O'Connor et al., 2009).

Further research led to the synthesis of the first orally administered proteasome inhibitor, ixazomib. Ixazomib (MLN2238), a boronic acid inhibitor, demonstrated to be a more potent inhibitor of the β5 subunit of the proteasome in blood and tumour tissue than bortezomib (Kupperman et al., 2010). It also displayed a proteasome dissociation half-life almost six times shorter than that of bortezomib (18 mins compared to 110 mins), which was believed to improve its tissue distribution (Kupperman et al., 2010). Patients treated with a single dose of ixazomib at its maximum tolerated dose of 1.76 mg/m^2 exhibited a maximum 20S proteasome inhibition in the blood of 60%, and activity levels returned to pre-treatment levels within 24 hours (Smith et al., 2015). Ixazomib is administered as the pro-drug ixazomib citrate which is hydrolysed to its biologically active form when exposed to the blood plasma under physiological conditions (Kupperman et al., 2010; Offidani et al., 2014). Like other drugs of its class in 2015 ixazomib was also FDA-approved for the treatment of multiple myeloma in combination with previous treatments of lenalidomide and dexamethasone (Moreau et al., 2016). Common side effects seen by patients treated with ixazomib are minor skin and soft tissue disorders such as dermatitis and maculo-

papular rashes as well as reduced platelet count (thrombocytopenia) (Gupta et al., 2016; Smith et al., 2015).

Newer class proteasome inhibitors currently being evaluated include delanzomib, a peptide boronic acid inhibitor with a similar chemical profile to bortezomib (Berkers et al., 2012). It inhibits chymotrypsin and caspase-like sites of the 26S proteasome to a similar extent to bortezomib, with no impact on the tryptic activity (Berkers et al., 2012). Delanzomib (also known as CEP-18770) has undergone phase I clinical trials against multiple myeloma (Gallerani et al., 2013; Vogl et al., 2017) and a range of solid tumour types including colorectal cancer and non-small cell lung cancer (Gallerani et al., 2013). No significant improvements were seen in patients treated with delanzomib, so its clinical development was discontinued (Gallerani et al., 2013; Vogl et al., 2017). More recently delanzomib has been shown to sensitize breast cancer (Wang et al., 2019) and cervical cancer (Guo et al., 2017) cell lines to doxorubicin induced apoptosis, providing hope that combination regimens including delanzomib may benefit patients.

The second-generation proteasome inhibitor oprozomib (PR-047) is an orally bioavailable epoxyketone derivative with a similar structure to the irreversible inhibitor, carfilzomib (Zhou et al., 2009). Oprozomib has been shown to rapidly reach maximal levels in the blood stream within 1-2 hours, whilst also being eliminated rapidly (Hari et al., 2019). Oprozomib has undergone a phase Ib/II clinical trial against advanced multiple myeloma and Waldenström macroglobulinemia (Ghobrial et al., 2019). It exhibited a 25-40% overall response rate (defined as a partial or complete response in patients) (Ghobrial et al., 2019). The largest concerns raised by that study were the common gastrointestinal side effects in patients (Ghobrial et al., 2019). At its maximum tolerated dose, two patients died from gastrointestinal haemorrhaging, although gastrointestinal side-effects were reduced by

using a step-up dosing regimen as well as administering antidiarrhoeal medications (Ghobrial et al., 2019).

The inhibition of overactive proteasomes in cancer cells render them sensitive to cell cycle arrest and apoptosis because of the accumulation of cell cycle checkpoint inhibitors, otherwise degraded with an overactive proteasome (Huang et al., 2011; Rastogi & Mishra, 2012). Consequently, these treatments have been shown to disrupt the cell cycle which is the process of mitotic cell division which consists of G1 (Gap one), S (DNA synthesis) and G2 (Gap 2) phases then mitosis and cytokinesis (Israels & Israels, 2001). When melanoma cells (Beaumont et al., 2016), colon cancer (Hong et al., 2012) or osteosarcoma cells (Patatsos et al., 2018) were treated with bortezomib they demonstrated a dose-dependent G2 cell cycle arrest.

1.5.3 Sarcomas and proteasome inhibitors

Although less research has been undertaken on proteasome inhibitors in sarcomas than carcinomas, there is some evidence that sarcoma cells rely on proteasome activity for growth and survival. The EWS-FLI1 positive Ewing sarcoma cell line CHP100 contained 627 upregulated genes which were involved in the protein ubiquitination pathway (Shukla et al., 2016). Interestingly, shRNA-mediated knockdown of two of these genes (USP14 or UCHL5) in other EWS-FLI1 positive Ewing sarcoma cells (A673, TC-71) diminished expression of the proteins they encode, and diminished cell viability (Shukla et al., 2016). This showed the importance of the overactive protein ubiquitination pathway in the viability of human Ewing sarcoma cells.

I*n vitro* studies have revealed that sarcomas are sensitive to proteasome inhibitors. Bortezomib was able to induce cell death and G0/G1 phase arrest in chondrosarcoma cells *in vitro* (Bao et al., 2017). It was also shown that bortezomib, ixazomib and carfilzomib

greatly reduced cell viability in human and canine osteosarcoma cells *in vitro* at 10% of the concentration theoretically achievable in the blood-stream of treated patients (Patatsos et al., 2018). Bortezomib also inhibited the growth of a selection of various Ewing sarcoma cell lines *in vitro* at doses substantially lower than those achieved in patients' blood (Lu et al., 2008). Ixazomib was able to effectively reduce cell viability of osteosarcoma cells *in vitro* at theoretically achievable concentrations as well as reducing the levels of matrix metalloproteinases involved in cellular invasion (Liu et al., 2017).

Although proteasome inhibitors were identified as promising drug candidates for sarcomas on the basis of *in vitro* assays, animal experiments and clinical trials data did not support the *in vitro* data. However, it should be noted that bortezomib is the only proteasome inhibitor to have been examined in previous *in vivo* experiments against sarcomas. In one experiment, mice were implanted subcutaneously with rhabdomyosarcoma, rhabdoid or Ewing sarcoma cells, all of which were shown to be sensitive towards bortezomib *in vitro* (Houghton et al., 2008). The mice were treated with 1 mg/kg of bortezomib, but no effect was observed on rhabdoid or Ewing sarcoma growth and only minor tumour regression was reported in rhabdomyosarcoma-implanted mice (Houghton et al., 2008). A phase II clinical trial was undertaken using sarcoma patients suffering from recurrent or metastatic tumours of various sarcoma types, most notably from leiomyosarcoma, Ewing sarcoma and liposarcoma (Maki et al., 2005). Of the 21 patients, only one showed a minimal response to bortezomib, whilst others had no response to treatment and some patients were excluded due to drug toxicity (Maki et al., 2005).

Bortezomib also provoked no response in patients with other solid tumour types (Irvin et al., 2010). One hypothesis for this disappointing finding was that poor vascularisation of these solid tumours reduced the ability of bortezomib to penetrate and elicit a response. This was apparent in a study in which bortezomib was unable to reduce tumour volume in

poorly vascularised tumours but was active in well vascularised tumours (Williamson et al., 2009). On a more promising front, newer generation proteasome inhibitor ixazomib showed preclinical efficacy against the solid tumour type hepatocellular carcinoma (Augello et al., 2018), significantly reducing primary tumour volume in this mouse model compared to vehicle (Augello et al., 2018). Similarly, in a human xenograft prostate mouse model, ixazomib reduced the average tumour volume to a greater extent than bortezomib (Kupperman et al., 2010). However, the clinical testing of ixazomib in an advanced solid tumour setting has so far yielded limited results (Smith et al., 2015).

Recently, vorinostat and the VEGF inhibitor pazopanib was more effective than vorinostat plus ixazomib in a phase I clinical trial of patients with metastatic TP53 mutant solid tumours including sarcomas, colorectal cancer and breast cancer (Wang et al., 2020). Although the authors concluded that ixazomib "did not elicit an objective response", only 4 out the 59 patients were sarcoma patients (Wang et al., 2020). Consequently, studies such as these provide hope for potential clinical efficacy of the newer class proteasome inhibitors against solid tumour types including various sarcomas.

1.6 Sarcomas and the immune system

The immune system is known to play a major role in the growth and proliferation of tumours, and immunotherapies are very effective against some cancer types (Riley et al., 2019). Therefore, understanding the tumour-infiltrating lymphocyte composition is important when selecting new drug candidates to treat cancer. The most common immune cell type seen in sarcomas is macrophages, which accounted for around a third of lymphocytes in the tumour (Zhu & Hou, 2020). Sarcoma patients with high levels of NK and CD8 T cells and lower levels of macrophages had relatively good survival rates (Zhu & Hou, 2020). This finding indicated the importance in understanding the composition of

immune cells within a tumour microenvironment. In another study using soft tissue sarcomas, the leiomyosarcomas were classified as "immune desert" with very few immune cells and low vasculature compared to de-differentiated liposarcomas which were immune rich most namely, T cells and NK cells (Petitprez et al., 2020). Comparing the differing groups, those patients with minimal tumour immune cell filtration had lower overall survival rates than those with overall immune rich tumours (Petitprez et al., 2020). The use of immunotherapies in that study such as a PD-1 inhibitor showed the greatest effect on the tumours with higher compositions of immune cells (Petitprez et al., 2020). In a cohort of osteosarcoma and Ewing sarcoma patients no significant differences were seen in NK cells, T and B cells compared to normal patients in their blood stream, although lower levels of lymphocytes and higher levels of granulocytes were detected (Hingorani et al., 2015). These studies illustrated the importance of understanding the composition of the tumour microenvironment in sarcomas, as some express high whilst others express low levels of immune cells which could impact the effectiveness of immunotherapies against these cancers.

1.7 Aims of project

The aims of this project were to evaluate potential new therapies for sarcomas, initially through determining the *in vitro* sensitivity of cell lines from a range of sarcoma types to a panel of anti-cancer drugs. This panel of drugs included BH3 mimetics, SMAC mimetics, HDAC inhibitors as well as proteasome inhibitors. The most potent response produced was triggered by bortezomib, a proteasome inhibitor, against Ewing sarcoma cells, so further drug screening was undertaken using the newer class proteasome inhibitors ixazomib and carfilzomib, with a focus on Ewing sarcoma. To enable *in vivo* testing of proteasome inhibitors and other agents against Ewing sarcoma, novel extraskeletal Ewing xenograft models were established, via inoculation of A673 human Ewing sarcoma cells into the

muscle or the circulation of BALB/c nude mice. The aim was then to determine the efficacy of these proteasome inhibitors *in vivo* in both a primary setting, within the muscle, as well as establish a metastatic mouse model for Ewing sarcoma. This was an important aspect of this project as previous studies only reported metastasis to the lungs in mice, however Ewing sarcoma spreads to a wide number of sites in patients. Understanding the spread and growth of the metastatic disease was imperative as it resulted in poorer clinical outcomes for Ewing sarcoma patients. Other goals of this project were to investigate the impact that proteasome inhibitor therapies had on the cell cycle, proteasome, and caspase activity in Ewing sarcoma cells, as well as whether they could cooperate with current treatments.

Chapter 2: Materials and Methods

2.1 Cell culturing and drugs

The sarcoma cell lines A673, SK-UT-1, RD-1, SK-PN-DW were supplied by Lucy Coupland from Australian National University and CHLA-10 was provided by Dr Mark Hulett from La Trobe University. The PT67 cell line was supplied by Dr Belinda Parker (La Trobe University).

All human sarcoma cell lines (A673, SK-UT-1, RD-1, SK-PN-DW, CHLA-10) were maintained in a humidified incubator at 37 °C in air supplemented with 5% CO_2. A673, SK-UT-1, RD-1 and SK-PN-DW were cultured in DMEM media (+ 4.5 g/L D-glucose, L-Glutamine, 110 mg/L sodium pyruvate) (Thermo Fisher Scientific; MA, USA) supplemented with 10% Foetal Calf Serum (FCS). The Ewing sarcoma cell line CHLA-10 was cultured in IMDM media (+ L-Glutamine, 25 mM HEPES) (Thermo Fisher Scientific) supplemented with 20% FCS and Insulin Transferrin Selenium containing 10 mg/L Insulin, 5.5 mg/L Transferrin and 0.0067 mg/L Selenium (Thermo Fisher Scientific). All adherent cells were washed in Phosphate Buffered Saline (PBS) (135 µM potassium chloride, 500 µM phosphate buffer, 6.85 mM sodium chloride, pH 7.4) then detached using Trypsin-EDTA (5.3 mM potassium chloride, 0.44 mM potassium phosphate monobasic, 4.2 mM sodium bicarbonate, 138 mM sodium chloride, 0.34 mM sodium phosphate dibasic, 5.56 mM D-Glucose, 0.91 mM EDTA, 0.03 mM phenol red, 0.11 mM trypsin) (Thermo Fisher Scientific).

The drugs temozolomide, SN38, vincristine, doxorubicin, navitoclax and LCL-161 were purchased from Selleck Chemicals (TX, USA), whilst bortezomib, carfilzomib, ixazomib, delanzomib, oprozomib, cisplatin, vorinostat were purchased from Sigma-Aldrich (NSW,

Australia). All drugs were dissolved in DMSO except for doxorubicin which was dissolved in Milli-Q water.

2.2 CD44 staining

A673 and KRIB luc-4 cells were harvested, collected, and resuspended in 1:100 Mouse Anti-Human CD44-FITC (SouthernBiotech; Birmingham, USA) or 1:100 of the isotype control Mouse IgG_{2a}-FITC (SouthernBiotech). They were then immediately run on the FACS CytoFLEX (BD Biosciences) and plots were analysed to compare differences in peak shift for the FL1-A: FITC-A channel.

2.3 Pharmacodynamics (proteasome and caspase activity assays)

Protein was extracted for enzyme assays according to published method (Kisselev & Goldberg, 2005), with minor adaptations. A673, SK-PN-DW and CHLA-10 cells were seeded and left to adhere overnight before being treated with the proteasome inhibitors bortezomib, ixazomib and carfilzomib. These cells were then collected at 1, 24, and 48 hours and the pellets were stored at -20 °C until required. The pellets were then homogenised on ice using a Microson Ultrasonic Cell Disruptor (Misonix) using a hypotonic lysis buffer (50 mM HEPES, pH 8.0, 1 mM DTT (added fresh)) (Kisselev & Goldberg, 2005). The solution was then centrifuged at 13,000 *g* for 20 minutes at 4 °C and the supernatant was mixed 1:1 with stabilisation solution (40 mM HEPES pH 8.0, 1 mM EDTA, 20% glycerol) (Kisselev & Goldberg, 2005) and stored at -80 °C. Using a micro BCA kit (Thermo Fisher Scientific) as per the manufacturers protocol, the protein in each sample was quantified. The proteasome activity assay was prepared on ice in a clear curved-bottom 96 well plate standardised with 30 µg of protein per sample along with an equal volume of proteasome activity buffer (0.5 mM ATP, 1 mM DTT, 0.5 mg/ml BSA) (Kisselev & Goldberg, 2005) containing 100 µM of Suc-LLVY-AMC substrate (Enzo Life

Sciences; NY, USA). The fluorescence was measured over a 3-hour period using a SpectraMax M5^{e} (Molecular Devices) and fluorescence readings were compared to a no protein lysate control.

Similarly, the caspase activity assay was prepared in a clear curved-bottom 96 well plate on ice using universal citrate buffer (10 mM HEPES pH 7.0, 10% sucrose, 0.1% CHAPS, 100 mM NaCl, 1 mM EDTA, 0.65 M citrate) (Bloomer et al., 2019) with 10 mM DTT and 50 µM Ac-DEVD-AFC with equal volumes of 30 µg of protein lysate per sample. The fluorescence was then read using the SpectraMax M5^{e} (Molecular Devices) over a 1-hour period.

2.4 *In vitro* screening assays (MTT, CellTiter-Glo)

Non-adhered cell viability assays:

All drugs were prepared in clear (MTT assay) or white (CellTiter-Glo) flat-bottomed 96 well plates at double their desired concentrations and frozen at -80 °C until required (the cells were later added to this drug containing media in equal volumes to achieve the desired drug concentrations).

Once thawed for MTT assays, 5000 cells were added to the plates and incubated for 24 hours in a humidified chamber at 37 °C and 5% CO_2. MTT was added to a final concentration of 0.83 mg/ml per well and incubated for a further 4 hours. The formazan crystals were dissolved in acidified sodium dodecyl sulphate (SDS) (10% (w/v) in 0.01 M HCl) and returned to the incubator overnight where the absorbance was then read at 570 nm (Tada et al., 1986). The readings were taken on a SpectraMax M5^{e} (Molecular Devices; San Jose, USA), where absorbance of wells containing media alone was subtracted from the treatments.

To quantify ATP levels after treatments using the CellTiter-Glo assay, 2000 cells were counted and added to the thawed drug plates and incubated at 37 °C for either 24, 48 or 72 hours. Samples were analysed using CellTiter-Glo 2.0 (Promega) as per the manufacturer's instructions, using half the quantity of CellTiter-Glo reagent specified and the luminescence measured using a SpectraMax M5^{e} (Molecular devices). The luminescence for all samples were subtracted from wells containing media alone. All IC_{50} values were calculated using non-linear regression on GraphPad Prism 8.0.1 (GraphPad Software; La Jolla, California). CompuSyn (CompuSyn Inc; Paramus, New Jersey) was used to calculate the combination index for the synergy/antagonism of the drug combinations of bortezomib/ixazomib with cisplatin/doxorubicin (Chou, 2010).

Adhered cell viability assay:

CellTiter-Glo assays on adhered cells were undertaken by seeding either 2000 cells per well for 72-hour treatments or 5000 cells per well for 24- or 48-hour treatments in white-bottomed 96-well plates. The cells were left overnight to adhere in a 37 °C incubator, then the media in the wells was replaced with drug containing media. After the incubation, cell viability was measured in the same manner as the non-adhered viability assays described above using CellTiter-Glo 2.0 (Promega) and drug cooperation was analysed using CompuSyn.

2.5 Flow cytometry

One hundred thousand A673, CHLA-10 or SK-PN-DW cells were seeded per well in a 24 well plate and left overnight to adhere. The media was then replaced with the desired concentration of drug containing media and the plates were returned to the 37 °C incubator for 24 hours. After the appropriate drug incubations, the media containing the non-adhered cells was collected and the adherent cells were washed with PBS, detached with 0.25%

Trypsin-EDTA (Thermo Fisher) and collected in the same tube. They were then pelleted at 1200 *g* for 5 minutes at room temperature and the pellet was washed with PBS then repelleted. The pellets were then resuspended in binding buffer (10 mM HEPES, 140 mM NaCl, 2.5 mM $CaCl_2$, pH 7.4) with 10 µg/mL propidium iodide (PI; Sigma-Aldrich) and 750 ng/ml Annexin V-FITC (Abcam; Cambridge, England). The samples were run on the FACS Canto II (BD Biosciences) and analysed for PI and Annexin V-FITC positive cells using FlowJo version 10.6.0 (FlowJo; USA).

For cell cycle analysis post drug treatment, the cells were fixed in 70% cold ethanol (added dropwise) and kept at 4 °C overnight. The fixed cells were then repelleted and washed with PBS before being treated with 50 µg/ml PI and 100 µg/ml RNAse A (Qiagen; Maryland). Treated and untreated samples were analysed on a FACS Canto II, where the sub-G1, G1, S and G2/M phases were determined based on PI fluorescence (reflecting DNA content) using FlowJo (Becton, Dickinson, and company; Ashland, Oregon).

2.6 Lentiviral infection

PT67 packaging cells were seeded to 50% confluency and cultured overnight in DMEM substituted with 10% FCS in a P75 flask at 37 °C, 5% CO_2. The following day the media was replaced with fresh media. Next, 36 µg of pMSC-mcherry-luc-IRES plasmid (from Dr Belinda Parker) was prepared in 500 µl of serum free media. A second tube was prepared with 450 µl of serum free media and 50 µl of Lipofectamine 2000 and the tubes were left to incubate for 5 minutes. Next 125 µl of the plasmid solution was added to an equal volume of the Lipofectamine solution and left for 20 minutes to incubate. Following this incubation, the plasmid/Lipofectamine solution was added dropwise to the PT67 cells. The media was replaced on the packaging cells after 8 hours and returned to the incubator for a further 36 hours (until day three). On day two, 100,000 A673 cells were seeded into

wells of a 6-well plate to be used for the infection. On day three, the lentiviral supernatant from the PT67 cells was filtered through a 0.45 µM filter and 4 µg/ml of polybrene (Sigma-Aldrich) was added. Next, the filtered supernatant was diluted to 15 ml with fresh DMEM media and added to A673 cells. The plate was spun at 1800 rpm for 45 mins at 25 °C. The plates were then returned to 37 °C incubator and the media was replaced on the cells the next morning. On day five, the infection was repeated for a second time on the same cells to improve the uptake efficiency.

2.7 A673 stable transfection

A673 cells were seeded to 50-60% confluency in a 10 cm plate. The following day 100,000 A673 cells were seeded into wells of a 6-well plate and left overnight to adhere. 14 µg of the pcDNA3.1(+)/Luc2=tdT plasmid (Addgene) was prepared in 700 µl of serum free media. A second tube was prepared with 18 µl of Lipofectamine 2000 and made up to 250 µl using serum free media and incubated for 5 minutes. Next 125 µl of each tube were added together and incubated for 20 minutes. During this time the media was replaced on the A673 cells with 2 ml of fresh DMEM media containing 10% FCS. Next 250 µl of the Lipofectamine/plasmid solution containing 2.5 µg of the plasmid and 9 µl of Lipofectamine 2000 was added dropwise per well and, without mixing the contents, the plate was returned to the incubator. To determine ideal transfection conditions the media was replaced in the separate wells after 4, 16, (2ml fresh media added after 8 hours then replaced after 16 hours) or 24 hours later. Three days post transfection, the cells were analysed for tomato fluorescence using the PE channel on the FACS CytoFLEX Flow Cytometer (Beckman Coulter Life Sciences) to determine transient transfection efficiency and then sorted using the FACSAria III (BD Biosciences).

2.8 Sorting and screening of luciferase clones

The cells which had undergone the infection using the pMSC-mcherry-luc-IRES plasmid were resuspended in sorting buffer (PBS, 4% FCS, 5mM EDTA) and sorted into monoclonal populations by Dr Tanmay Shekhar using the FACSAria III (BD Biosciences). The transfected A673 cells using the pcDNA3.1(+)/Luc2=tdT plasmid were also resuspended in sorting buffer and sorted into 1 cell/well and 10 cells/well by Dr Margaret Veale using the FACSAria III (BD Biosciences). The monoclonal (1 cell/well) and polyclonal (10 cells/well) A673 populations were cultured in wells of a clear flat-bottom 96 well plate with DMEM media containing 20% FCS and 100 units/ml of penicillin and 100 µg/ml of streptomycin, and expanded to larger plates as required. As an early means to detect tomato positive cells (pcDNA3.1(+)/Luc2=tdT plasmid), the colonies were observed under an Olympus IX81 using the TRITC filter cube. The proportion of mCherry or tomato positive cells in the populations were determined via harvesting and resuspending the cells in PBS before being analysed on the FACS CytoFLEX (Beckman Coulter Life Sciences). To assess luciferase activity of the clones, 5000 cells were seeded from the monoclonal populations into a 96 well flat-bottom plate before being incubated with 150 µg/ml of D-luciferin (Gold Biotechnology, USA) and their luminescence was immediately measured using the SpectraMax M5^{e} (Molecular devices).

2.9 Limiting dilution of A673 tomato clones

A673 cells transfected with pcDNA3.1(+)/Luc2=tdT plasmid (Addgene) were sorted to isolate tomato positive cells. Aliquots mathematically containing 0.9 cells were added to individual wells of a 96 well plate, which was expected to result in 37% of wells containing a single cell and a 22% of wells containing more than one cell according to Poisson's distribution (Fuller et al., 2001; Gross et al., 2015). Monoclonal populations were selected

via microscopy through the identification of a single colony within the well. Monoclonal transfectants generated from this process were denoted A673 Luc1L, A673Luc2L etc.

2.10 G418 treatment of transfected A673 cells

A673 cells were transfected with the G418-selectable pcDNA3.1(+)/Luc2=tdT plasmid or the control (puromycin-selectable) pEF plasmid (Hawkins et al., 1996) as stated in 2.7. Two days post transfection, the cells were expanded into 10 cm plates where they were treated with either 0, 50, 100, 250, 500 or 1000 µg/ml of G418. Once all cells appeared dead in the plate containing cells transfected with the pEF control plasmid, individual colonies were selected from the pcDNA3.1(+)/Luc2=tdT plasmid treated at the identical concentration of G418. Colonies were then harvested under a light microscope into media containing 1000 µg/ml of G418 and 100 units/ml of penicillin and 100 µg/ml of streptomycin. To ensure the A673 colonies selected were of a clonal nature, sparsely distributed colonies were chosen. Sterility was maximised by wiping down all equipment with ethanol prior to use and removing lids off cells only when necessary. All monoclonal populations generated from this protocol were named numerically using the nomenclature A673 Luc1G, A673 Luc2G etc.

2.11 Luciferase gene PCR

DNA was extracted from sarcoma cells using the DNeasy Blood and tissue kit (Qiagen, Victoria, Australia) as per manufacturer's instructions. Sets of luciferase primers designed by Dr Christine Hawkins for the luciferase gene were tested to determine the most specific pair for the A673-Luc clones (from lentiviral infection with pMSC-mcherry-luc-IRES plasmid) (Table 1).

Table 1: **PCR primers for luciferase and vimentin gene**

Primer#, gene, (expected size)	**Forward primer**	**Reverse primer**
1978-1979, luciferase (146 bp)	GCAACCAGATCATCCCCGAC	GCTGCGCAAGAATAGCTCCT
1976-1977, luciferase (293 bp)	CCGGCTTCAACGAGTACGAC	CTCCTCCTCGAAGCGGTACA
1980-1981, luciferase (131 bp)	TGCAGTTCTTCATGCCCGTG	GCTCACGAATACGACGGTGG
1982-1983, vimentin (81 bp)	AGCTGCTAACTACCAGGACACTATTG	CGAAGGTGACGAGCCATCTC

Primers used to amplify the vimentin gene (1982-1983; Table 1) were as previously published (Rautela et al., 2015). PCR was prepared using OneTaq DNA Polymerase (New England Biolabs; MA, USA) and 100 ng of DNA per sample for consistency. The conditions used for this PCR were an initial incubation at 95 °C for 2 minutes, then 39 cycles of [95 °C for 15 seconds, 56 °C for 15 seconds and 72 °C for 1 minute]. The samples were run on a 1.8% agarose gel containing 1X SYBR Safe (Thermo Fischer Scientific, MA, USA) and imaged in a G:BOX F3 (Syngene, Cambridge, UK).

2.12 A673 -xenograft models

The tumourigenicity and efficacy experiments in this project were all approved by the La Trobe Animal Ethics Committee (AEC17-76), using 6-week-old BALB/c nude mice (Animal Resource Centre, Murdoch, WA). For the primary Ewing sarcoma model, 50,000 A673 Luc-4 cells were implanted in the *tibialis anterior* using a 26 gauge needle in the left hind leg of five BALB/c nude mice, with a 1:1 ratio of media containing cells and Cultrex (Trivigen, MD, USA), as published (Shekhar et al., 2019). Once tumours were detected,

primary tumour size was monitored three times a week using calipers (as luminescence was not detected in any A673 luciferase clones generated using the mCherry/luciferase plasmid) and the tumour volume was determined via the equation (Tumour length (mm) * (Tumour width (mm))^2)/2).

For the metastatic mouse model, 150,000 or 500,00 A673 Luc3L tomato positive cells (generated via limiting dilution cloning of transfectants) were intravenously implanted in ten BALB/c nude mice, 24 hours after half of which had been administered 50 µl of anti-asialo-GM1 (Wako, Osaka, Japan) antibody via intraperitoneal injection and the other half were administered 50 µl of saline. The mice were anesthetised twice weekly for four weeks via the inhalation of 2.5% isoflurane and administered 150 mg/kg of D-luciferin via intraperitoneal injections. Bioluminescence emitted by the tumour cells was detected once per minute for 10 minutes using an *in vivo* imaging system (IVIS) (Perkin Elmer; MA; USA). The peak luminescence reading over this period was recorded. All bioluminescent organs also underwent *ex vivo* analysis at the endpoint by harvesting them and soaking them in 15 mg/ml D-luciferin and instantly reading the bioluminescence.

2.13 A673 efficacy using proteasome inhibitors bortezomib and ixazomib

Mice intramuscularly implanted with A673 Luc-4 cells were monitored daily until tumours were detected by eye and palpation and were then sorted into treatment groups. Eight mice received twice-weekly doses of saline via intraperitoneal injection using a 26-gauge needle, eight mice received 5 mg/kg of ixazomib (twice weekly) via oral gavage and eight mice were administered 1 mg/kg of bortezomib (twice-weekly) via intraperitoneal injection using a 26-gauge needle. The primary tumour size was measured three times a week using callipers and tumour volume calculated using the equation in section 2.12. The mice were treated twice weekly for up to four weeks after the detection of a primary tumour, followed

by two weeks without treatments before the endpoint. Culling was performed before the planned endpoint if their movement was impaired by the tumour, if they displayed breathing difficulties, the tumour became ulcerated or if the primary tumour volume reached the limit of 1000 mm^3, specified by the ethics committee.

2.14 A673 Luc-4 *ex vivo* sensitivity

One quarter of the primary tumour from each mouse was resected at the endpoint of the primary efficacy experiment and incubated in collagenase/dispase 1 mg/ml (Sigma-Aldrich) at 37 °C for 3-4 hours. This cell sample was passed through a 0.45 µm filter into DMEM media containing 10% FCS and cultured in a 37 °C incubator. One week after culturing the cells, they were washed with PBS and the media was replaced before undergoing a CellTiter-Glo experiment the following day using bortezomib and ixazomib as described in 2.4.

2.15 Immunophenotyping

Organs from the A673 Luc3L tumour-bearing mice were collected at the endpoint of the 500,000 A673 Luc3L metastatic model experiment, along with a mouse spleen without any detectable metastasis. All the organs were minced finely using a scalpel blade and then placed into 1 ml of digestion solution (0.1% collagenase A and 0.2% dispase II (Sigma-Aldrich)) and incubated at 37 °C shaking gently for 30 minutes. The suspension was transferred to a 50 ml tube containing DMEM media (+ 4.5 g/L D-glucose, L-Glutamine, 110 mg/L sodium pyruvate) (Thermo Fisher Scientific; MA, USA) supplemented with 10% FCS and gravity filtered through 70 µM strainer. The process was repeated for the remaining minced tissue for a further 30 minutes. During the second incubation the mouse spleen was mashed using the serrated end of the syringe plunger in DMEM media and the solution was centrifuged at 1200 *g* for 5 minutes. The pellet was resuspended in filter-

sterilized red blood cell lysis buffer (10 mM potassium bicarbonate, 0.15 M ammonium chloride, and 0.1 mM ethylenediaminetetraacetic acid (EDTA)) and incubated at room temperature for 10 minutes and then resuspended in 3 ml of fresh media. After the second incubation, the 50 ml tubes containing the tumour cells were then pelleted at 1200 *g* for 5 minutes and resuspended in 10 ml of fresh DMEM media. Parental A673 cells, cultured A673 Luc3L cells, spleen cells, as well as cells from each tumour-bearing organ were stained with Ly-6G-APC clone 1A8 #560599 (BD Biosciences, Franklin Lakes, NJ), CD335/NKp46-BV421 clone 29A1.4 #562850 (BD Biosciences) and F4/80-Pe-Cy7 clone BM8 #25-4801-82 (ThermoFisher Scientific) antibodies diluted 1/300 (or their isotype controls, sourced from the same companies) for 30 minutes. The samples were then washed with PBS and resuspended in sorting buffer (PBS containing 4% FCS, 1mM EDTA) and analysed using the FACS CytoFLEX (Beckman Coulter Life Sciences).

2.16 Hematoxylin & Eosin staining

Organs from tumour-bearing mice were placed in cassettes and stored in formalin. Next, the tissue was processed in 70% ethanol for 1 hour, 100% ethanol for 1 hour, fresh solutions of 100% ethanol twice for 1.5 hours each, three consecutive incubations in xylene for 1 hour, one incubation in xylene for 1.5 hours and lastly three incubations in paraffin wax (60 °C) for 1 hour each. The tissue was then embedded in molten paraffin wax and the block was left at room temperature overnight to solidify. The block was then sectioned using a microtome to a thickness of 4 µm before the ribbon was added to a 42 °C water bath and placed immediately on the positive (+) surface of a clean glass slide. The slides were then H & E stained using the protocol shown in table 2 below (Cardiff et al., 2014).

Table 2: **Protocol for H & E staining**

Part 1: Dewaxing	
1: Xylene (two incubations)	4 minutes
2: 100% ethanol (two incubations)	2 minutes
3: Tap water	5 minutes
Part 2: Haematoxylin and Eosin staining:	
1: Mayer's Haematoxylin	3 minutes
2: Tap water	10 seconds
3: Scott's tap water	1 minutes
4: Tap water	1 minutes
5: 1% Aqueous Eosin	3 minutes
6: Tap water	Rinse
Part 3: Dehydrating in alcohols and clearing in xylene	
1: 100% Ethanol (three incubations)	10 dips
2: Xylene (two incubations)	2 minutes
*Slides were then mounted in DPX (Sigma-Aldrich, NSW, Australia)	

All reagents for staining purchased form Amber scientific, WA, Australia.

The slides were then imaged on an Olympus IX81 using the Olympus UPLSAPO 10X objective lens.

2.17 Mouse experimental workload

The workload involved in weighing the mice was evenly split between Carmelo Cerra and Michael Harris. The mouse intramuscular injections, IVIS imaging and mouse treatments were done by Carmelo with assistance from Michael. Carmelo and Michael contributed equally to the removal of mouse organs at the endpoints of these mouse studies. Intravenous injections were administered by animal technicians at the La Trobe Animal and Teaching Facility (LARTF).

2.18 Statistical calculations

All statistical calculations were generated using the GraphPad Prism software. A one-way ANOVA with Tukey's multiple comparisons was used to compare proteasome activity means 1 h to 48 h post drug treatment. A one-way ANOVA with Sidak's post-tests was used to compare A673 primary tumour volume between saline, bortezomib and ixazomib treated mice in the primary efficacy experiment. To compare the survival rate of the mice

between the different treatment groups (saline, bortezomib, ixazomib) in the A673 primary efficacy experiment, a Mantel-Cox test with Bonferroni correction for multiple comparisons (2) was used. A one-way ANOVA with Dunnett's multiple comparisons was used to compare the *ex vivo* sensitivity of each of the A673 primary mouse tumours to the proteasome inhibitors.

Chapter 3: Results

3.1 *In vitro* sarcoma cell line drug sensitivity screening

Three cell lines representing different sarcoma types were screened in an *in vitro* setting against current and novel anti-cancer agents at their maximum peak plasma concentration achievable in patients (C_{max}). The C_{max} were chosen to predict which drugs could possibly have activity i*n vivo*. Treating cells with concentrations that would be experienced by cells within the tumour would be ideal, but those drug concentrations have not been determined for these sarcomas. C_{max} is the next best option as it reflects the highest dose a cell could theoretically receive, but is probably higher than what will reach the tumour tissue.

An initial screen was achieved using an MTT assay to compare differences in cell metabolic activity (as a surrogate measure of cell viability) (Präbst et al., 2017; Tada et al., 1986) after the treatment of a cell lines derived from a Ewing sarcoma (A673), rhabdomyosarcoma (RD-1) and leiomyosarcoma (SK-UT-1) with various anti-cancer agents for 24 h (Figure 3). The purpose of this was to identify the most effective drug candidate for further *in vitro* sarcoma screening. Bortezomib, a proteasome inhibitor, was the most effective agent on average at reducing metabolic activity. The Ewing sarcoma cell line A673 and to a lesser extent the leiomyosarcoma cell line SK-UT-1 were particularly sensitive to this drug.

A

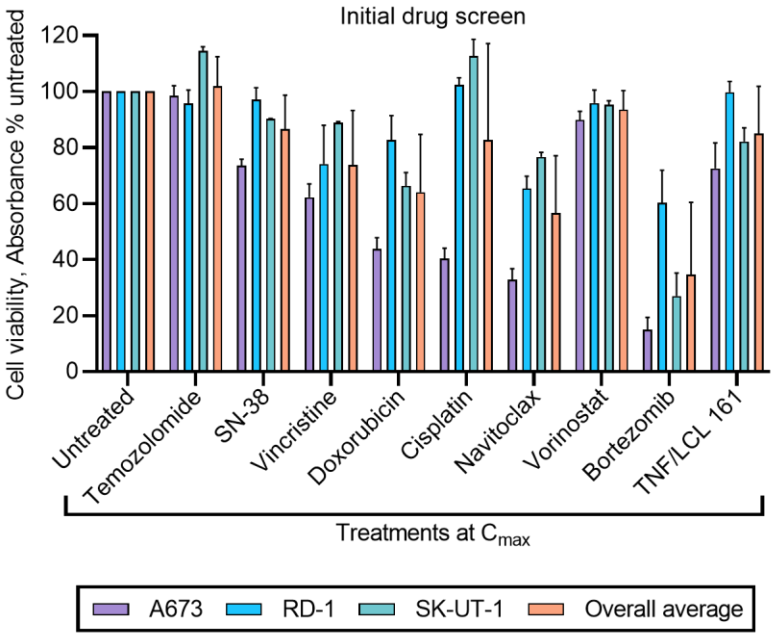

B

Drug	**C_{max}**	**Reference**
Temozolomide	35 µM	(Brada et al., 1999)
SN-38	45 nM	(Hamaguchi et al., 2010)
Vincristine	3.9 µM	(Shah et al., 2016)
Doxorubicin	1.7 µM	(Rushing et al., 1993)
Cisplatin	5.5 µM	(van Hennik et al., 1987)
Navitoclax	6.6 µM	(Wilson et al., 2010)
Vorinostat	1.8 µM	(Hummel et al., 2013)
Bortezomib	580 nM	(Moreau et al., 2012)
LCL 161	12 µM	(Infante et al., 2014)
TNFα (endogenous)	12 pg/ml	(Xiao et al., 2014)

Figure 3: **Ewing sarcoma cells are most sensitive to the proteasome inhibitor bortezomib**. Three sarcoma cell lines, Ewing sarcoma (A673), rhabdomyosarcoma (RD-1) and leiomyosarcoma (SK-UT-1), were incubated for 24 h with various anti-cancer agents all at their respective C_{max}. (A) All treatments were standardised relative to the untreated samples and averages (n = 9) for each drug were determined. The metabolic activity was measured via an MTT assay as an indirect measure of cell viability (n = 3, +/- SEM). (B) The C_{max} concentration for each drug used in the MTT assay.

To determine whether bortezomib sensitivity of A673 cells reflected a general sensitivity of Ewing sarcoma cells to proteasome inhibitors, two Ewing sarcoma cell lines, one derived from a muscle tumour (A673) and one derived from a bone tumour (SK-PN-DW) were treated with various proteasome inhibitors (Figure 4). A range of clinically relevant proteasome inhibitors which have been previously FDA-approved in treating multiple myeloma including bortezomib, ixazomib and carfilzomib as well as newer class inhibitors oprozomib and delanzomib were used.

The cell viability was determined using a CellTiter-Glo assay as it is a more precise and sensitive technique than MTT (Harris et al., 2020a), with the ability to detect below 300 cells in a sample (Appendix 1). This assay quantifies the ATP in each sample as a measure of the change in cell viability in different treatment groups.

These 48 hour *in vitro* CellTiter-Glo assays confirmed that Ewing sarcoma cells were very sensitive to the entire class of proteasome inhibitor therapies at clinically relevant concentrations. This was important as it implied that the sensitivity in Figure 3 was a general feature of this drug class and cell type.

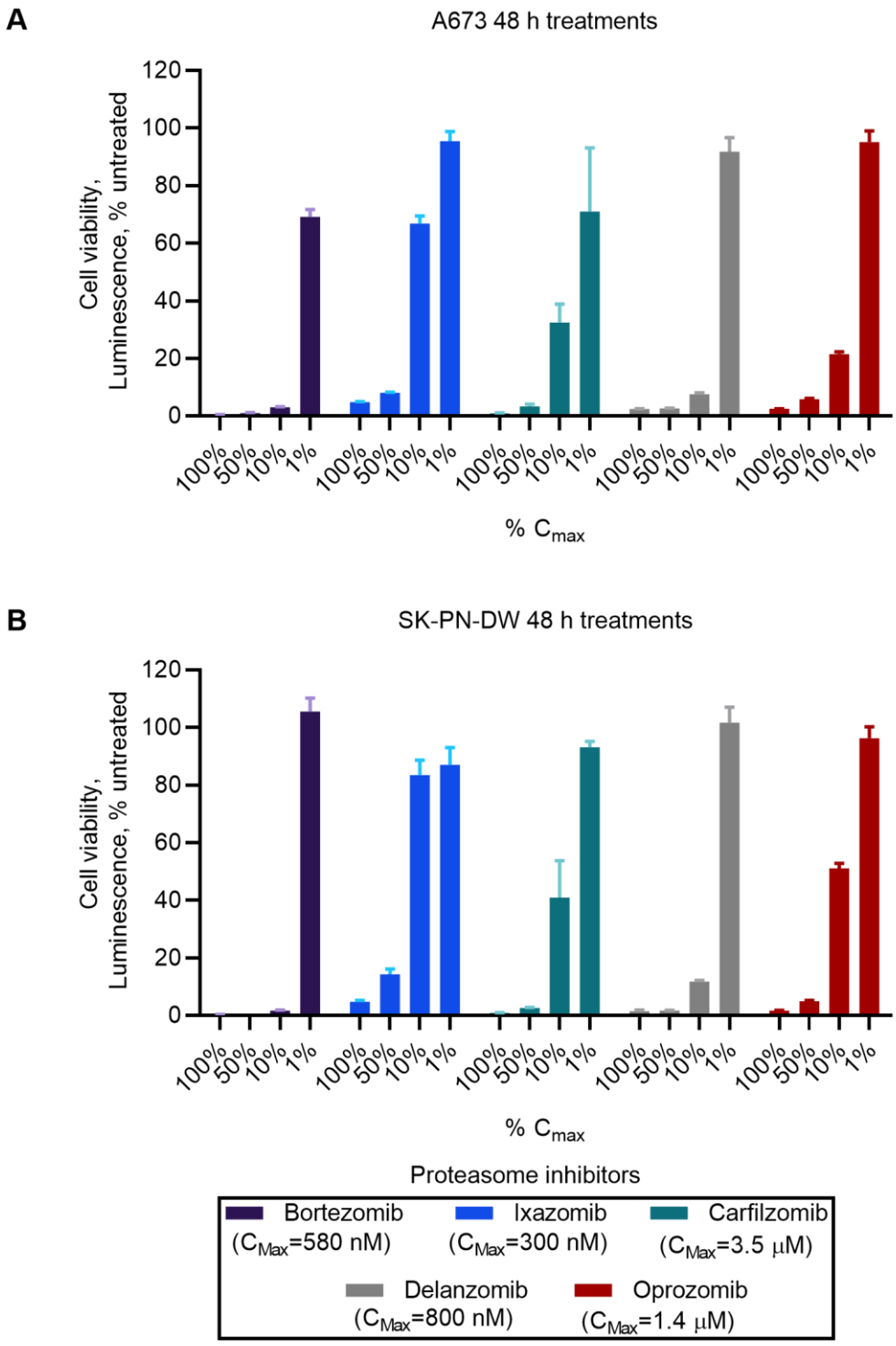

Figure 4: **Ewing sarcoma cells are sensitive many proteasome inhibitors.** A673 (A) and SK-PN-DW (B) cells were treated for 48 h with varying doses of C_{max} of the proteasome inhibitors bortezomib (580 nM (Moreau et al., 2012)), ixazomib (300 nM (Richardson et al., 2014)), carfilzomib (3500 nM (Quach et al., 2017)), delanzomib (800 nM (Gallerani et al., 2013)) and oprozomib (1400 nM (Infante et al., 2016)). (n = 3, +/-SEM). The cell viability was determined using the CellTiter-Glo assay, with the signals from all samples expressed relative to untreated cells.

The results in Figures 3 and 4 led to the focus for the remainder of this project on proteasome inhibitors and Ewing sarcoma.

The sensitivity of the Ewing sarcoma cell lines A673 (derived from a muscle) (Giard et al., 1973), CHLA-10 (from a thoracic lymph node) (Batra et al., 2004) and SK-PN-DW (derived from a bone) (Potluri et al., 1987) was investigated further using additional incubation times and cells both adhered and not adhered prior to drug treatments. These Ewing sarcoma cell lines were treated with bortezomib, ixazomib and carfilzomib compared to current chemotherapy drugs cisplatin and doxorubicin over a range of concentrations, using the CellTiter-Glo assay (Figure 5,6). Cisplatin is used for recurrent Ewing sarcoma patients (van Maldegem et al., 2015), whilst doxorubicin is used as a first-line treatment for Ewing sarcoma (Womer et al., 2012). This process was undertaken on Ewing cell lines before they had adhered to the plate (Figure 5) and once they had adhered to the plate (Figure 6), to observe the impact that cell adhesion had on drug sensitivity.

Overall, A673 cells were the most sensitive Ewing sarcoma cell line to the proteasome inhibitors at 24, 48 and 72 h. Bortezomib was the most effective drug at reducing cell viability in all three Ewing cell lines. Also, bortezomib and carfilzomib were just as effective and, in some cases, more effective at reducing ATP levels than current chemotherapies in the SK-PN-DW and CHLA-10 cells. Using this data, the concentrations of the drugs required to reduce ATP levels by half (IC_{50}) were calculated for both the non-adhered (Table 3) and adhered cell (Table 4) experiments. To put these concentrations into further clinical relevance the percentage C_{max} required for each IC_{50} was calculated as a means of comparing drug effectiveness between treatments.

In general, the adhered cells tended to be slightly less sensitive to all treatments although similar sensitivity profiles were observed within each of the two experiments (non-adhered

vs adhered cells). This may have been due to changes in cell morphology or cell adhesion-mediated drug resistance discussed in section 4.1.3 (Damiano et al., 2001; Huang et al., 2019). The adhered IC_{50}'s were used for all further experiments in this project, unless otherwise specified for consistency to the literature as these Ewing sarcoma cells are all adherent cells. Also, since Ewing sarcoma is a solid tumour type *in vivo* it would be expected that the cells would be more likely to be in an adhered morphology in a patient.

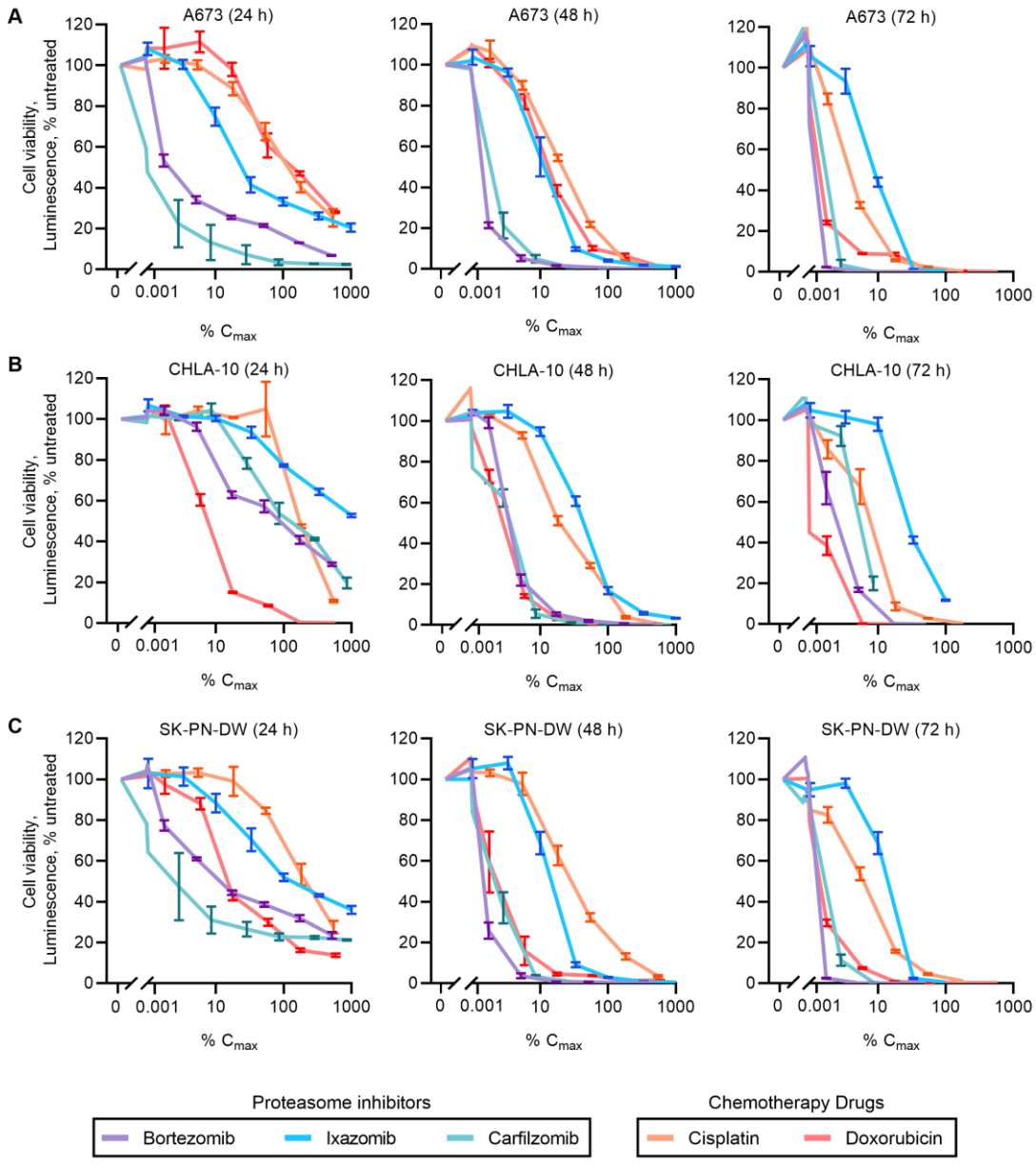

Figure 5: **Ewing sarcoma cell lines (<u>non-adhered protocol</u>) are sensitive to the proteasome inhibitors, compared to current chemotherapies**. Three Ewing sarcoma cell lines A673 (A), CHLA-10 (B) and SK-PN-DW (C) were incubated for either 24, 48 or 72 h with the proteasome inhibitors bortezomib (C_{max}= 580 nM), ixazomib (C_{max}= 300 nM) and carfilzomib (C_{max}= 3500 nM) as well as current treatments cisplatin (C_{max}= 5500 nM) and doxorubicin (C_{max}= 1700 nM) (n = 3, +/-SEM). The levels of ATP were determined using the CellTiter-Glo assay, with all samples compared relative to untreated cells.

Table 3: **The calculated concentrations of each drug required to reduce ATP levels by half (IC_{50}), for the Ewing sarcoma lines A673, CHLA-10, SK-PN-DW (<u>non-adhered protocol</u>), after 24, 48 or 72h.** In each case the values in brackets indicate the percentage C_{max} required to achieve this IC_{50} (n=3, +/- SEM). Where the C_{max} was taken from the following references bortezomib (Moreau et al., 2012), ixazomib (Richardson et al., 2014), carfilzomib (Quach et al., 2017), cisplatin (van Hennik et al., 1987), doxorubicin (Rushing et al., 1993).

		Bortezomib (C_{max}=580 nM)	Ixazomib (C_{max}=300 nM)	Carfilzomib (C_{max}=3500 nM)	Cisplatin (C_{max}=5500 nM)	Doxorubicin (C_{max}=1700 nM)
24 h	A673	9.17 ± 0.893 nM (1.58 ± 0.02%)	43.7 ± 6.87 nM (14.6 ± 2.30%)	10.9 ± 32.5 nM (0.31 ± 0.93%)	4.03 ± 0.27 µM (73.3 ± 0.01%)	871 ± 125 nM (51.2 ± 7.35%)
	CHLA-10	132 ± 23.6 nM (22.7 ± 0.04%)	379 ± 91.1 nM (126 ± 30.4%)	2.60 ± 0.74 µM (74.1 ± 0.02%)	9.64 ± 0.63 µM (175 ± 3.18%)	651 ± 9.61 nM (38.3 ± 0.57%)
	SK-PN-DW	21.5 ± 1.79 nM (3.70 ± 0.31%)	105 ± 37.0 nM (35.0%)	16.8 ± 3.07 nM (0.48 ± 0.09%)	8.17 ± 1.40 µM (149 ± 0.03%)	213 ± 9.60 nM (12.5 ± 0.56%)
48 h	A673	6.80 ± 0.89 nM (1.17 ± 0.15%)	31.7 ± 5.00 nM (10.6 ± 1.67%)	64.9 ± 7.06 nM (1.85 ± 0.20%)	1.05 ± 0.05 µM (19.0 ± 0.001%)	204 ± 13.5 nM (12.0 ± 0.79%)
	CHLA-10	22.1 ± 1.41 nM (3.81 ± 0.24%)	116 ± 4.13 nM (38.7 ± 1.38%)	118 ± 12.4 nM (3.37 ± 0.35%)	1.09 ± 0.13 µM (19.9 ± 0.002%)	44.9 ± 2.54 nM (2.64 ± 0.15%)
	SK-PN-DW	9.03 ± 0.89 nM (1.56 ± 0.15%)	37.7 ± 4.28 nM (12.6 ± 1.43%)	71.1 ± 16.5 nM (2.05 ± 0.47%)	1.42 ± 0.17 µM (25.8 ± 0.003%)	34 ± 12 nM (2.00 ± 0.71%)
72 h	A673	3.46 ± 0.05 nM (0.60 ± 0.01%)	24.8 ± 0.85 nM (8.26 ± 0.28%)	45.6 ± 3.09 nM (1.30 ± 0.09%)	173 ± 3.08 nM (3.15 ± 0.06%)	15.7 ± 0.90 nM (0.93 ± 0.05%)
	CHLA-10	13.1 ± 1.08 nM (2.25 ± 0.19%)	78.2 ± 4.38 nM (26.1 ± 1.46%)	227 ± 5.44 nM (6.48 ± 0.16%)	389 ± 42.9 nM (7.06 ± 0.78%)	15.7 ± 6.44 nM (0.92 ± 0.38%)
	SK-PN-DW	4.51 ± 0.12 nM (0.78 ± 0.02%)	36.9 ± 2.02 nM (12.3 ± 0.67%)	65.7 ± 10.4 nM (1.88 ± 0.30%)	368 ± 25.6 nM (6.70 ± 0.47%)	18.5 ± 1.95 nM (1.10 ± 0.12%)

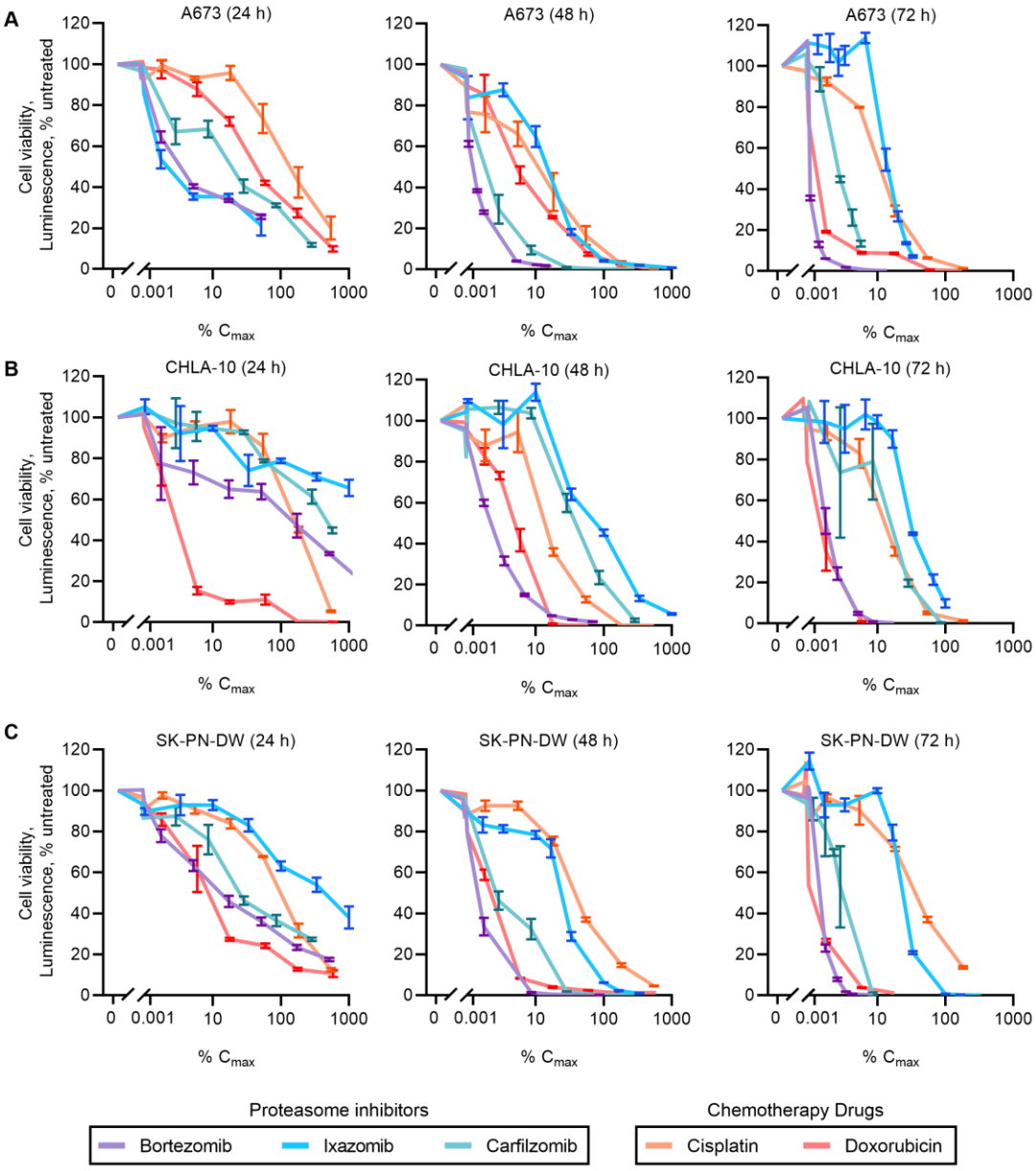

Figure 6: **Ewing sarcoma cell lines (<u>adhered cell protocol</u>) are sensitive to the proteasome inhibitors**. Three Ewing sarcoma cell lines, A673 (A), CHLA-10 (B) and SK-PN-DW (C) were seeded into plates then the next day were incubated for either 24, 48 or 72 h with the proteasome inhibitors bortezomib (C_{max}= 580 nM), ixazomib (C_{max}= 300 nM) and carfilzomib (C_{max}= 3500 nM) as well as current treatments cisplatin (C_{max}= 5500 nM) and doxorubicin (C_{max}= 1700 nM) (n = 3, +/-SEM). The levels of ATP were determined using the CellTiter-Glo assay, with all samples compared relative to untreated cells.

Table 4: **The calculated concentrations of each drug required to reduce ATP levels by half (IC_{50}), for the Ewing sarcoma lines A673, CHLA-10, SK-PN-DW (adhered cell protocol), after 24, 48 and 72h incubations.** In each case the values in brackets demonstrate the percentage C_{max} required to achieve this IC_{50} (n = 3, +/- SEM).

		Bortezomib (C_{max}=580 nM)	Ixazomib (C_{max}=300 nM)	Carfilzomib (C_{max}=3500 nM)	Cisplatin (C_{max}=5500 nM)	Doxorubicin (C_{max}=1700 nM)
24 h	A673	11.2 ± 0.89 nM (1.93 ± 0.15%)	71.8 ± 9.54 nM (23.9 ± 3.18%)	807 ± 86.8 nM (23.1 ± 2.48%)	6.37 ± 0.809 µM (116 ± 14.7%)	716 ± 253 nM (42.1 ± 14.9%)
	CHLA-10	246 ± 32.4 nM (42.4 ± 5.60%)	33.6 ± 0.63 µM (11205 ± 209%)	19.1 ± 2.73 µM (545 ± 77.9%)	10.1 ± 6.29 µM (184 ± 114%)	118 ± 6.04 nM (6.94 ± 0.36%)
	SK-PN-DW	32.7 ± 8.27 nM (5.64 ± 1.43%)	372 ± 80.0 nM (124 ± 26.7%)	618 ± 80.2 nM (17.7 ± 2.29%)	5.70 ± 0.77 µM (104 ± 14.0%)	119 ± 31.1 nM (7 ± 1.83%)
48 h	A673	6.62 ± 0.19 nM (1.14 ± 0.03%)	48.5 ± 3.82 nM (16.2 ± 1.27%)	63.1 ± 16.9 nM (1.80 ± 0.48%)	896 ± 437 nM (16.3 ± 7.95%)	104 ± 26.9 nM (6.12 ± 1.58%)
	CHLA-10	12.6 ± 0.36 nM (2.17 ± 0.06%)	177 ± 30.3 nM (59 ± 10.1%)	1.31 ± 0.26 µM (37.3 ± 7.39%)	812 ± 43.1 nM (14.8 ± 0.78%)	86.9 ± 7.64 nM (5.11 ± 0.45%)
	SK-PN-DW	8.41 ± 0.56 nM (1.45 ± 0.10%)	82.7 ± 3.12 nM (27.6 ± 1.04%)	124 ± 27.9 nM (3.54 ± 0.80%)	2.26 ± 0.05 µM (41.0 ± 0.97%)	35.6 ± 6.46 nM (2.09 ± 0.38%)
72 h	A673	5.07 ± 0.23 nM (0.87 ± 0.04%)	38.9 ± 1.09 nM (13 ± 0.36%)	33.0 ± 3.39 nM (0.94 ± 0.10%)	655 ± 9.65 nM (11.9 ± 0.18%)	92.1 ± 1.06 nM (5.42 ± 0.06%)
	CHLA-10	9.97 ± 0.43 nM (1.72 ± 0.07%)	86.9 ± 3.41 nM (29 ± 1.14%)	617 ± 196 nM (17.6 ± 5.59%)	747 ± 40.2 nM (13.6 ± 0.73%)	20.7 ± 5.63 nM (1.22 ± 0.33%)
	SK-PN-DW	8.49 ± 0.19 µM (1.46 ± 0.03%)	70.6 ± 1.56 nM (23.5 ± 0.52%)	114 ± 7.52 nM (3.26 ± 0.21%)	1.95 ± 0.24 µM (35.5 ± 4.31%)	11.5 ± 0.61 nM (0.68 ± 0.04%)

As a further means of determining the sensitivity of Ewing sarcoma cells to proteasome inhibition, a flow cytometry experiment was undertaken to measure cell death post treatments with Annexin V-FITC and Propidium Iodide staining (Figure 7). These stains allow for the detection of early apoptotic and dead cells respectively (Banfalvi, 2017). Annexin V-FITC has high affinity for phosphatidylserine which is found on the inner surface of the plasma membrane in viable cells and becomes exposed when a cell undergoes apoptosis (Wlodkowic et al., 2012). Propidium iodide is a DNA binding dye which stains cells which have accessible DNA usually due to the damage or the absence of nuclear membranes (Nicoletti et al., 1991).

The proteasome inhibitors induced apoptosis in all three cell lines at 10% theoretically achievable concentrations in patients' blood. A673 and SK-PN-DW were more sensitive to the drugs than CHLA-10 cells. This was highlighted as at least 50 % of these cells bound annexin V 24 hours post treatment with C_{max} doses. This supports previous CellTiter-Glo data that CHLA-10 cells were the least sensitive cell line to the proteasome inhibitors as well as confirming that the A673 cells were most sensitive to bortezomib.

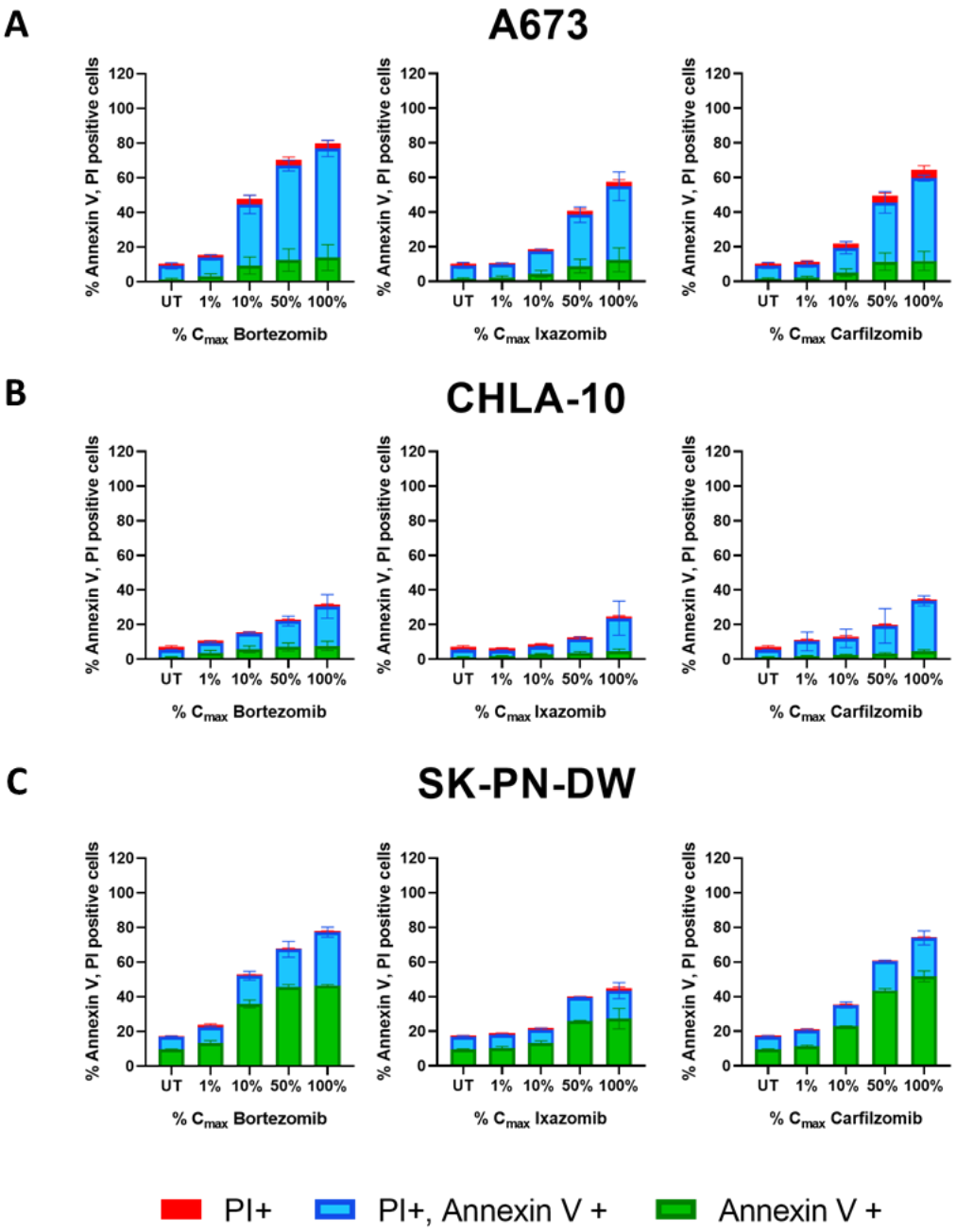

Figure 7: **The proteasome inhibitors induce high levels of apoptosis in Ewing sarcoma cell lines**. The Ewing sarcoma cell lines A673 (A), CHLA-10 (B) and SK-PN-DW (C) were treated with the proteasome inhibitors bortezomib (580 nM), ixazomib (300 nM) and carfilzomib (3500 nM) at their C_{max} and analysed via Annexin V/PI Flow cytometry after 24 h, (UT = untreated) (n = 3, +/-SEM).

To explore the mode of cell death provoked by the proteasome inhibitors, a caspase activity assay was completed (Figure 8). A673, SK-PN-DW and CHLA-10 cells were treated with doses of 5 and 10 nM bortezomib and 50 and 100 nM of ixazomib for 1, 24 and 48 h and levels of caspase activity was monitored. Caspase activity was measured using the fluorogenic substrate Ac-DEVD-AFC which can be efficiently cleaved by active caspase-3 and less efficiently caspase-7 (McStay, 2016; Vickers et al., 2013). Proteasome inhibitors have been shown to enhance caspase activity within osteosarcoma cells (Patatsos et al., 2018). It was expected that the more effective the drug, the larger the increase in caspase activity following treatments (Lau et al., 2006; Staib et al., 2005).

In all three cell lines, the proteasome inhibitors induced high levels of caspase activity at the higher drug concentrations (10 nM bortezomib and 100 nM ixazomib) with a peak at 24 hours. At the lower drug concentrations (5 nM bortezomib and 50 nM ixazomib) caspase activity did not reach the same levels and instead the overall activity peaked at 48 hours, consistent with previous studies using bortezomib and chondrosarcoma cells (Lohberger et al., 2016). This was supported by the Annexin V-FITC, PI flow cytometry experiment (Figure 7), as the detection of apoptosis by the staining implied caspases were activated against Ewing sarcoma cells when treated with the proteasome inhibitors. As a result, it was confirmed that the treatments activated caspases and induced apoptosis *in vitro*.

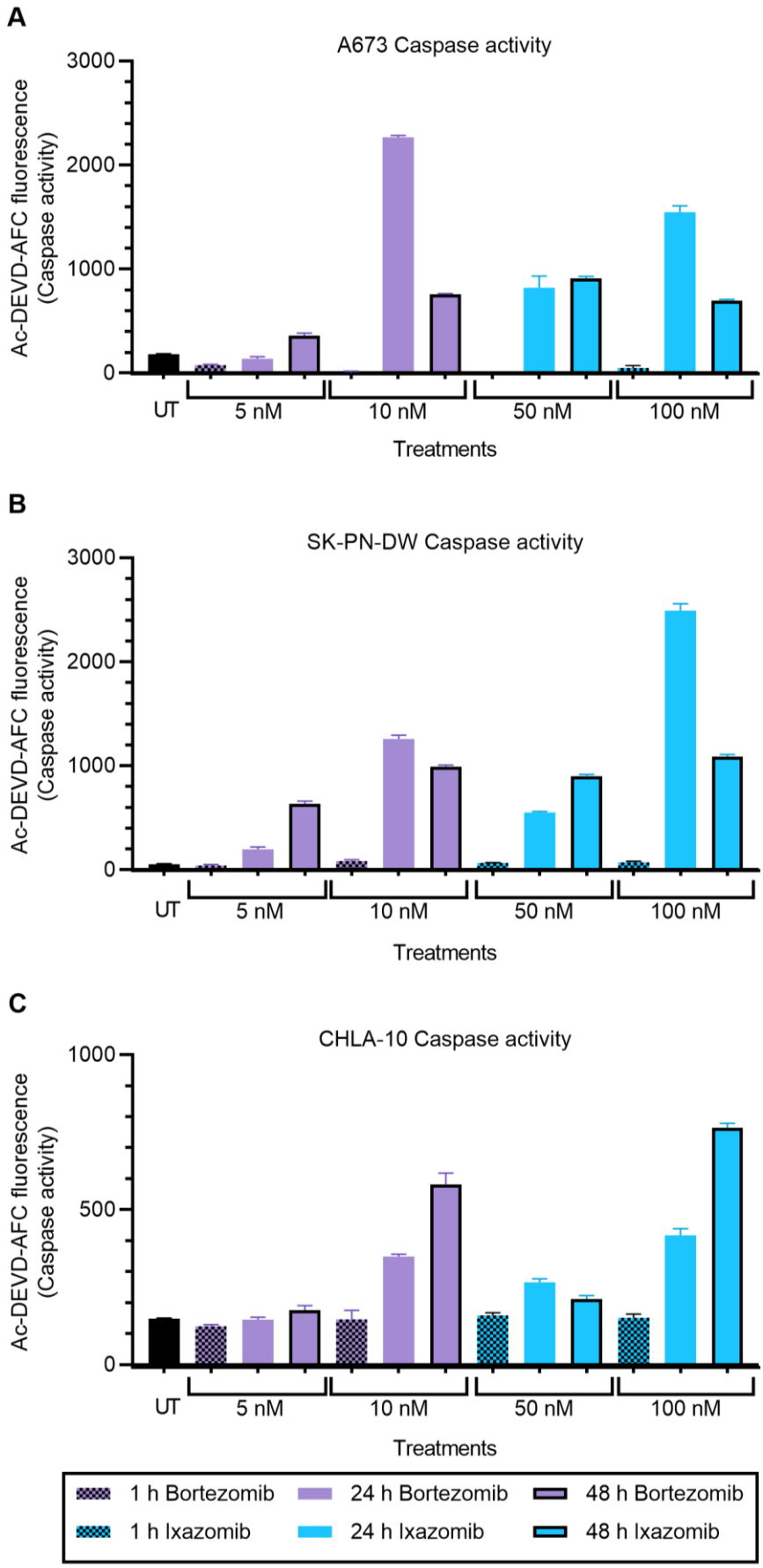

Figure 8: **Proteasome inhibitors induce high levels of caspase activity in Ewing sarcoma cells.** The Ewing sarcoma cell lines A673 (A), SK-PN-DW (B) and CHLA-10 (C) were treated with 5 and 10 nM of bortezomib and 50 and 100 nM of ixazomib for 1, 24 or 48 h (UT = Untreated cells). Caspase activity was determined over a 1 h period using the fluorogenic substrate Ac-DEVD-AFC. (n = 3, +/-SEM).

To investigate whether proteasome inhibitors induced apoptosis through causing a reduction in proteasome activity, a proteasome activity assay was conducted (Figure 9). This involved treating A673, SK-PN-DW and CHLA-10 cells with previously calculated 48 h IC_{50} (Table 4) concentrations of bortezomib, ixazomib and carfilzomib for 1, 24 and 48 hours to monitor changes in activity. The changes in proteasome activity were recorded using the fluorogenic substrate Suc-LLVY-AMC, specific for the chymotrypsin-like sites of the 26S proteasome (Kisselev & Goldberg, 2005).

With all the Ewing sarcoma cell lines, the proteasome inhibitors were able to significantly reduce proteasome activity compared to untreated cells. Also, a pattern was observed, that although proteasome activity was greatly reduced 1-hour post treatment, the levels began to return to untreated levels by 48 hours. There were statistically significant differences in the proteasome activity means at the 1-hour time point compared to 48 hours, with only A673 cells treated with ixazomib and carfilzomib not demonstrating significant recovery in activity. This finding confirmed that proteasome inhibitors were performing their role of reducing 26S proteasome activity in Ewing sarcoma cells. The vast reductions in their chymotrypsin-like sites of the 26S proteasome within Ewing sarcoma cells affected their viability, highlighting the importance of this pathway in the viability of Ewing sarcomas.

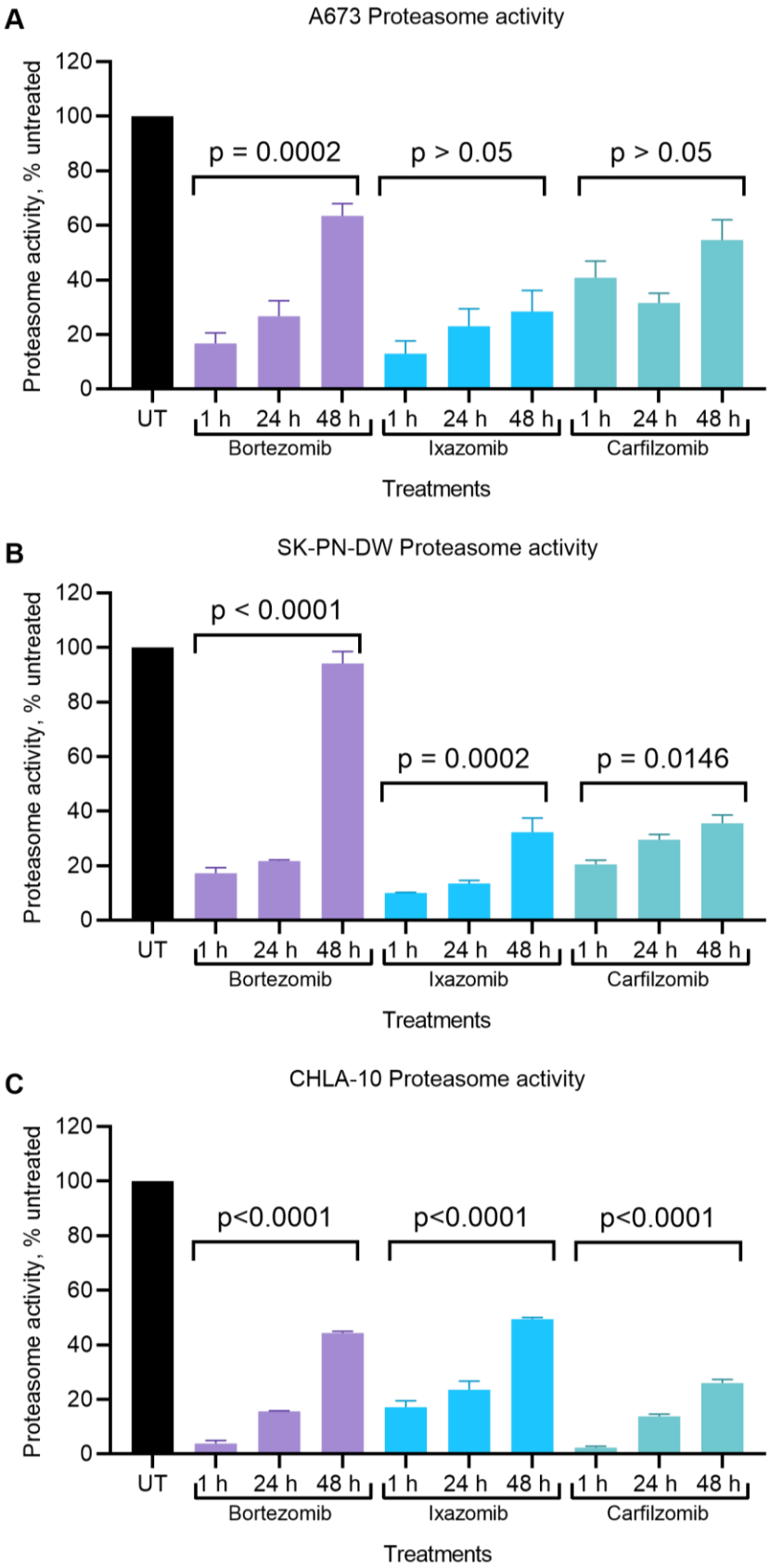

Figure 9: **Proteasome inhibitors significantly reduce proteasome activity in Ewing Sarcoma cells.** A673 (A), SK-PN-DW (B) and CHLA-10 (C) cells were incubated with the proteasome inhibitors bortezomib, ixazomib and carfilzomib at previously determined 48 h IC_{50} (adhered cell protocol) for 1, 24 and 48 h. The level of proteasome activity was determined using the substrate Suc-LLVY-AMC (n = 3, +/-SEM), compared relative to untreated cells (UT). Statistical analysis was undertaken to compare 1 h to 48 h treatment means using a One-way ANOVA with Tukey's multiple comparisons, with all p-values shown on the graph (significant $p < 0.05$, not significant $p > 0.05$).

A frequently-reported activity of proteasome inhibitors is to cause cell cycle arrest, as a result of preventing the degradation of cell cycle checkpoint inhibitors (Dou et al., 2003; Thibaudeau & Smith, 2019). Proteasome inhibitors have previously been shown to induce G2 cell cycle arrest in osteosarcoma cells (Patatsos et al., 2018) and human non-small cell lung cancer lines (Ling et al., 2003) and G1 cell cycle arrest in multiple myeloma cells (Li et al., 2020). Consequently, a cell cycle experiment was performed to observe the effect of proteasome inhibitors on the cell's DNA content and therefore their impact on the cell cycle (Figure 10). The purpose of this experiment was to determine whether proteasome inhibitors induced cell cycle arrest in A673 cells and the timeframe in which the cells could overcome this.

In this experiment A673 cells were incubated with either 5 nM of bortezomib or 30 nM of ixazomib and the changes in DNA content were determined from 8 h to 32 h post treatment using flow cytometry. Compared to untreated A673 cells, there were increases in the percentage of cells in the G2/M phase when treated with the proteasome inhibitors. This was consistent across both proteasome inhibitors used in this study. By 32 h, in both cases, the overall DNA content profile returned towards untreated levels. Although the changes were subtile, probably due to the low concentrations of drug used, these data indicate that these drugs induced G2/M cell cycle arrest.

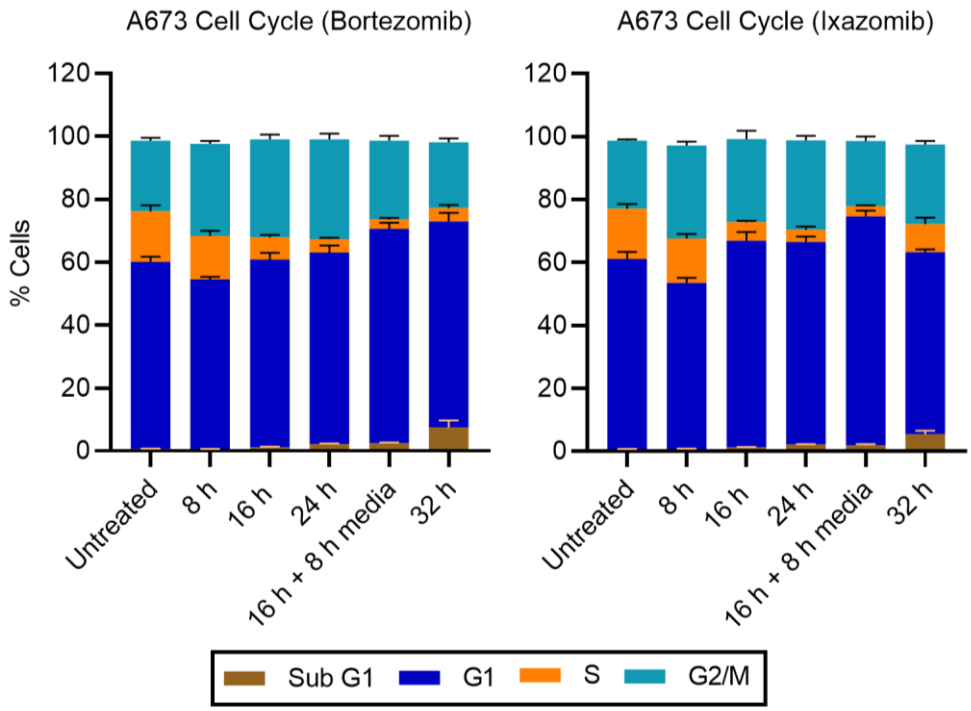

Figure 10: **Proteasome inhibitors cause G2 cell cycle arrest in A673 cells.** A673 cells were treated with either 5 nM bortezomib or 30 nM ixazomib for 8 h, 16 h, 16 h then 8h fresh media or 32 h, their DNA content was then determined via propidium iodide (PI) flow cytometry. (n = 3, +/-SEM)

An experiment was performed to determine any potential drug combinations which could be used *in vivo* for treating Ewing sarcomas. A673, SK-PN-DW and CHLA-10 cells were treated with bortezomib, or ixazomib, with doxorubicin (Figure 11) or cisplatin (Figure 12), alone and in combination to observe any potential cooperation *in vitro*, using the Chou-Talalay (CI = combination index) method (Chou, 2010). The drugs were either added together for 48 h or applied in sequential 24 h incubations. This time point of 24 h was chosen to unveil any potential drug antagonism if the cell cycle arrest caused by the proteasome inhibitors (Figure 10) impaired the toxicity of chemotherapies, which require an active cell cycle to cause cytotoxicity and cell death (Mills et al., 2018).

Treatment of Ewing sarcoma cells with a proteasome inhibitor along with doxorubicin or cisplatin in combination for 48 h yielded average CI values of around 1-1.5 indicating slight to moderate drug antagonism. Only minor synergy/additive effects were seen with SK-PN-DW cells treated with ixazomib and cisplatin (Ix+C) and CHLA-10 cells treated with

bortezomib and cisplatin (B+C). Furthermore, treating these cells sequentially with the drugs in different orders yielded differences in drug interactive effects. Overall, when the chemotherapy agents (cisplatin, doxorubicin) were added prior to the addition of the proteasome inhibitor, lower average combination index values were recorded. This finding indicated that the order of drug addition was important to avoid antagonism with these drug combinations. Unfortunately, major synergy was not observed in any cases. Before contemplating clinical application of combined chemotherapy and proteasome inhibitor drugs, mechanisms for avoiding antagonism should be explored.

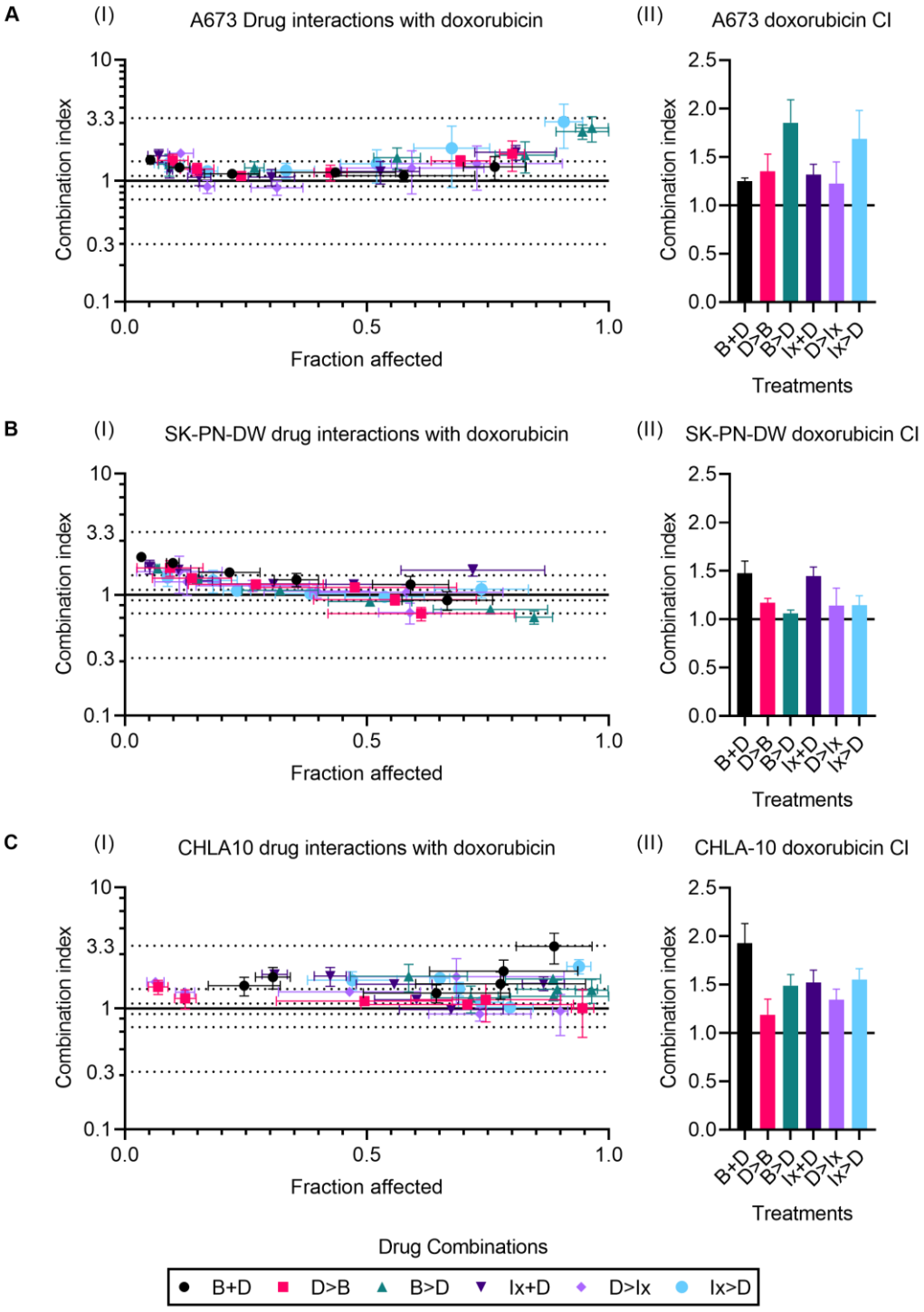

Figure 11: **The order of drug addition alters the drug interaction effect on Ewing sarcoma cells between proteasome inhibitors and doxorubicin.** A673 (A), SK-PN-DW (B) and CHLA-10 (C) cells were treated with the previously calculated 48 h IC_{50} for adhered cells. The cells were treated either with bortezomib and doxorubicin together for 48 h (B+D), doxorubicin for 24 h, then bortezomib for 24 h (D>B) or bortezomib for 24 h then doxorubicin for 24 h (B>D). The same was also achieved for the ixazomib and doxorubicin combination. The viability was quantitated comparing ATP levels using a CellTiter-Glo assay. The combination indices (CI) from each treatment were calculated using the Chou-Talalay method using CompuSyn (n = 3, +/-SEM). Strong antagonism CI>3.3, antagonism 1.45<CI<3.3, slight/moderate antagonism 1.1<CI<1.45, approximately additive 0.9<CI<1.1, slight/moderate synergy 0.7<CI<0.9), synergy 0.3<CI<0.7, strong/very strong synergy CI<0.3. The fraction affected denotes the fraction of cells which have been killed due to the treatment. (II) The average combination index (CI) was also graphed to compare between drug combinations. Overall CI > 1 denotes antagonism, CI = 1 signifies an additive effect (identified by solid line at CI = 1) and CI < 1 denotes synergy.

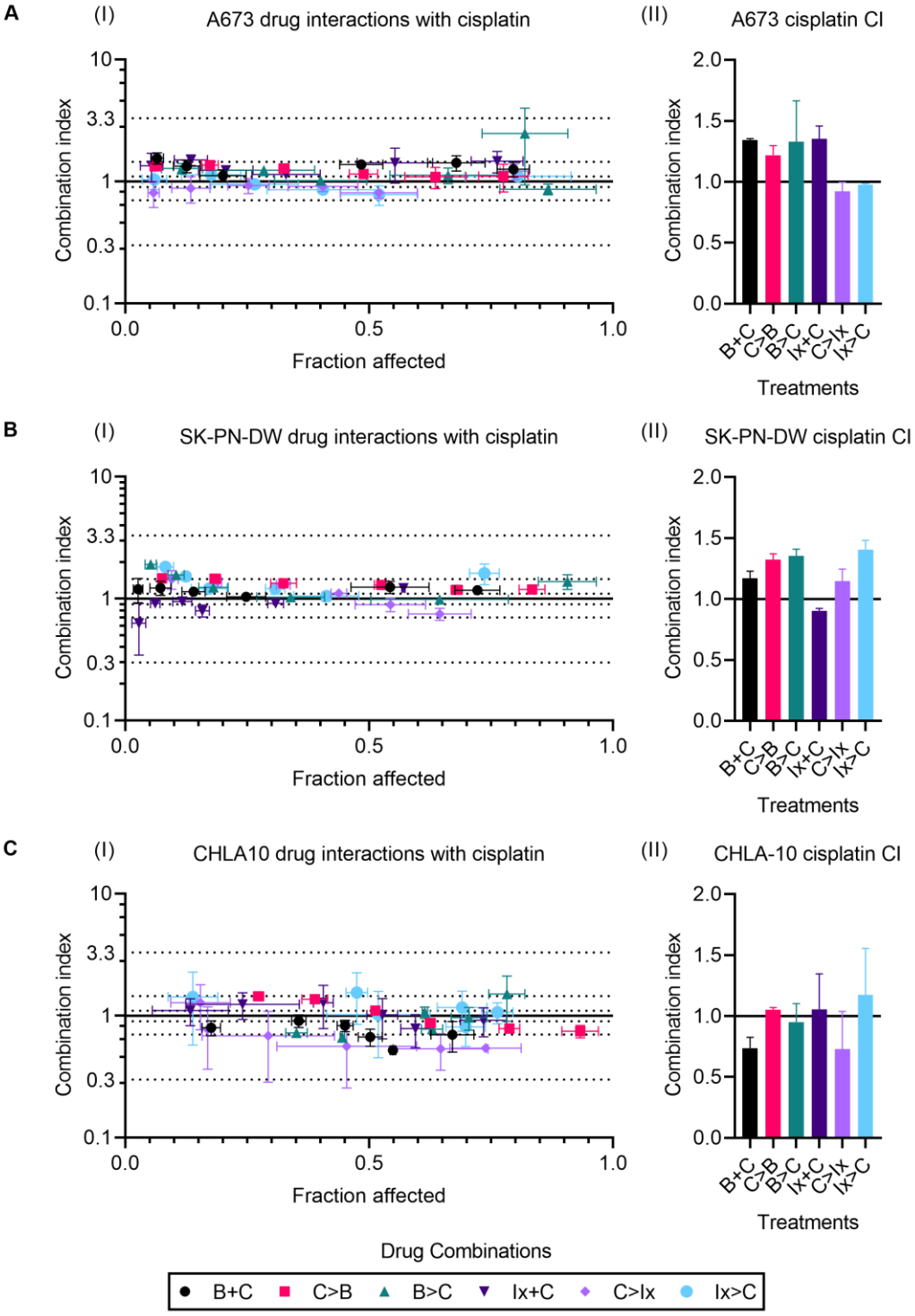

Figure 12: **The order of drug addition alters the drug interaction effect on Ewing sarcoma cells between proteasome inhibitors and cisplatin.** A673 (A), SK-PN-DW (B) and CHLA-10 (C) cells were treated with the previously calculated 48 h IC_{50} for adhered cells. The cells were treated either with bortezomib and cisplatin together for 48 h (B+C), cisplatin for 24 h, then bortezomib for 24 h (C>B) or bortezomib for 24 h then cisplatin for 24 h (B>C). The same was also achieved for the ixazomib and doxorubicin combination. The viability was quantitated comparing ATP levels using a CellTiter-Glo assay. The combination indices (CI) from each treatment were calculated using the Chou-Talalay method using CompuSyn (n = 3, +/-SEM). Strong antagonism CI>3.3, antagonism 1.45<CI<3.3, slight/moderate antagonism 1.1<CI<1.45, approximately additive 0.9<CI<1.1, slight/moderate synergy 0.7<CI<0.9), synergy 0.3<CI<0.7, strong/very strong synergy CI<0.3. The fraction affected denotes the fraction of cells which were killed due to the treatment. (II) The average combination index (CI) was also graphed to compare between drug combinations. Overall CI > 1 denotes antagonism, CI = 1 signifies an additive effect (identified by solid line at CI = 1) and CI < 1 denotes synergy.

3.2 Lentiviral infection of A673

The *in vitro* sensitivity of Ewing sarcoma cells toward proteasome inhibitors justified testing their efficacy in an *in vivo* setting, using mice implanted with Ewing sarcoma cells. The A673 cell line was chosen over the other Ewing sarcoma lines as it was previously published to be tumourigenic in BALB/c nude mice (Rouleau et al., 2015), whilst being sensitive to bortezomib and ixazomib *in vitro* (Figures 4, 5, 6). A673 cells were virally infected to express luciferase by the candidate and cell-sorted with the help of Dr Tanmay Shekhar (Figure 13). The purpose of tagging these cells was to provide a means of detecting and quantifying tumour burden via bioluminescent imaging, which is a more sensitive and accurate measure of tumour burden than using callipers. This would also provide a way of detecting and monitoring any metastasis in the mice and evaluating the effects of treatments on the primary and metastatic disease. The cells were transduced with a virus encoding luciferase and mCherry (pMSC-mCherry-luc-IRES). The levels of mCherry positive cells (which were deemed to have been successfully transduced) were compared in the infected verses untreated A673 samples (Figure 13). This flow cytometry plot confirmed a successful, although very inefficient infection of the A673 cell line, when comparing mCherry intensity in the A673 cells to OSCA40 luc-2 (Appendix 2). Single cells were then sorted based on their mCherry fluorescence into a 96 well plate, to derive monoclonal populations (Figure 13C).

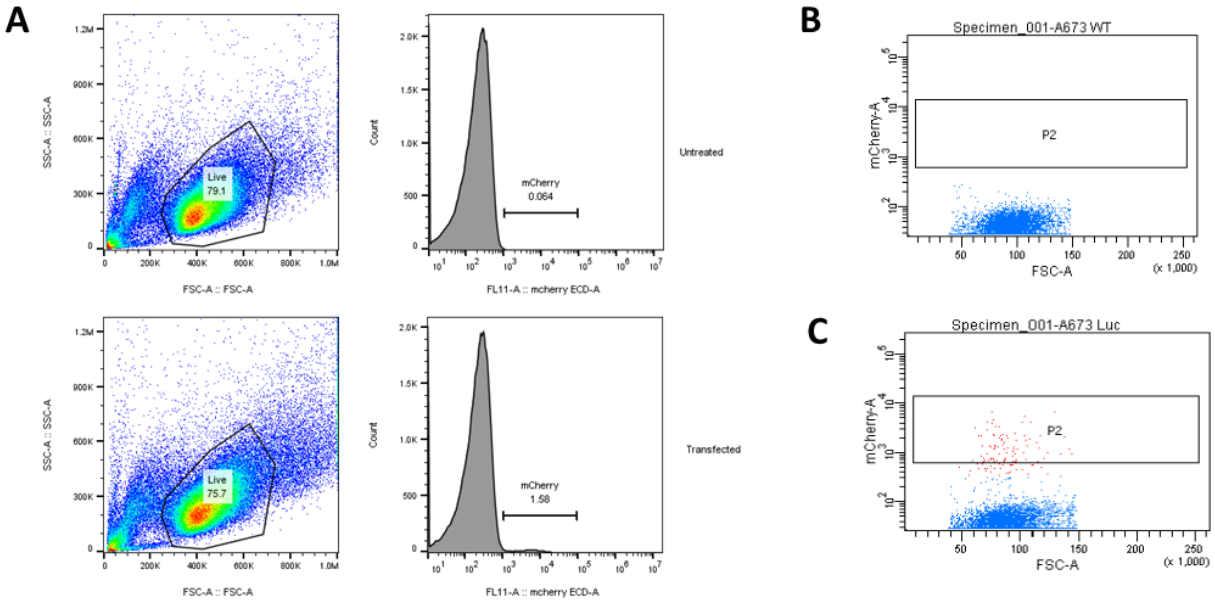

Figure 13: **Lentiviral infection of A673 cells using Luciferase-mCherry plasmid.** (A) After the infection, the percentage of mCherry positive cells was determined via flow cytometry compared to the untreated A673 parental cells. The cells were single cell sorted into monoclonal populations by comparing mCherry fluorescence between the parental A673 (B) and the infected A673 cells (C).

Once sorted, the mCherry-positive monoclonal populations were cultured and expanded to generate clones. To select an appropriate A673 expressing subclone for *in vivo* implantation, four clones that exhibited normal morphology and growth rates were tested for sensitivity towards bortezomib and ixazomib (Figure 14A). This was performed to select a clone which had comparable sensitivity to the parental cells for *in vivo* use. The four transduced clones as well as the polyclonal population all had similar sensitivity to the parental A673 cell line after 24 h incubations with varying doses of bortezomib and ixazomib.

The luciferase activity of each clone was determined after an incubation with D-luciferin, with immediate detection of the luminescence emitted (Figure 14B). D-luciferin is converted via the luciferase enzyme with oxygen into 1,2-dioxetane, which is unstable and decays emitting one photon of light per second (Baklaushev et al., 2017). Although these monoclonal populations were selected from mCherry positive cells (indicating cells had undergone a successful infection), none of the cell lines except the positive control (OSCA-

40 luc-2) expressed any detectable luminescence after a D-luciferin incubation. Therefore, the transduced clones could not be used for bio-luminescence imaging in an *in vivo* setting to monitor primary tumour growth/regression or detect metastasis.

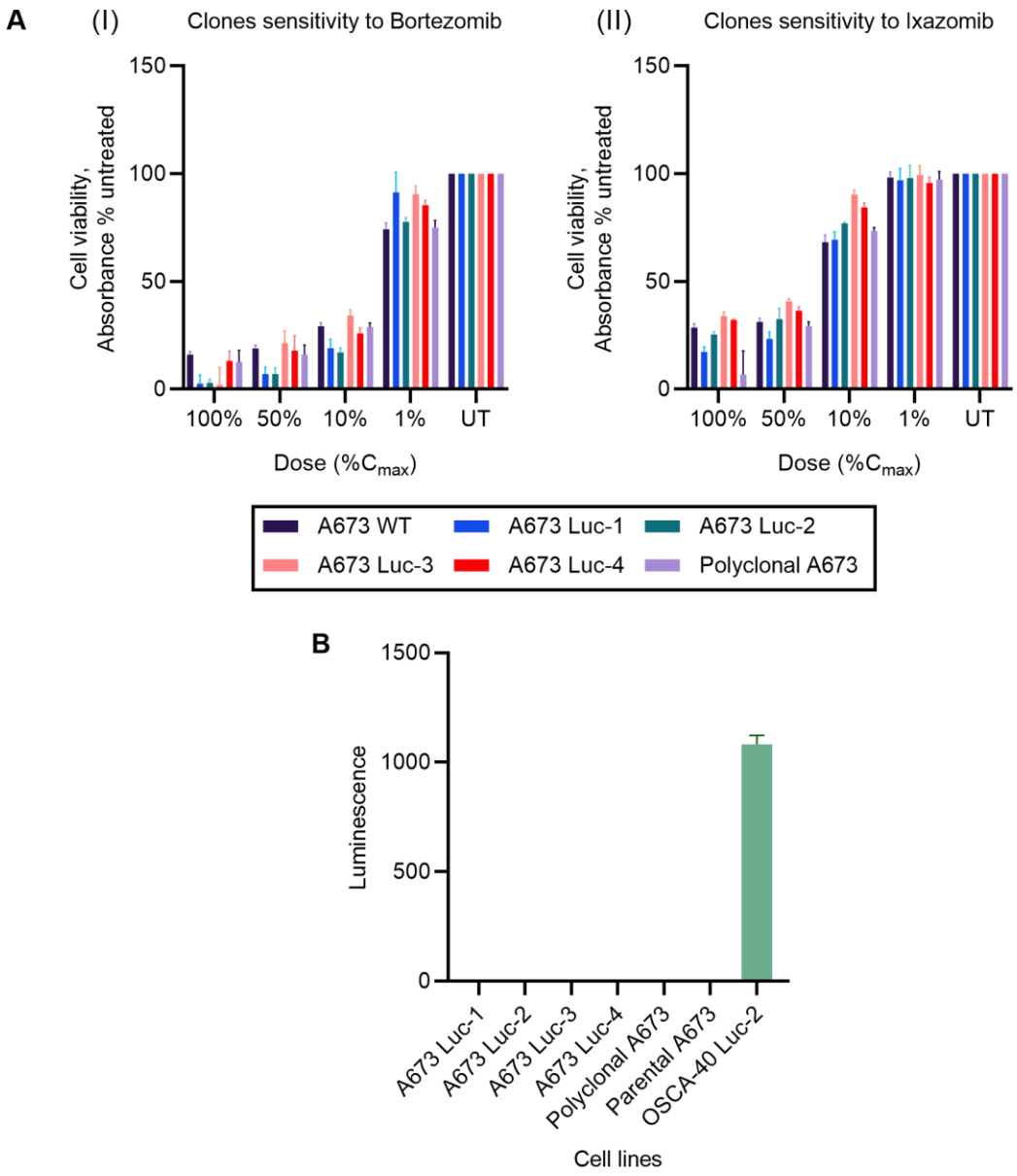

Figure 14: **Luciferase clones have similar drug sensitivity (cell metabolic activity) profiles to the parental A673 cells but lack luciferase activity.** (A) Four monoclonal populations as well as the polyclonal A673 populations were numbered and incubated with either bortezomib (AI) or ixazomib (AII) for 24 h and their residual metabolic activity was determined via an MTT assay (n=3, +/- SEM). The concentrations of drug used were increments of the drugs C_{max} (580 nM for bortezomib and 300 nM for ixazomib) and all the calculated cell metabolism was compared relative to the untreated sample. (B) The clones were then incubated with D-luciferin and emitted luminescence was measured immediately (n=3, +/- SEM).

No luciferase activity was detected in the subclones (Figure 14B) that emitted low mCherry fluorescence (Appendix 2), so the next step was to test whether the luciferase gene was present in the cell lines. Using PCR and three sets of primers specific for the luciferase gene, it was identified that clone A673 Luc-4 contained the luciferase gene (Figure 15). Using the parental A673 and virally transduced KRIB cells as negative and positive controls respectively, the most specific primer set with minimal non-specific binding was determined to be primer set 1976 and 1977. To detect the presence of the luciferase gene, four separate samples of DNA were extracted from each luciferase sub-clone and treated as separate templates in PCR reactions and run on a gel (Figure 16). The PCR results suggested that sub-clones 1, 2 and 4 contained the luciferase gene. Although the lower intensity of the product formed in the reaction using genomic DNA from the A673 clones suggested a lower viral insertion copy number than in the positive control cell line KRIB luc-4 (Shekhar et al., 2019). Possible mechanisms that could account for the presence of luciferase DNA but not enzymatic activity in the virally-transduced A673 clones are presented in section 4.2.1. While the cells could not be detected via luminescence *in vivo*, this PCR finding indicated that the transduced clones could be useful, as tumour burden could be quantitated in organs of tumour-bearing mice after culling using luciferase-specific PCR.

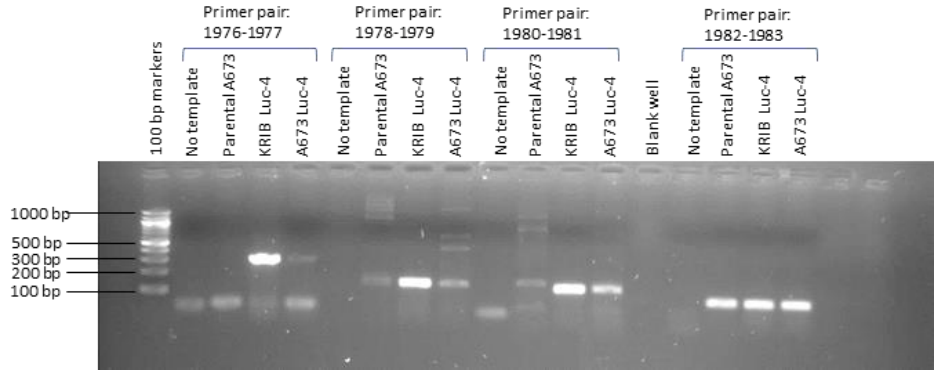

Figure 15: **The most specific luciferase primer set for A673 Luc-4 is 1976-1977.** Luciferase primers 1976-1977, 1978-1979 and 1980-1981 were tested for specificity against subclone A673 Luc-4. The vimentin primers 1982-1983 were used as loading control. Parental A673 was used as a negative control and KRIB Luc-4 as a positive control. Each PCR reaction used 100 ng of genomic DNA as a template and was loaded on a 1.8% agarose gel.

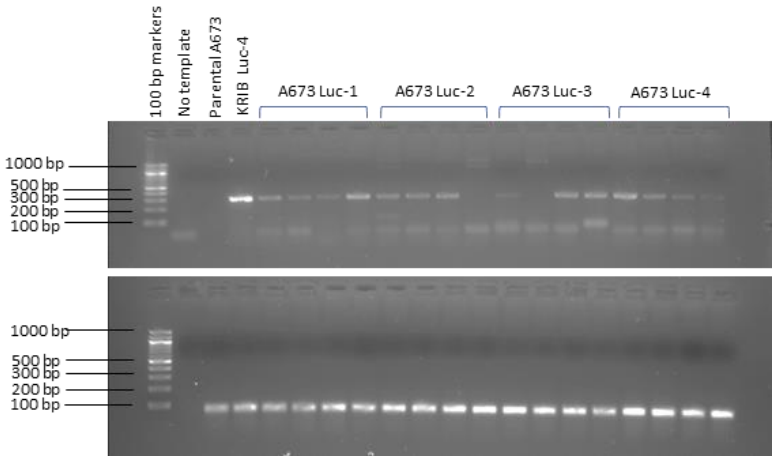

Figure 16: **PCR confirmation that A673 sub clones contain luciferase gene.** The top gel used the luciferase primer set 1976 and 1977 and bottom gel used vimentin control primer set 1982-83. Four individual samples of DNA from each subclone underwent separate PCR reactions, using 100 ng of genomic DNA as templates, and were run on a 1.8% agarose gel.

3.3 Tumourigenicity of A673 cells in BALB/c nude mice

Although no luciferase expression was detected from the subclones, the presence of the luciferase gene (which may facilitate PCR-based quantitation of tumour burden) made those derivatives preferable, compared to the parental cells, for a tumourigenicity experiment. Based on sensitivity and cell morphology, A673 Luc-4 was chosen to develop a BALB/c nu/nu Ewing sarcoma mouse model. Previous Ewing sarcoma studies in nude mice have used subcutaneous implantation (Stolte et al., 2018) but the muscle is a more relevant site for Ewing tumours as the A673 cell line originated from a muscle tumour (Giard et al., 1973). After *tibialis anterior* implantation, all mice had detectable primary tumours by day 14, measured using callipers (Figure 17A). At the endpoint (day 28), all mice had similar sized primary tumours (Figure 17A). With the assistance of Michael Harris, a Hematoxylin & Eosin stained section of each primary A673 tumour revealed invasion of the muscle by A673 tumour tissue (Figure 17B).

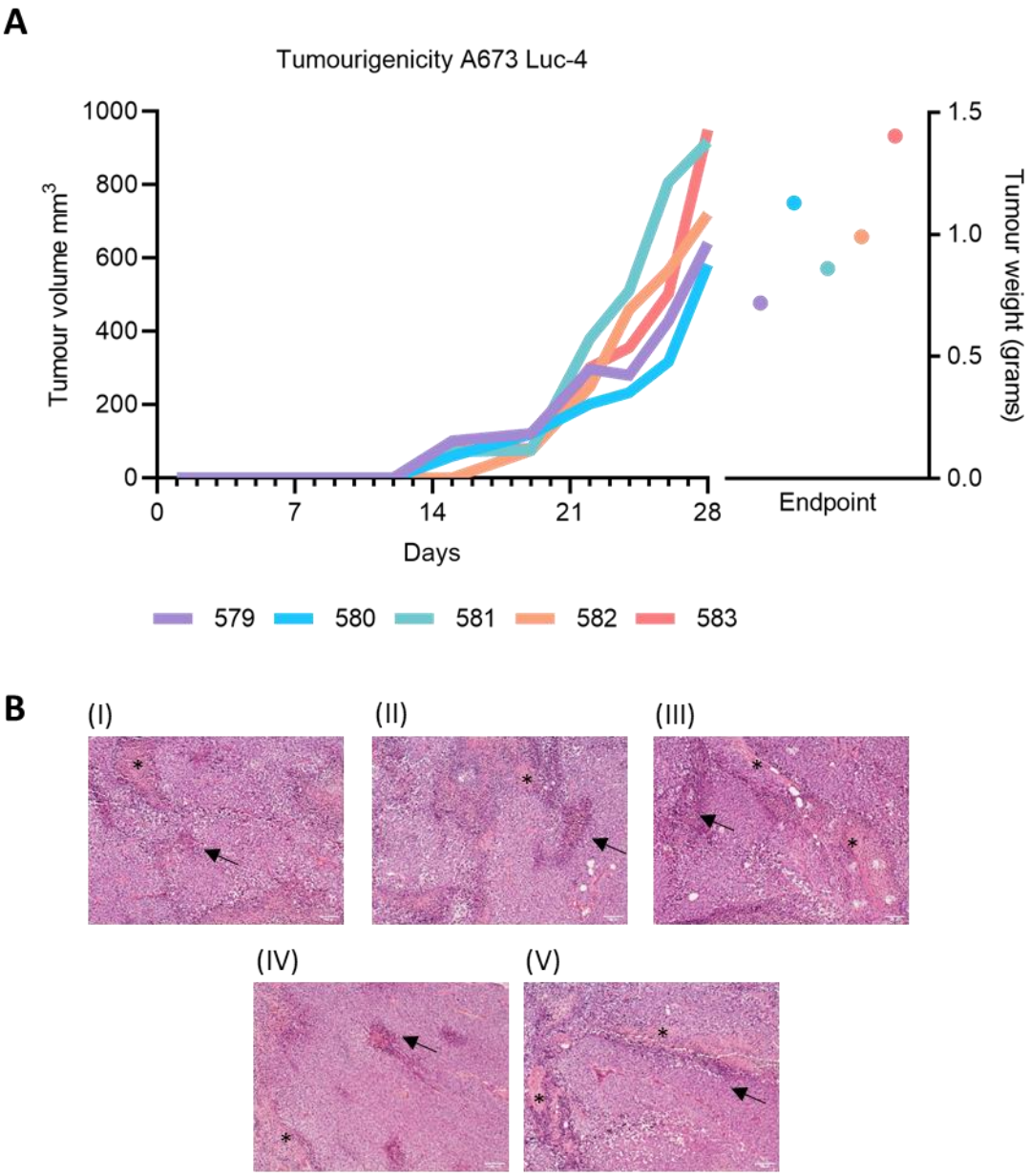

Figure 17: **A673 cells are tumourigenic in BALB/c nude mice.** (A) 50,000 A673 Luc-4 cells were implanted intramuscularly into the *tibialis anterior* leg muscle of five nude mice and the tumour size was measured by callipers over a four-week period. At the endpoint of the experiment the primary tumours from each mouse were weighed. (B) The primary tumour from each mouse (I: mouse 579, II: mouse 580, III mouse 581, IV: mouse 582, V: mouse 583) underwent H & E Staining, tumour cells (arrow), muscle tissue (asterisk). (Scale = 100 µm). The tissue for staining was processed by Michael Harris and the photos were taken by Carmelo Cerra.

3.4 Efficacy of bortezomib and ixazomib against primary Ewing sarcoma

Based on successful tumourigenicity data, nude mice were implanted with A673 Luc-4 cells into the *tibialis anterior* and separated into three equivalent treatment groups once tumours were detected by eye (Figure 18). The doses of bortezomib and ixazomib had been previously established by Dr Tanmay Shekhar (in the Hawkins laboratory) to be tolerated by nude mice. Mice were treated with saline (Figure 18A) or the maximum tolerated doses of bortezomib (1 mg/kg, twice weekly) (Figure 18B), or ixazomib (5 mg/kg, twice weekly) (Figure 18C). The intent was to treat them twice weekly for four weeks, but due to the aggressive nature of the tumours none of the mice survived to this point.

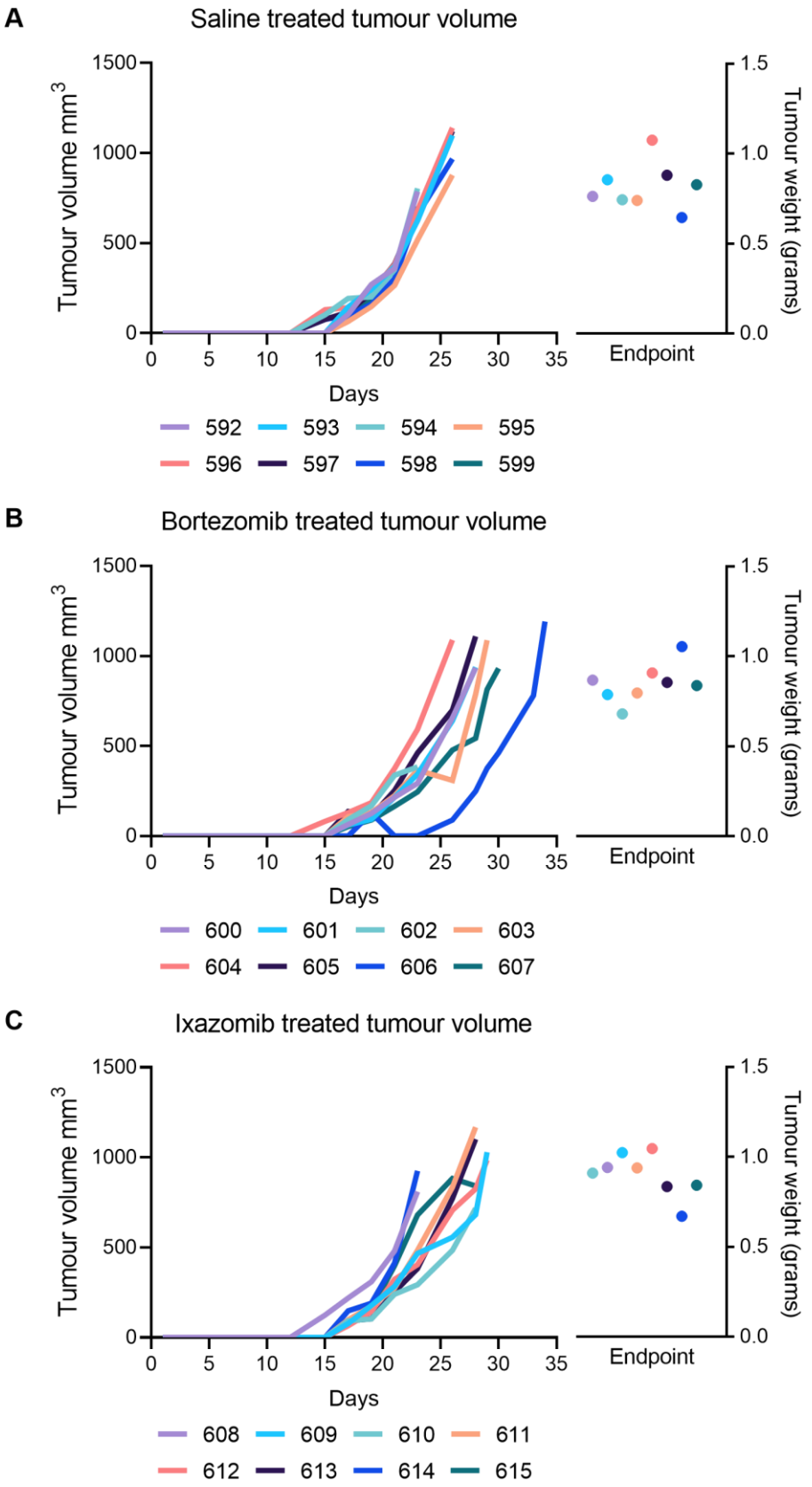

Figure 18: **Bortezomib and ixazomib reduced A673 primary tumour size and progression.** BALB/c nude mice were implanted with 50,000 A673 Luc-4 cells intramuscularly into the *tibialis anterior* and were randomised into groups of eight once the tumour was detected (n = 8). From detection they were treated twice weekly with either saline (A), bortezomib (B) or ixazomib (C), with the endpoint primary tumour weight of each mouse also shown.

On average, mice treated with the proteasome inhibitors bortezomib and ixazomib had reduced primary tumour growth compared to the saline treatment group (Figure 19A). From days 15 to 23, bortezomib was able to significantly reduce primary tumour volumes compared to the saline treatment group ($p = 0.0018$), with no significant differences identified between ixazomib and saline ($p= 0.5209$). The bortezomib-treated mice also survived significantly longer ($p = 0.0112$) than the saline treated mice (Figure 19B). To a lesser extent this was also the case for the mice treated with ixazomib compared to saline ($p = 0.0246$). Similarly, by day 26 all saline treated mice were culled, whereas all ixazomib treated mice were culled by day 29 and bortezomib mice by day 34. These data support the *in vitro* data that the A673 cells are sensitive to proteasome inhibitors. Although statistically significant, the magnitude of the effect of these drugs would not be expected to translate into a clinical response.

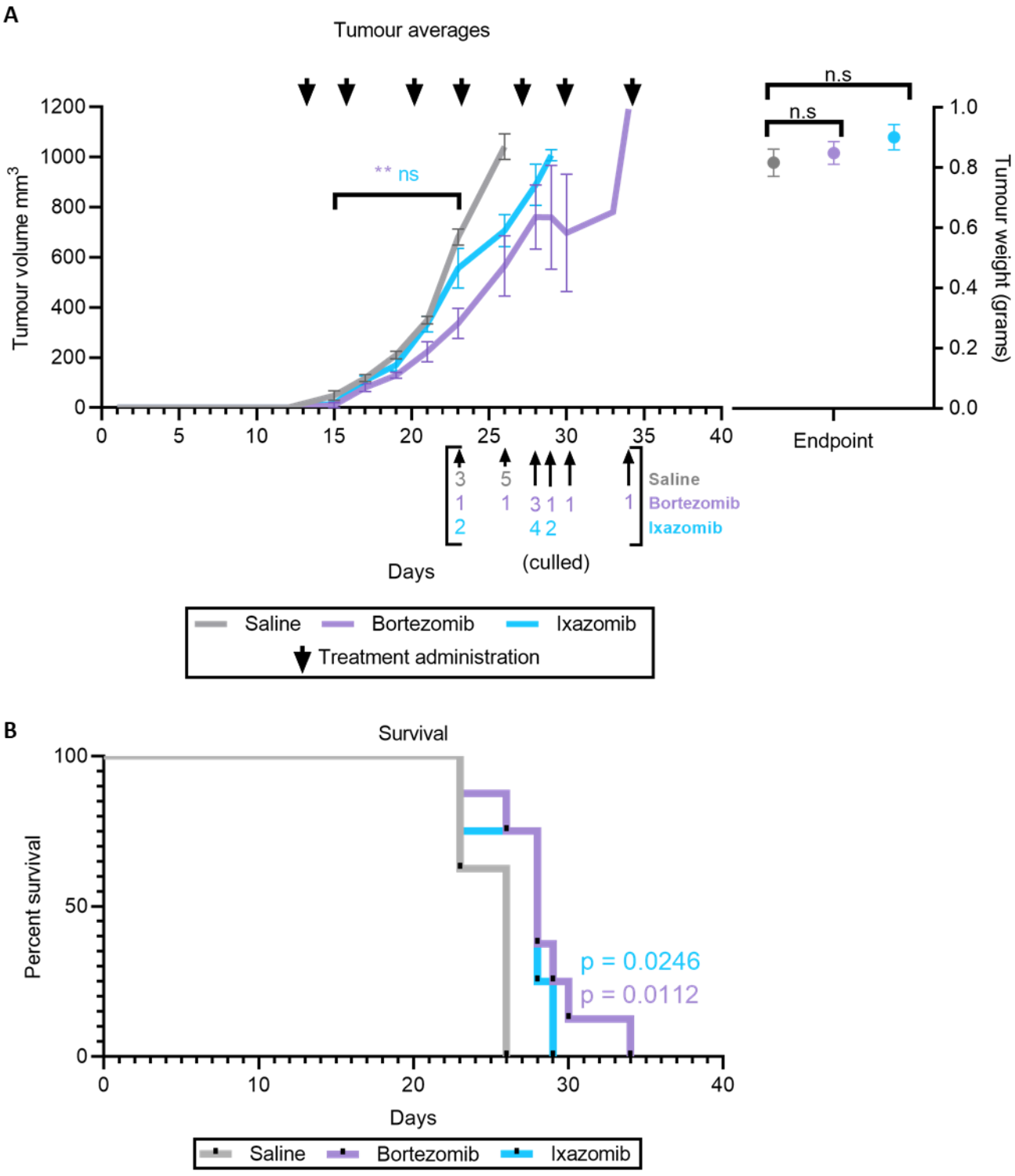

Figure 19: **Bortezomib and ixazomib prolong survival of BALB/c nude mice bearing primary A673 tumours.** Mice were implanted with A673 Luc-4 cells and treated twice weekly until the endpoint. (A) The average tumour volume was measured via callipers for mice treated with either saline, bortezomib or ixazomib as well as the average tumour weight at the endpoint of the experiment (n = 8). The black arrows indicate treatment days, whilst the colour coded numbers below the x-axis shows the number of mice from each treatment group that were culled on each day. A one-way ANOVA with Sidak's post-tests, identified a significant difference in tumour volume from day 15 to 23 between saline and bortezomib treated mice **(p = 0.0018) and no significant difference with ixazomib treated mice (p = 0.5209). A one-way ANOVA with Dunnett's multiple comparisons identified no significant differences in average endpoint tumour weight (saline vs. bortezomib p = 0.8123, saline vs ixazomib p = 0.2820). (B) The survival curve for all mice included in this efficacy experiment, Mantel-Cox test with Bonferroni correction for multiple comparisons (2) was used to compare survival rate of the different treatment groups, *saline vs ixazomib (p = 0.0246), **saline vs bortezomib (p = 0.0112).

3.5 *Ex vivo* sensitivity

The primary A673 tumours were removed from the mice and a small section was used for *ex vivo* sensitivity analysis (Figure 20) to determine whether their sensitivity changed to bortezomib or ixazomib after *in vivo* growth and/or drug exposure. If this was the case it could provide a reason for limited efficacy seen *in vivo* even though the cells were sensitive to proteasome inhibitors *in vitro*. Tumour cells from the saline, bortezomib and ixazomib treated mice were separately incubated for 24 h with the IC_{50} (Table 3) concentrations of bortezomib or ixazomib for A673 cells. Some tumours became significantly more resistant to the proteasome inhibitors, although drug exposure *in vivo* did not impact on the tumour's sensitivity to these proteasome inhibitors. Note that mouse 592 was not analysed in this section due to contamination during the tissue processing for cell culturing. This indicated that changes in drug sensitivity because of *in vivo* growth may be one small aspect as to differences seen in drug sensitivity of Ewing sarcoma cells *in vivo* compared to *in vitro*.

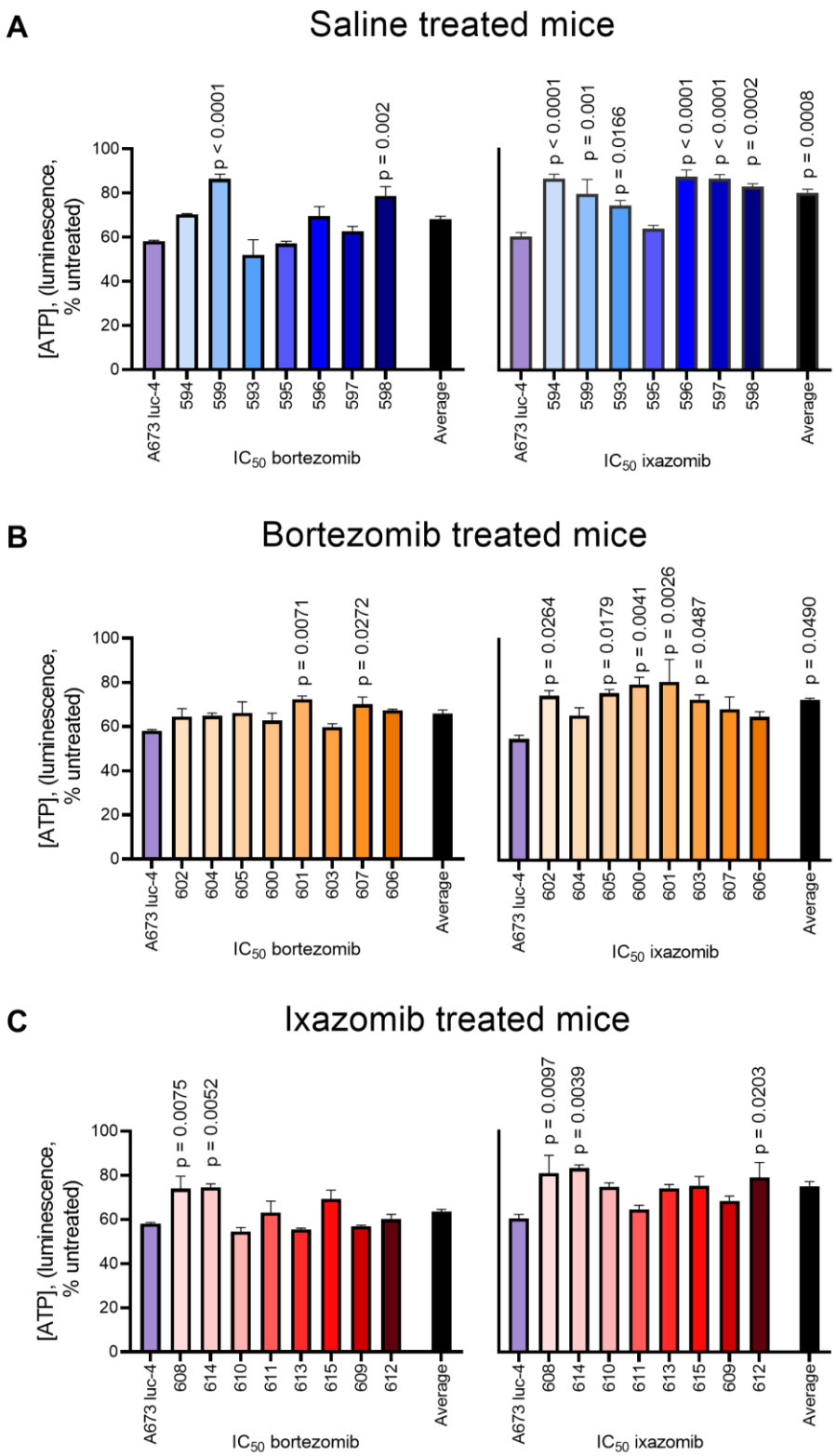

Figure 20: ***Ex vivo* Ewing sarcoma sensitivity**. All primary tumours (except 592) from efficacy experimental groups saline (A), bortezomib (B), ixazomib (C) were cultured *ex vivo* and treated for 24 h with previously calculated IC_{50} (non-adhered IC_{50}) of either bortezomib (9.17 nM) or ixazomib (43.7 nM). The sensitivity was compared to A673 Luc-4 which was initially implanted in the mice to generate tumours via CellTiter-Glo (n = 3, +/- SEM). Averages for each group were also calculated and mouse samples were ordered from earliest culled to last culled, from left to right respectively. The average in each group is shown on the right of each graph in black. A one-way ANOVA with Dunnett's multiple comparisons was used to compare the sensitivity of each separate tumour sample (technical replicates) and average (biological replicates) to the sensitivity of A673 Luc-4. Significant p values were shown above the bar graphs, the bars without any p values were determined to be not significant compared to A673 Luc-4 sensitivity.

3.6 Primary Ewing sarcoma Haematoxylin & Eosin staining

Tumour samples from the primary A673 mouse efficacy experiment were stained with Haematoxylin and Eosin to further analyse their tumour anatomy (Figure 21). These slides revealed the invasiveness of the A673 tumour (purple) within the smooth muscle (pink) as shown in four independent tumour samples. This finding also confirmed that the Ewing sarcoma cells were implanted correctly in the mice as they grew primarily within the mouse's leg muscle. Other H & E stained images of primary tumours are in appendix 5.

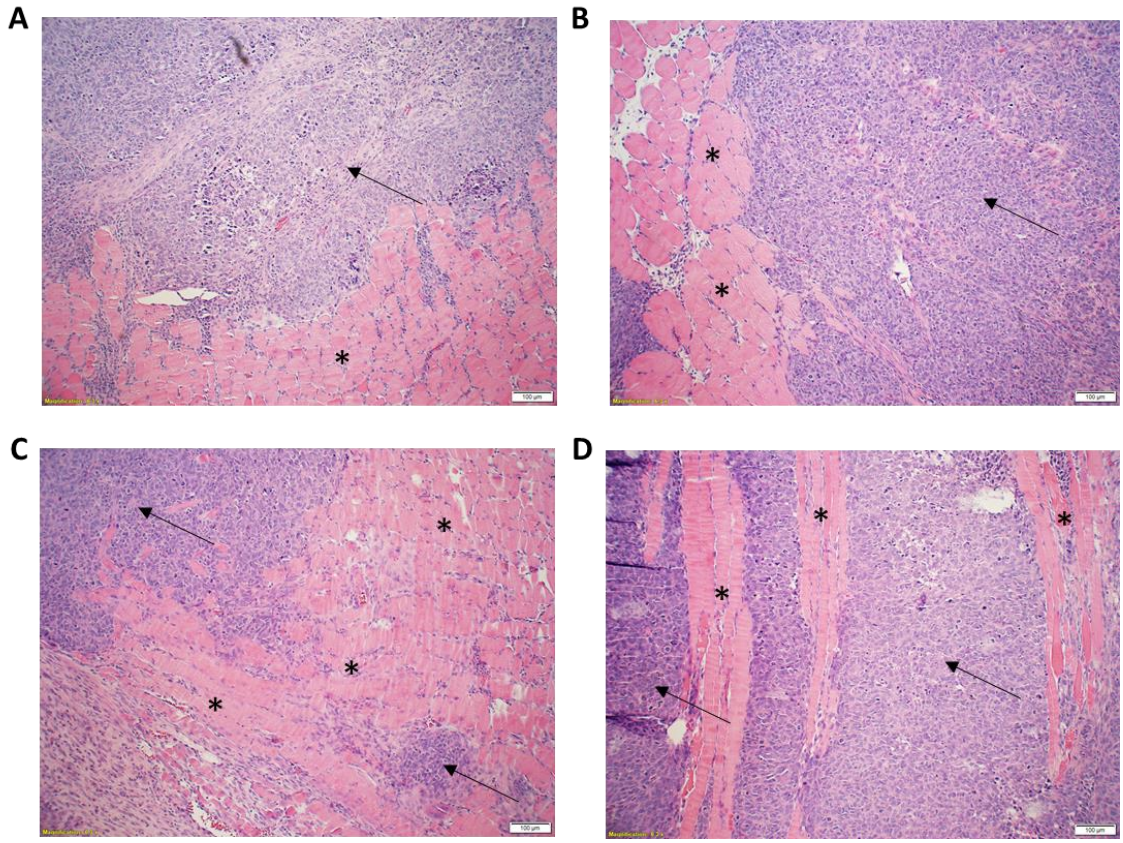

Figure 21: **Primary A673 invasiveness in smooth muscle**. Primary tumour samples were stained under H & E with tumour tissue in purple (arrow) and muscle tissue shown in pink (asterisk) with a selection from four independent mice to analyse tumour anatomy. A cross section of (A) mouse # 592 (saline treated), (B) mouse #595 (saline treated), (C) mouse #613 (ixazomib treated) and (D) mouse #604 (bortezomib treated) were used. (scale = 100 µm). The tissue was sectioned and stained by Michael Harris and the photos were taken by Carmelo Cerra.

The lungs of the tumour-bearing mice then underwent H & E staining as a way of identifying any potential metastasis (Figure 22). The lungs were chosen as they were identified in patients as being one of the most common metastatic sites for Ewing sarcoma (Chen et al., 2014). In previous Ewing mouse models the subcutaneous implantation of A673 cells provoked metastasis to the lungs (Ambati et al., 2014) but no prior data has shown this from an intramuscular implantation. This staining revealed that intramuscular A673 Ewing sarcoma tumours were able to metastasise to the lungs, allowing the establishment of a metastatic Ewing sarcoma mouse model. Unfortunately, time did not permit a comparison of any potential lung metastasis between treatment groups.

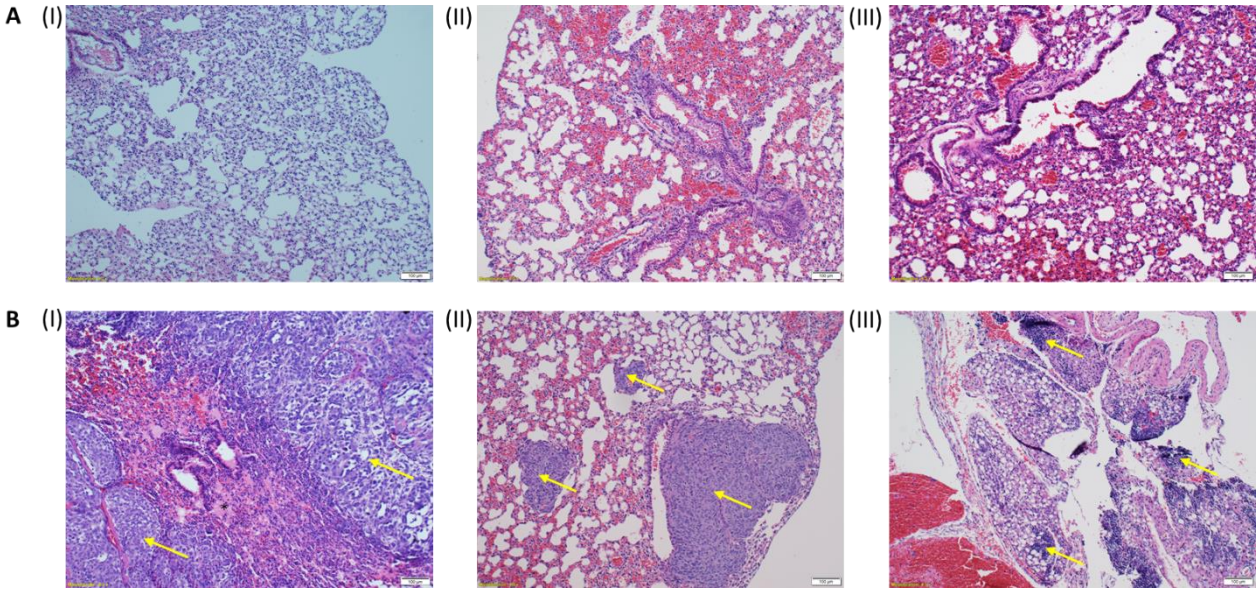

Figure 22: **Pulmonary metastasis in A673 tumour bearing mice.** Lungs were removed from mice in the primary efficacy experiment and stained with H & E. Panel A shows three healthy mouse lung tissues and panel B shows three mouse lungs (I: #581 (from tumourigenicity and was untreated), II: #604 (efficacy- bortezomib treated), III: #596 (efficacy-saline treated) with A673 tumour metastasis (identified with yellow arrow). (Scale = 100 µm). The tissue was sectioned and stained by Michael Harris and the photos were taken by Carmelo Cerra.

3.7 A673 stable transfection (tomato/luciferase plasmid)

To generate a metastatic mouse model and observe the spread of Ewing sarcoma cells in live nude mice, a non-viral method was used to enforce luciferase expression in A673 cells. It seemed possible that viral elements may have led to silencing of the reporter genes using the retroviral vector employed in the previous model. A673 cells were stably transfected with the pcDNA3.1(+)/Luc2=tdT plasmid (Figure 23). A 4 h incubation with the Lipofectamine 2000 and plasmid solution generated around 15% tomato positive (successfully transiently-transfected) cells which was determined as being the ideal transfection conditions for this cell line and plasmid (Figure 23A). Using this condition, transfected cells were then single cell sorted via flow cytometry (FACSAria) based on their fluorescence in the PE channel for tomato fluorescence (Figure 23B). The flow cytometry sorting was undertaken by Dr Margaret Veale, part of the Bioimaging platform at La Trobe University. A polyclonal population was also generated, which was analysed weeks later to ensure that all single cells selected via flow cytometry contained the plasmid of interest. The analysis of this population (A673 Luc-polyclonal-1) only detected 1.14% tomato positive cells (Figure 23C). Consequently, the flow cytometry sorting to generate clonal A673 luciferase/tomato populations was deemed unsuccessful and other means of sorting were explored to achieve clonal populations.

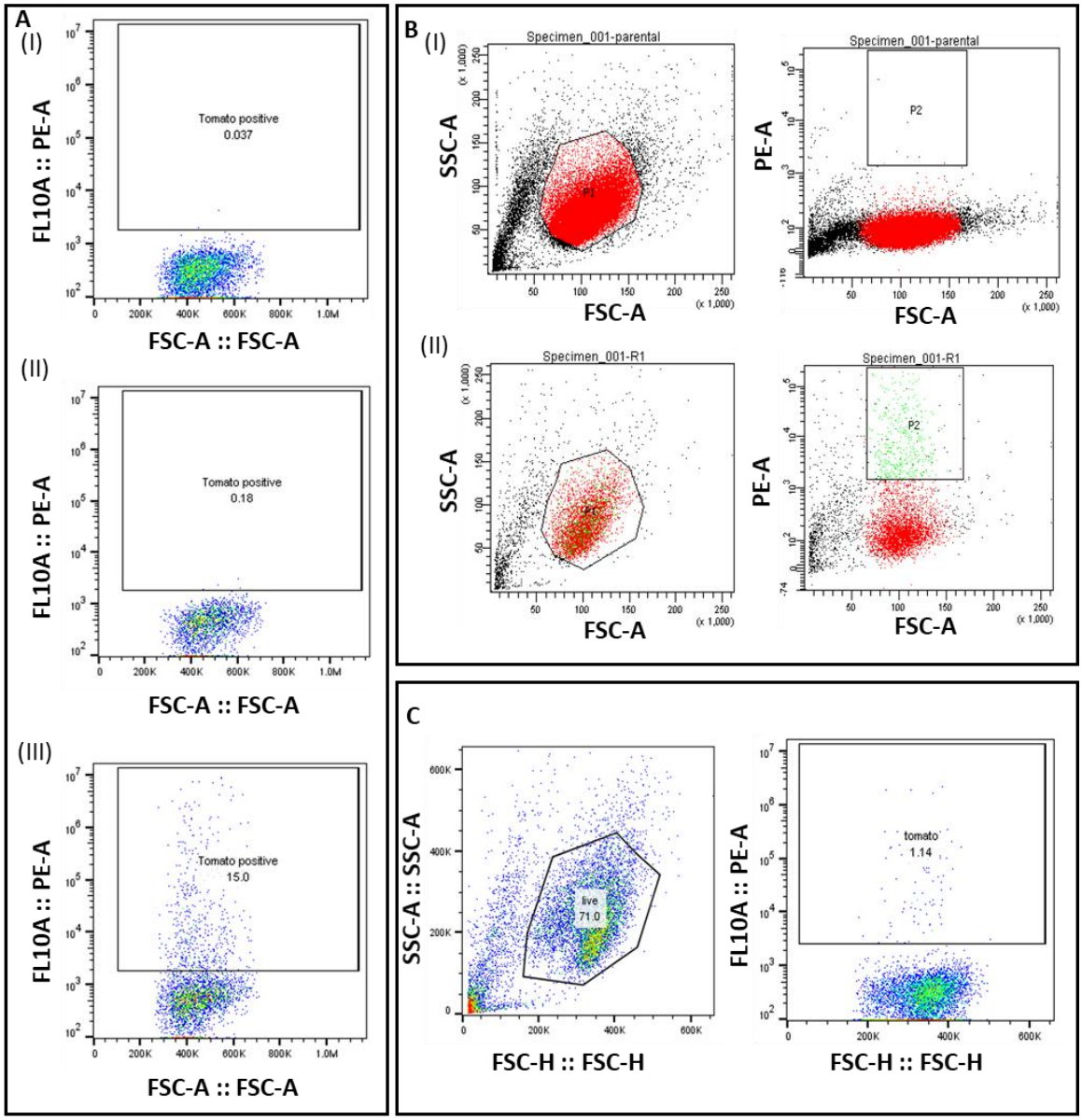

Figure 23: **A673 Stable transfection analysis using the pcDNA3.1(+)/Luc2=tdT plasmid**. (A) A673 cells were transfected with the tdTomato plasmid and levels of tomato fluorescence were compared between A673 parentals (I), A673 cells transfected with pEF plasmid (II) and A673 cells transfected for 4 h with pcDNA3.1(+)/Luc2=tdT plasmid (III). (B) The cells were then sorted using the FACSAria with both parental (I) and A673 cells (4 h transfection) (II) with cells gated for tomato fluorescence using the PE channel. (C) A673 luciferase/tomato polyclonal (A673 Luc-polyclonal-1) cells were then analysed on the FACS CytoFLEX using the PE channel for tomato fluorescence.

A smaller polyclonal population (A673 Luc-polyclonal-2) which was also sorted via the flow cytometry method described above (Figure 23) was later deemed to contain a greater frequency of tomato positive cells than the initial A673 Luc-polyclonal-1 population (Appendix 7). This population was used to generate A673 clonal populations via limiting dilution (Fuller et al., 2001; Gross et al., 2015), with clones denoted A673 Luc1L, A673 Luc2L etc. Other clones were generated via transfecting A673 parental cells with pcDNA3.1(+)/Luc2=tdT then treating them with G418. Only the cells which had taken up the plasmid (contain the antibiotic resistant marker) survived the treatment and formed colonies. Those colonies were harvested and each clone denoted A673 Luc1G, A673 Luc2G etc.

Clones with appropriate luciferase activity were required for the generation of a metastatic Ewing sarcoma mouse model. All clones produced via limiting dilution and G418 selection were incubated with D-luciferin and the luminescence was measured immediately (Figure 24A) as in section 3.2 in Figure 14. Luminescence was compared to KRIB Luc-20 cells, used previously by the Hawkins lab in mouse studies (Harris et al., 2020b; Harris et al., 2020c). All clones with detectable luciferase activity contained higher luminescence readings than the positive control KRIB Luc-20, whilst A673 Luc2L-6L had no detectable luminescence. The clones were then analysed via flow cytometry for tomato fluorescence to ensure they were clonal (Figure 24B, C). A673 Luc1L-6L and 1G contained appropriate luciferase activity and tomato intensity for this study.

The clones were then treated with varying doses of bortezomib and ixazomib to check whether the transfection experiment altered the A673 cells' drug sensitivity compared to the parental cells (Figure 25). All 12 clones generated exhibited similar proteasome inhibitor sensitivity to the parental cells (Figure 25). Taking into consideration all the data presented in Figures 24 and 25, A673 Luc3L was chosen for generating the mouse model as it contained appropriate luciferase activity, was clonal and had similar proteasome inhibitor sensitivity to parental A673 cells.

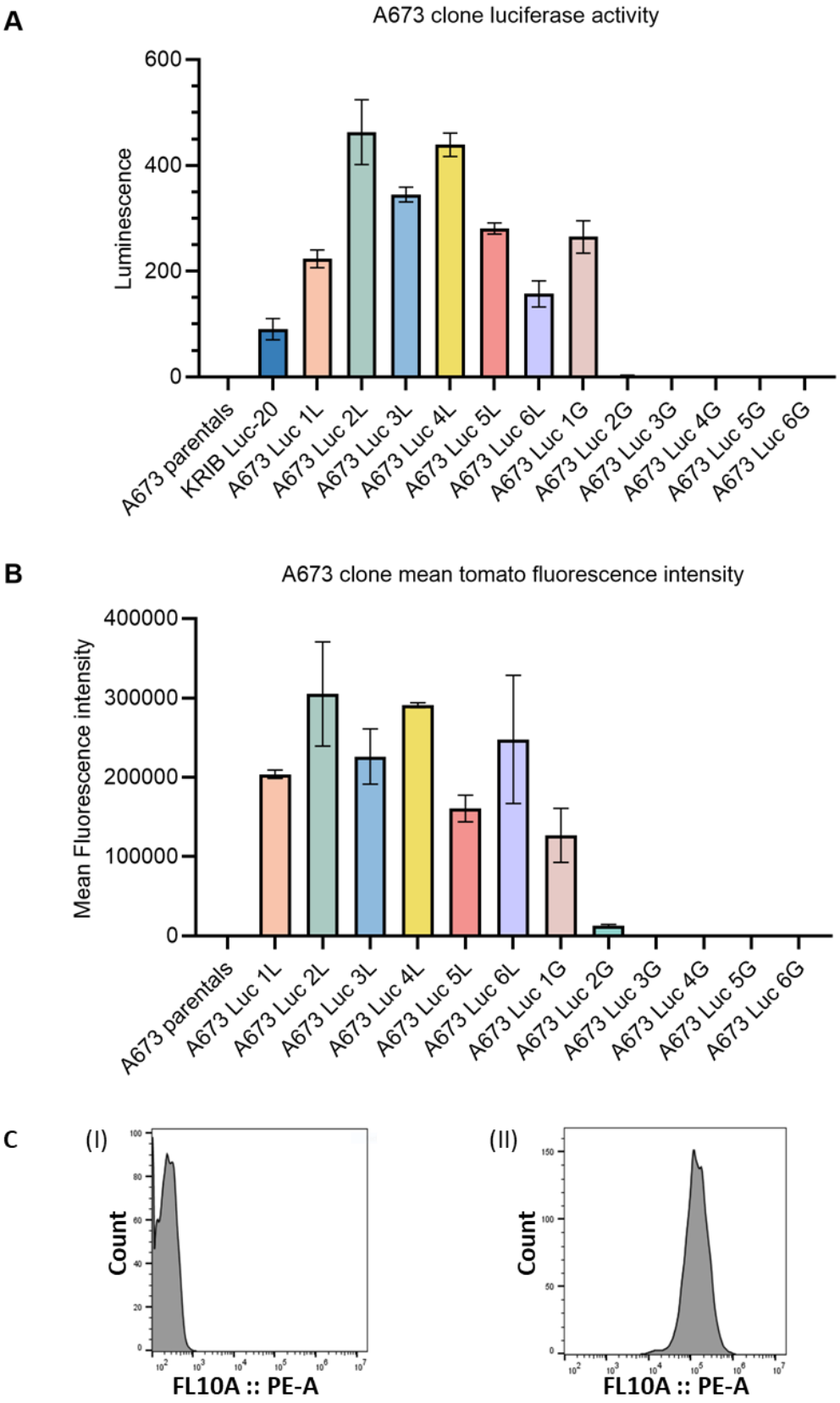

Figure 24: **Stably transfected A673 luciferase clones have appropriate fluorescence intensity and luciferase activity and are of a clonal nature.** (A) A673 clones generated via limiting dilution denoted A673-Luc1L and clones generated via G418 treated denoted A673-Luc1G were treated with 15 mg/kg of D-luciferin and emitted luminescence was measured immediately (n = 3, +/- SEM). (B) The tomato fluorescence for each clone was determined by running the samples on the FACS CytoFLEX and analysed using the PE channel (n = 3, +/- SEM). (C) The fluorescence readings on the PE channel was compared between parental A673 cells (I) and selected clone A673 Luc3L (II) after they were analysed on the FACS CytoFLEX.

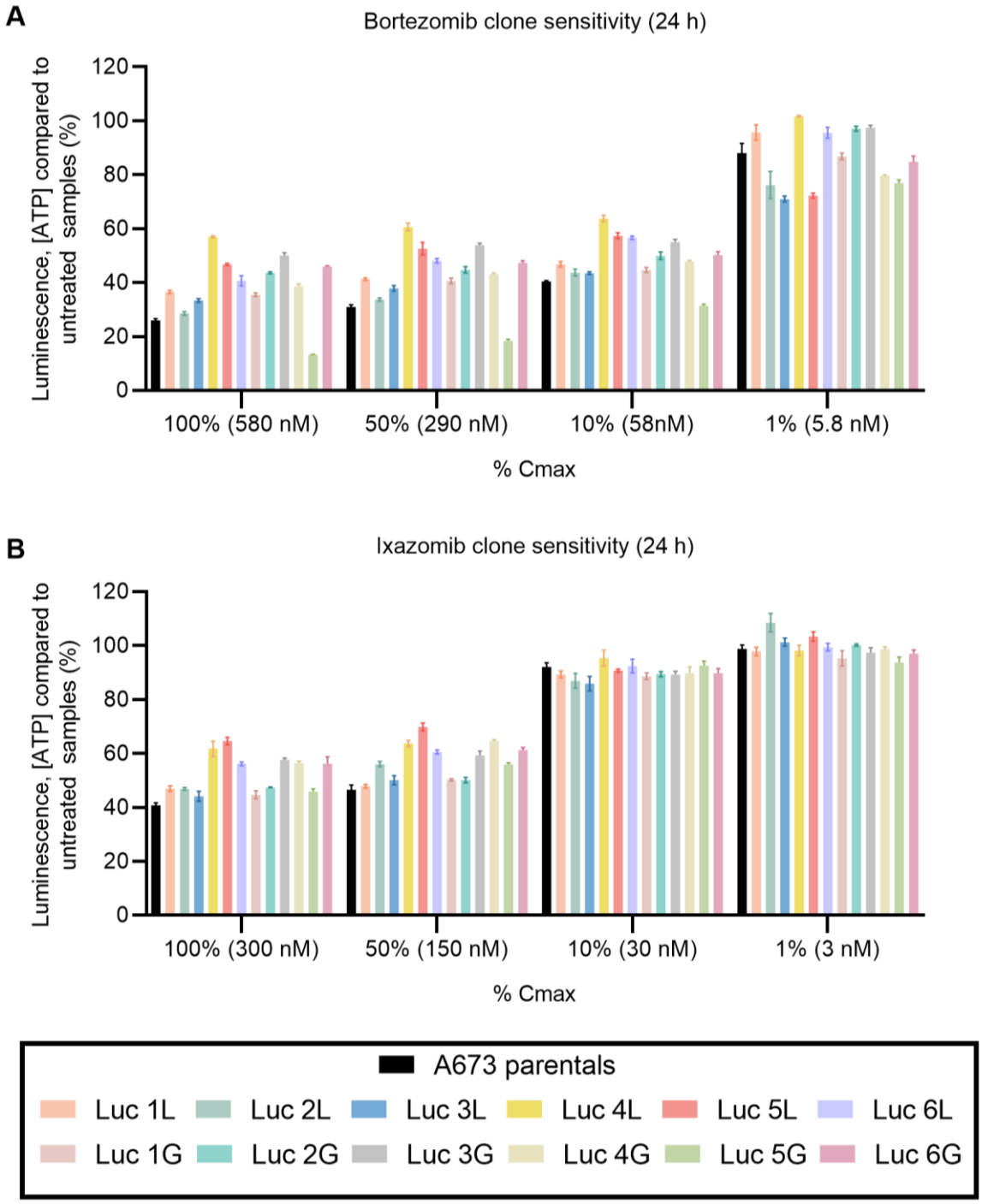

Figure 25: **Stably transfected A673 luciferase clones have similar proteasome inhibitor drug sensitivity to A673 parental cells.** A673 luciferase stable transfected clones were treated with varying C_{max} doses of the proteasome inhibitors bortezomib-580 nM (A) and ixazomib- 300 nM (B). The ATP content was determined via a CellTiter-Glo assay and all luminescence was calculated relative to the untreated cells, where all cell viability was compared to the A673 parental cells (n = 3, +/- SEM). All clones are denoted in shorthand in the legend, i.e. Luc 1L= A673 Luc1L.

3.8 A673 Metastatic mouse model

The next aim was to establish a Ewing sarcoma metastatic mouse model that could be used to screen novel therapies as a means of improving outcomes for patients with the metastatic disease. It has previously been shown that NK cells are important in destroying circulating cancer cells to prevent metastatic spread, with nude mice injected intravenously with osteosarcoma cells only showing detectable metastatic disease if previously treated with an anti-asialo-GM1 (NK depletion) antibody (Harris et al., 2020c). Previously published Ewing sarcoma metastatic mouse models established lung metastasis requiring 1-2 million cells (Lagares-Tena et al., 2016; Richter et al., 2009). It seemed likely that NK depletion may enable the establishment of a more efficient experimental metastasis model.

To test this hypothesis, ten nude mice were intravenously inoculated with 150,000 A673 Luc3L cells, with half the mice receiving anti-asialo-GM1 (NK depletion) antibody 24 h prior and the others receiving saline (Figure 26). Metastatic spread was monitored via bioluminescent signals over a 28-day period (Figure 26A). Only two mice (mouse 766, 767) from the NK-depletion group had detectable metastatic disease *in vivo*, with no tumour burden detected in any mice from the saline group. In the subsequent experiment, all organs were removed from the mice and tumour burden was quantified *ex vivo* (Figure 26B), by soaking the organs in D-luciferin. Bioluminescence was detected in numerous sites such as the brain, liver, kidneys, adipose tissue, muscle, and heart in the NK depletion group. Less frequently, some smaller metastases were detected *ex vivo* in the saline treated mice. Also, mice 767-770 had weak widespread signals *in vivo* that were only detected on day 28 (Figure 28C). The *in vivo* finding of small widespread weak signals in mice 767-770 on day 28 along with luminescence detected in numerous organs *ex vivo* demonstrated small widespread metastasis which was not as significant in the saline group. The *in vivo* and *ex*

vivo bioluminescent images (Figure 26C) demonstrated the site and intensity of the A673 tumours.

These data indicate that, NK depletion did assist with the overall formation of metastasis, although only two mice developed detectable *in vivo* metastatic sarcomas within four weeks. Some of the smaller tumours detected *ex vivo* indicated the variability and spread of this cell line. We explored the possibility that this could be enhanced with an increase in cell inoculation numbers.

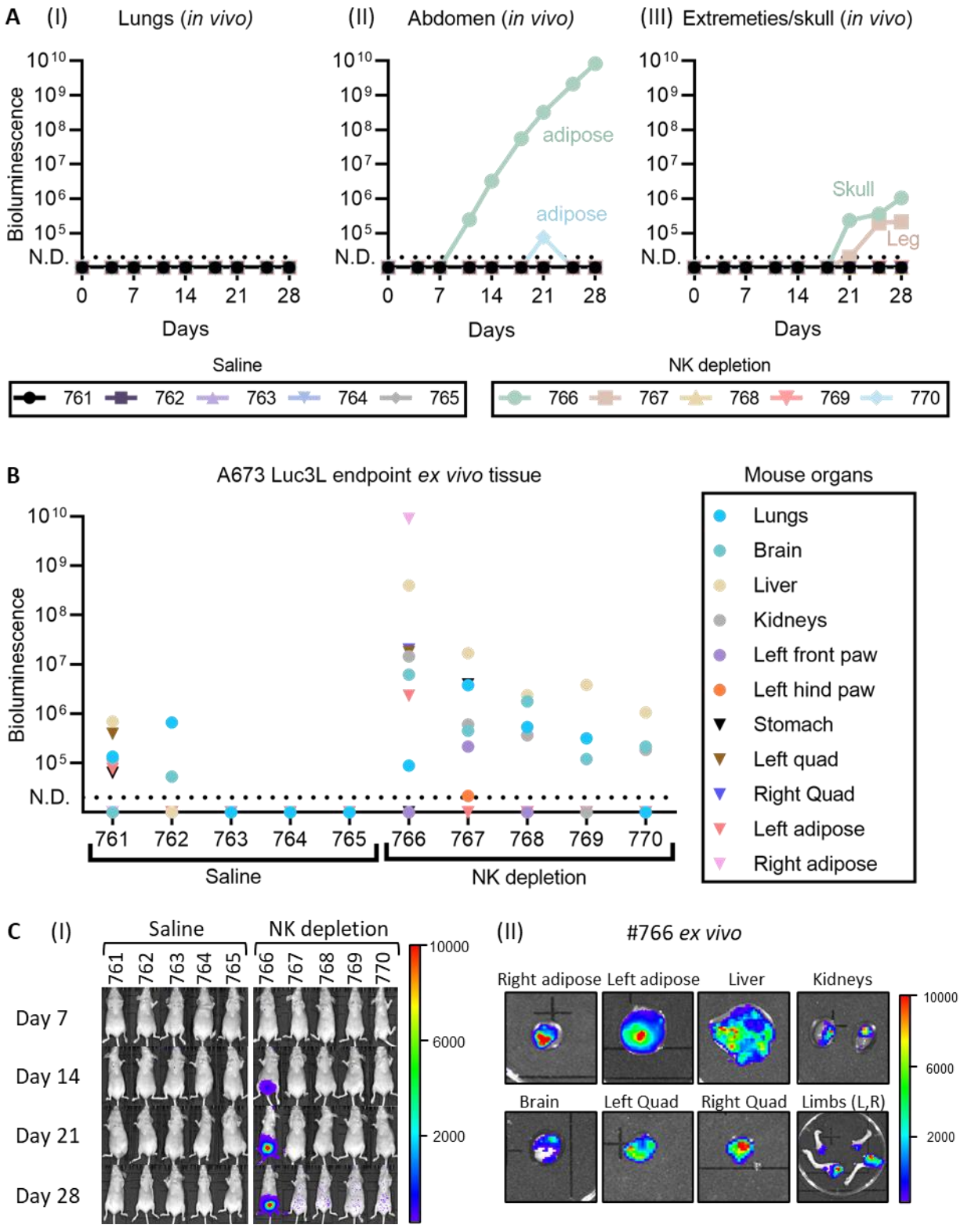

Figure 26: **NK depletion facilitates the formation of small Ewing sarcoma metastases in nude mice inoculated with 150,000 A673 Luc3L cells.** (A) BALB/c nude mice were intravenously inoculated with 150,000 A673 Luc3L cells and bioluminescence was detected twice weekly for 4 weeks via D-luciferin administration. 24 h prior to cell administration half the mice received NK depletion (anti-asialo-GM1) antibody (766-770) and half received saline (761-765). *In vivo* bioluminescence was compared in lungs (AI), abdomen (AII) and extremities/skull (AIII). (B) All tissue samples from the mice in this study were removed and their luminescence was determined *ex vivo* at the endpoint (day 28). (C) *In vivo* images of each mouse are shown taken along the entirety of this experiment (CI) and a representative image of *ex vivo* analysis of mouse #766 and its tissue, luminescence was indicated using a colour scale. N.D (not detectable) denotes a luminescence reading of 20,000 or below which is the detection limit.

In the hope of increasing the reproducibility of the model, the previous experiment was repeated with 500,000 A673 Luc3L cells (Figure 27), 24 h after the nude mice received NK depletion antibody or saline. Four out of the five NK depleted mice had detectable metastatic disease *in vivo* in the lungs, rib cage (later determined via *ex vivo* analysis) and in the leg. These tumours were detected in 4 to 5 consecutive imaging sessions with the signal intensity doubling every few days. In contrast, none of the saline-treated mice formed any metastatic disease that could be detected *in vivo*. Subsequent *ex vivo* analyses of the mice's tissue showed a similar pattern to the previous experiment in which fewer cells were introduced, with bioluminescence only detected in mice whose NK cells were depleted prior to cell inoculation. There was a wide variety of metastatic sites detected encompassing the lungs, brain, liver, kidneys muscles and bones (Figure 27B). An indication of the spread and intensity of the metastasis can be seen in the IVIS images both *in vivo* and *ex vivo* (Figure 27C).

Four out of five of the mice whose NK cells were depleted prior to A673 cell inoculation formed large detectable *in vivo* metastases, hence an A673 metastatic nude mouse model was successfully established. Considerable heterogeneity was observed in the sites of metastatic tumour growth (mirroring the diversity in metastatic sites of clinical extra-osseous (extraskeletal) Ewing sarcomas). This variability, coupled with time constraints, led to the abandonment of the initial plan of evaluating the efficacy of proteasome inhibitors against metastatic Ewing sarcoma.

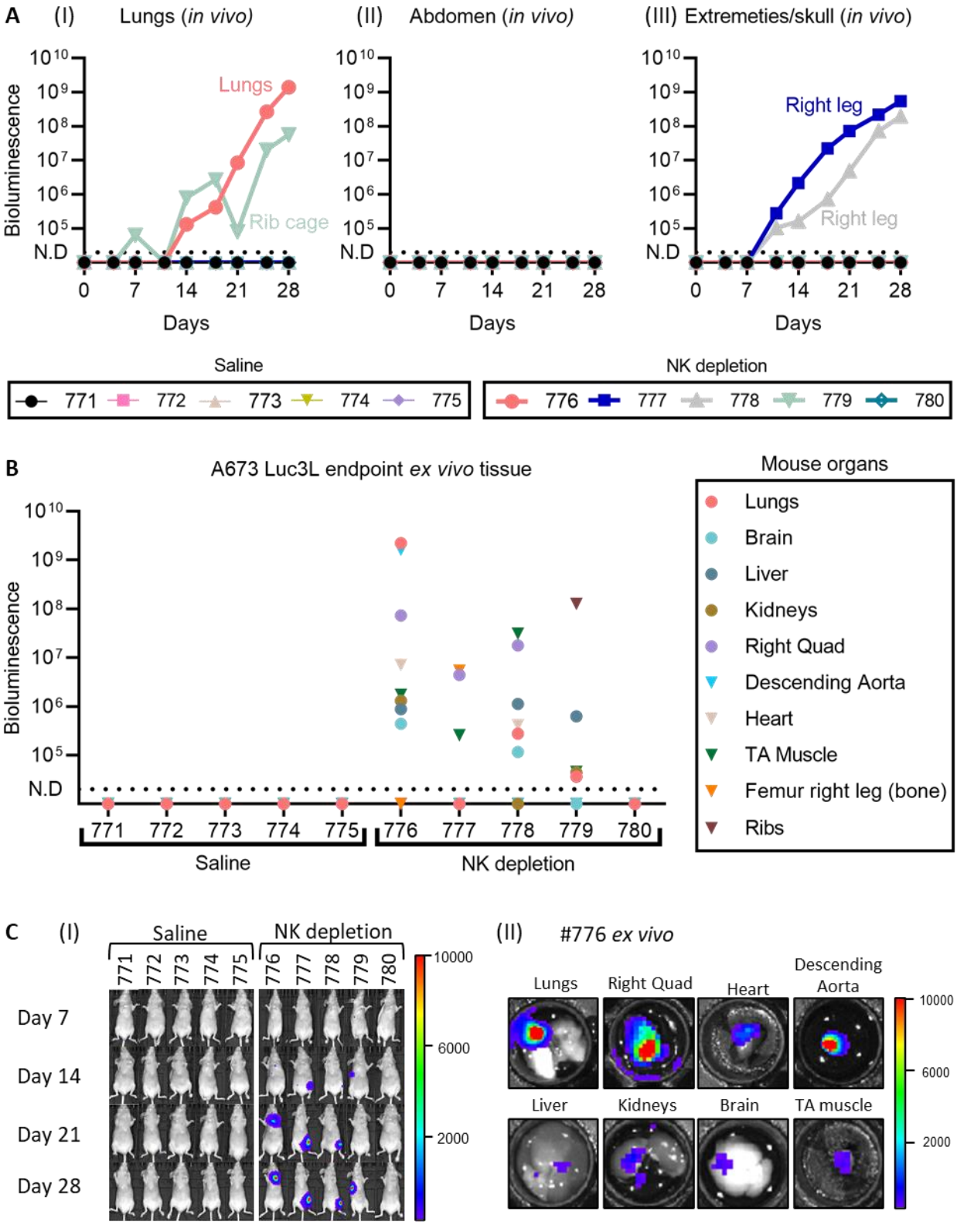

Figure 27: **Inoculation of 500,000 A673 Luc3L cells facilitates widespread metastasis following NK depletion in nude mice.** Mice 776-780 were administered anti-asialo-GM1 (NK depletion antibody) and mice 771-775 were administered saline 24 h prior to being inoculated with 500,000 A673 Luc3L cells. (A) The mice's bioluminescence was detected twice weekly. Detectable metastases were graphed according to their anatomical location; either lungs (I), abdomen (II) and extremities/skull (III). (B) At day 28 (endpoint) the mouses organs were all removed and quantified for tumour burden via *ex vivo* analysis (TA muscle = *tibialis anterior* muscle). (C) Images of each mouse are shown (I) as well as the luminescence detected *ex vivo* from organs in mouse 776 (II), all luminescence was indicated using colour scales. N.D (not detectable) denotes a luminescence reading of 20,000 bioluminescence or lower which is the detection limit.

The immune system plays a major role in the growth and maintenance of the tumour microenvironment (Gonzalez et al., 2018) and provides an insight into the potential use of immunotherapies, so the composition of immune cells in Ewing sarcoma tumours was explored (Figure 28A). Metastases from the A673 Luc3L metastatic mouse model were stained with antibodies recognising natural killer cells (CD335/NKP46-BV421), neutrophils (Ly-6G-APC), and macrophages (F4/80-PE-Cy7). Two independent tumours (from the aorta and lung) used in this experiment were extracted from mouse 776. A healthy mouse spleen was used as positive control to gate the detected immune cells (Appendix 8). Overall, immune cells made up less than one quarter of the cells within the tumours. The more prevalent immune cells in the descending aorta tumour were macrophages and neutrophils, but neutrophils were the least common immune cell in the lung tumour. Low immune cell infiltration was seen in the aorta and lung metastasis in mouse 776, demonstrating a potential minimal role of immune cells in these microenvironments, although conclusions could not definitively be made with a small sample size using immunodeficient mice. As immunotherapies are more effective in immune rich environments (Bonaventura et al., 2019) a larger sample size would be required to determine if they could be a viable therapy against Ewing sarcoma.

Ewing sarcoma metastases were stained using H&E (Figure 28B). Successfully stained lung, muscle, and liver tissue from mice with detectable tumours indicated these metastases formed via extravasation rather than embolisms. This is vital in this model as embolisms form when a cluster of cells dislodge and grow in a blood vessel (Mitchell et al., 2007), whereas most tumour metastasis in patients start from extravasation events (Chen et al., 2013; Pachmayr et al., 2017). Undertaking H&E indicated that this model is consistent to what occurs in a patient setting.

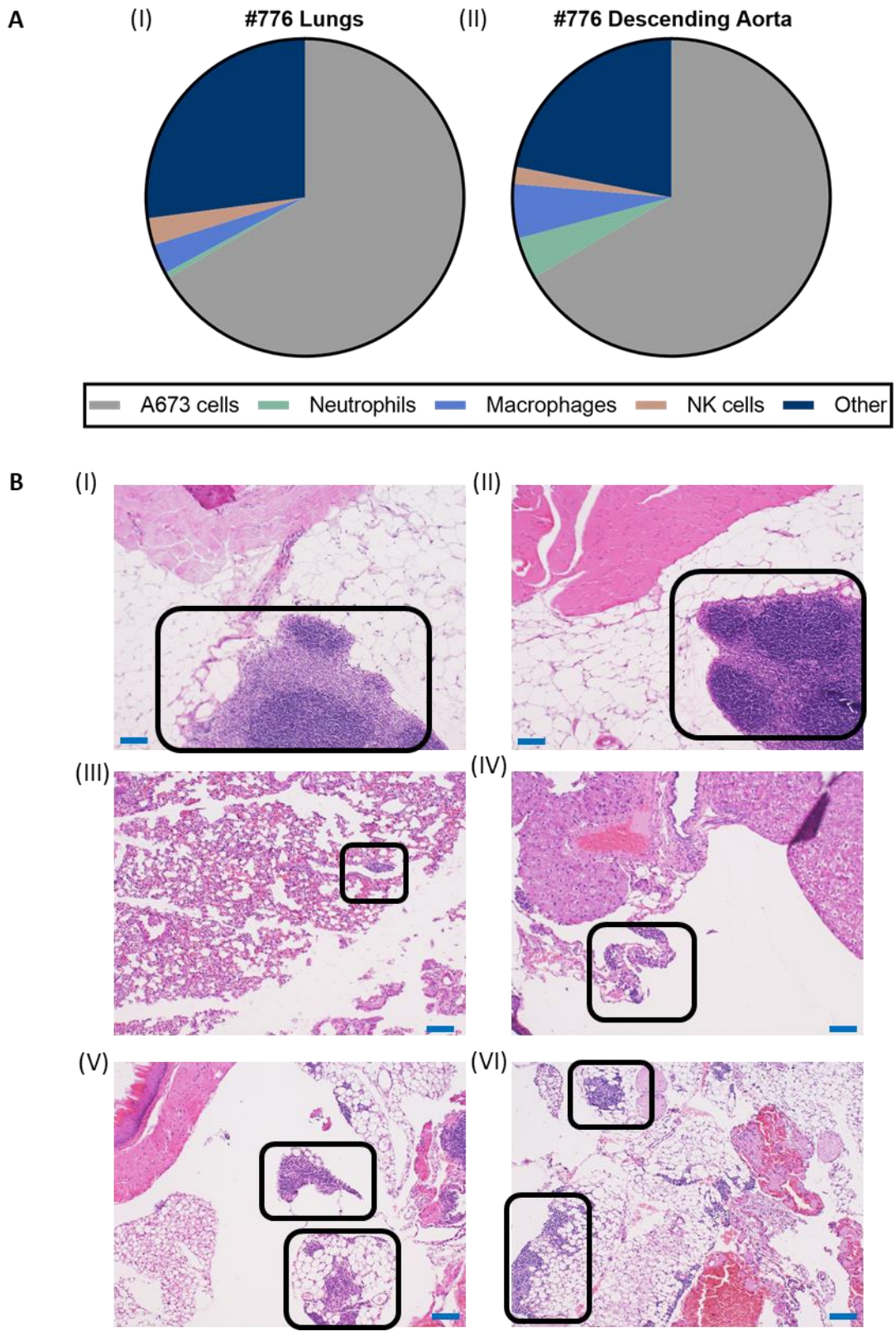

Figure 28: **A673-derived experimental metastases contain relatively few immune cells and are not embolisms.** (A) Tumours from mouse #776 (500,000 A673 Luc3L tumourigenicity experiment) were stained with antibodies recognising Ly6G (neutrophils), F4/80 (macrophages), NKp46 (NK cells) and then quantitated via flow cytometry (raw values in appendix 8). (B) Mouse tissues from animals intravenously inoculated with A673 Luc3L cells after NK depletion were subjected to H&E staining after endpoint organ removal. The tissues used for this staining were from mouse #766 left quad (I) and right quad (II), #767 lungs (III), mouse #767 liver (IV), as well as mouse #766 lungs (V), (VI). Indicative tumours are highlighted using black rectangles. Note: blue line denotes 100 µm.

Chapter 4: Discussion

With a median age of diagnosis of 15 years, Ewing sarcoma is the second most common malignant bone cancer in adolescents, exceeded only by osteosarcoma (Paulussen et al., 2009). Treatment of Ewing sarcoma prior to the 1960s involved surgery and radiation which led to overall 5-year survival rates below 20% (Nesbit, 1976). More recently, concurrent chemotherapy using vincristine, cyclophosphamide, doxorubicin with alternating cycles of ifosfamide and etoposide increased 5-year survival rates for patients with the primary disease to 70% (Womer et al., 2012). Unfortunately, 5-year survival rates remain below 40% for the metastatic disease with identical chemotherapies to the primary disease (Karski et al., 2016). These survival rates provide scope for new research into combating the primary and metastatic diseases.

Proteasome inhibitors have become a new promising drug class for the treatment of cancers, after being FDA-approved for multiple myeloma (Gandolfi et al., 2017). The proteasome inhibitor bortezomib was ineffective in clinical trials against Ewing sarcoma and other solid tumour types (Muscal et al., 2013). Publications suggested that ixazomib may have better tumour penetration against solid tumours (Kupperman et al., 2010). These data, along with the *in vitro* sensitivity of proteasome inhibitors against Ewing sarcoma cells (Figure 4,5,6) led to these drugs becoming the focus of this project. Where a goal of this project was to observe the primary and metastatic extraskeletal Ewing sarcoma disease in a mouse model as A673 cells were resected from a primary muscle tumour.

4.1 *In vitro* sensitivity

Ewing sarcoma cells were sensitive to the proteasome inhibitors, as measured via MTT, CellTiter-Glo and flow cytometry.

4.1.1 Initial sarcoma drug screen

In an *in vitro* setting, sarcoma cells were more sensitive to the proteasome inhibitor bortezomib than BH3 mimetics, HDAC inhibitors and SMAC mimetics including current treatments of vincristine and doxorubicin (Figure 3). Other sarcoma types such as rhabdomyosarcoma (RD-1) and uterine leiomyosarcoma (SK-UT-1) cell lines were less sensitive in general to all treatments compared to Ewing sarcoma A673 cells. Whilst this is the case, BH3 mimetics in combination with other therapies have been effective *in vitro* against soft tissue sarcomas (Rello-Varona et al., 2019), whilst synovial sarcoma cells were sensitive to HDAC inhibitors (Laporte et al., 2017). Osteosarcoma cells were sensitive to SMAC mimetics even at concentrations well below what's achievable in a patient's blood stream (Shekhar et al., 2019). Whilst BH3 mimetics, HDAC inhibitors and SMAC mimetics have been shown to be effective *in vitro* against various sarcomas, no previous work has been done using Ewing sarcoma cells. Other previous work in this field has shown that bortezomib has been effective at inducing cell cycle arrest and apoptosis in a variety of Ewing sarcoma cells *in vitro* (Lu et al., 2008; Nakamura et al., 2007). Whilst embryonal and alveolar rhabdomyosarcoma cells exhibited high sensitivity to the proteasome inhibitor bortezomib through the activation of caspase 3 and 7 (Bersani et al., 2008) and leiomyosarcomas were also sensitive to bortezomib induced proteasome inhibition *in vitro* (Perez et al., 2016). These publications supported the sensitivity data of bortezomib against the Ewing sarcoma and leiomyosarcoma cells in this project. The lack of drug potency seen against rhabdomyosarcoma cells compared to published data (Bersani et al., 2008) could be due to different drug incubation periods and cell lines used between the studies. As a result of this finding, the project's focus shifted to better understanding the effectiveness of proteasome inhibitors against Ewing sarcoma.

4.1.2 Ewing sarcoma sensitivity towards proteasome inhibitors *in vitro*

Ewing sarcoma cells were sensitive to proteasome inhibition at clinically achievable concentrations (Figures 4,5,6). This was confirmed via CellTiter-Glo and flow cytometry analysis.

The entire class of proteasome inhibitor therapies were able to reduce viability to below 5% at 50% C_{max} after 48 hours (Figure 4). A673 and SK-PN-DW Ewing cell lines demonstrated the greatest sensitivity at even 10% the dose of bortezomib, ixazomib and carfilzomib that is theoretically achievable in patients (C_{max}) (Figure 5,6). To put this in context, to achieve 50% reduction in ATP content (IC_{50}) in A673 cells, it required less than 1% C_{max} of bortezomib and carfilzomib compared to around 12% and 5% of C_{max} for cisplatin and doxorubicin (Table 4).

The flow cytometry experiment was undertaken as another means of determining how effective the proteasome inhibitor therapies were in reducing cell viability and causing apoptosis in Ewing sarcoma cells. The data confirmed what was seen via CellTiter-Glo, where the A673 and SK-PN-DW lines were more sensitive than CHLA-10 cells to proteasome inhibition derived apoptosis. The similarities in the Annexin V^+ and PI^+ profiles between the A673 and SK-PN-DW cells further confirmed their similarities in sensitivity to proteasome inhibition as seen via CellTiter-Glo. As this was the case, the A673 cell line was deemed to be the most sensitive cell line to proteasome inhibitors at 24 hours due to having a greater quantity of cells in late apoptosis (Annexin V^+, PI^+), compared to early apoptosis (Annexin$^+$,PI^-).

Various studies have demonstrated the apparent sensitivity of Ewing sarcoma cells to proteasome inhibition *in vitro* (Lu et al., 2008; Nakamura et al., 2007). Other upstream proteasome inhibitors, b-AP15 and VLX1570 (proteasome deubiquitinating enzyme

inhibitors) were shown to be effective against Ewing sarcoma, both *in vitro* and *in vivo* (Shukla et al., 2016). Both b-AP15 and VLX1570 inhibited proteasome function through inhibiting USP14 and UCHL5, which were both deubiquitinating enzymes, demonstrating an upstream inhibition in the proteasome pathway compared to bortezomib and it's analogous (Shukla et al., 2016). Proteasome inhibition through deubiquitinating inhibition of USP19 also caused a depletion in Ewing sarcoma cell growth and delayed tumour growth in mouse xenografts (Gierisch et al., 2019). These papers support the findings that Ewing sarcoma cells rely on proteasome activity for growth and metabolism and are therefore sensitive to cell death when this process is inhibited. Whilst these publications demonstrated how sensitive Ewing sarcoma cells were to proteasome inhibition, no previous work has been undertaken using the inhibitors ixazomib, carfilzomib, delanzomib and oprozomib against Ewing sarcoma. Consequently, it was worth exploring this aspect further due to the sensitivity of Ewing sarcoma cells *in vitro* to proteasome inhibition. This presented a potential novel treatment for Ewing sarcoma which was more effective *in vitro* than current treatments. It could be especially important for patients with recurrent and refractory Ewing sarcoma, with 5-year survival rates below 20% (Leavey et al., 2008; Xu et al., 2019), considering there is no standard second-line of therapy for these patients (Xu et al., 2019).

It would be interesting to repeat the flow cytometry experiment in the future with 48- and 72-hour incubations of the proteasome inhibitors with these Ewing cell lines as a comparison to the viability data generated via CellTiter-Glo. Previous *in vitro* research in this field has shown the effectiveness of bortezomib to inhibit cell proliferation in numerous Ewing sarcoma cell lines (Lu et al., 2008). The sensitivity data generated on the other proteasome inhibitors highlights how sensitive Ewing sarcoma cells were to proteasome inhibition and consequently how important proteasome activity must be in the growth and maintenance of these tumours.

4.1.3 Adhered versus suspension Ewing sarcoma cells sensitivity

Ewing sarcoma cells which were adhered to the plate prior to drug incubations were overall less sensitive to all treatments, compared to experiments where a cell suspension was added to wells containing the drug (Figure 5,6) and (Tables 3,4). Although not published for Ewing sarcoma cells, it has been shown that adhered K562 chronic myelogenous leukemia cells (Damiano et al., 2001) and human myeloma cell lines (Damiano et al., 1999; Huang et al., 2019) were more resistant to DNA damaging agents when adhered to a plate, than when grown in suspension. This phenomenon was termed cell adhesion-mediated drug resistance (Hazlehurst & Dalton, 2001). The exact reason as to why this occurs is not well understood but is believed to occur through multiple mechanisms such as increased $p27^{kip1}$ which is a cell cycle regulatory protein, as well as increases in topoisomerase II activity and changes in cell architecture (Shain & Dalton, 2001). This was also seen in a clinical setting with patients with multiple myeloma, where myeloma cells once adhered to the bone marrow or fibronectin displayed increased drug resistance towards chemotherapies (Abdi et al., 2013; Noborio-Hatano et al., 2009). Also, multiple myeloma cells with a higher expression of adhesion molecules such as ICAM-1 (intercellular adhesion molecule 1), VLA-4 (very late antigen 4) and VCAM (vascular adhesion molecule) had increased drug resistance to chemotherapies (Schmidmaier et al., 2006). These findings aligned with what was seen in this study as it seems as if Ewing sarcoma cells when adhered to the plate were also undergoing cell adhesion-mediated drug resistance against the proteasome inhibitors. As Ewing sarcoma is a solid tumour type, the adhered cell set-up was more likely to mirror an *in vivo* context which was the intention of this experiment. Because the suspension cells were trypsin-treated prior to being incubated with drug, this would have caused a proteolysis of many transmembrane proteins including those involved in cell adhesion (Huang et al., 2010). This may explain why the suspension cells were more sensitive to the proteasome inhibitors than these same cells adhered to the plate. Future experiments

could be undertaken using 3D cell culturing which would provide an improved technique for testing drug sensitivity that imitated an *in vivo* setting (Huang et al., 2013). This has previously been established using a 3D electrospun PCL scaffold, where it was demonstrated that TC-71 Ewing sarcoma cells had reduced growth rates compared to 2D cell culture, but which mimicked *in vivo* xenografts (Fong et al., 2013). At the same time this apparent drug resistance to proteasome inhibitors when adhered (which is a similar morphology to what is seen in a solid Ewing sarcoma tumour) may also explain as to why previous clinical trials with bortezomib have been ineffective against solid tumours (Huang et al., 2014). If this could be overcome, then there could be further clinical success with bortezomib in the clinic.

4.1.4 Proteasome and caspase activity assays

Proteasome inhibitors bortezomib and ixazomib induced high levels of caspase activity (Figure 8). A673 and SK-PN-DW cells demonstrated similar drug sensitivity profiles towards bortezomib and ixazomib which correlated to similar levels of caspase activity post treatments. As expected, the proteasome inhibitors induced significantly lower caspase activation in the less sensitive CHLA-10 Ewing cell line, at the same drug concentrations. The overall pattern observed in two out of three cell lines was that at low drug concentrations (5 nM bortezomib, 50 nM ixazomib) caspase activity peaked at 48 hours post treatment, compared to 24 hours post treatment at higher proteasome inhibitor treatments (10 nM bortezomib, 100 nM ixazomib). This pattern was similar to previously published data, showing higher doses of bortezomib induced maximal caspase activity in chondrosarcoma cells at 24 hours but caspase activity peaked at 48 hours after exposure to a lower dose (Lohberger et al., 2016). A plausible hypothesis for this finding was that those cell lines were more sensitive to proteasome inhibition triggered caspase activity and

apoptosis (by 24 hours) and by 48 hours fewer viable cells were present to undergo apoptosis, reducing the overall caspase activity.

Previous literature has demonstrated that proteasome inhibitors b-AP15 and VLX1570 (deubiquitinate proteasome inhibitors) were able to induce high levels of caspase activity in Ewing sarcoma cell lines *in vitro* (Shukla et al., 2016). Although these therapies induce proteasome inhibition in a different manner to bortezomib (and other inhibitors used in this project) they induced caspase activation most significantly in A673 cells compared to other Ewing sarcoma cell lines tested (CHP100,TC-71) (Shukla et al., 2016). This confirmed the data generated using the proteasome inhibitors in this project, specifically highlighting the sensitivity of A673 to proteasome inhibition. To further confirm the requirement for caspase activity in cell death triggered by proteasome inhibition, the cells could be treated with pan-caspase inhibitor Q-VD-OPh (Caserta et al., 2003). Caspase-dependant cell death could be confirmed if proteasome inhibitors had no effect on cell viability of Ewing sarcoma cells with prior pan-caspase treatment (Patatsos et al., 2018). The ability of Ewing sarcoma cells to undergo apoptosis could be further analysed in the future using the other proteasome inhibitors (carfilzomib, delanzomib, oprozomib) and longer timepoints to observe any effects after 48 hours.

The proteasome inhibitors were able to mostly induce reductions in proteasome activity below 25% 1-hour post treatments in the Ewing sarcoma cell lines *in vitro* (Figure 9). The rationale for this experiment was to explore the kinetics and extent of proteasome inhibition in Ewing sarcoma cells, given the drugs tested vary in their reversibility. As expected, from 1 to 48 hours bortezomib and ixazomib both recovered in activity due to their reversible mode of action. On the other hand, it was expected that the proteasome would recover to a lesser extent when treated with the carfilzomib due to its irreversibility for the 26S proteasome. This was seen in A673 treatments, also the proteasome did not recover as

significantly when treated with carfilzomib compared to the other proteasome inhibitors in SK-PN-DW cells. Alternatively, the CHLA-10 cells recovered their proteasome activity quickly, regardless of which proteasome inhibitor they had been exposed to. This provided a possible justification that CHLA-10 cells were not as sensitive to proteasome inhibitor therapies due to their ability to recover proteasome activity more significantly than A673 and SK-PN-DW lines. The activity of the proteasome in A673, SK-PN-DW and CHLA-10 cells recovered but did not approach untreated levels until at least 48 hours post treatment. Only A673 and SK-PN-DW cells fully recovered by 48 hours when treated with bortezomib, with other cell lines recovering to 40% activity by this timepoint.

In contrast, published data using melanoma mouse models treated with bortezomib demonstrated a similar reduction in proteasome activity 1-hour post treatments, which significantly recovered closer to untreated levels by 24 hours (Mlynarczuk-Bialy et al., 2014). In other clinical settings bortezomib has been shown to inhibit the proteasome activity at the maximum tolerated dose of 1 mg/kg by up to 60% one hour post treatment (Orlowski et al., 2002). Bortezomib was able to reduce proteasome activity levels to 10% by 4 hours which only recovered to around 50% at 48 hours *in vitro*, using previously calculated IC_{50} values against renal cell carcinoma cells (Vaziri et al., 2009). The authors also saw concentration dependant changes in proteasome activity where lower doses of this drug only reduced proteasome activity to 25% after 4 hours and 75% by 48 hours (Vaziri et al., 2009). Although this was the case it did seem to be cell line dependant as renal cells derived from lymph node metastasis showed minimal proteasome activity recovery by 48 hours (Vaziri et al., 2009).

The results in this study were compared to previously published data for bortezomib, as these assays have not been undertaken for other proteasome inhibitors, to which similar patterns in proteasome inhibitions and recoveries post treatments were observed.

Understanding the kinetics and extent of proteasome activity would be an important aspect when designing better treatments for Ewing sarcoma. Ewing sarcoma cells rely on a functional overactive 26S proteasome, as treatments render these cells apoptotic, so designing drugs with reduced side effects that could prolong inhibition would be of great clinical relevance in the treatments of Ewing sarcoma patients.

Future experimentations could be undertaken using these proteasome and caspase activity assays in an *in vivo* setting to provide an insight into how these treatments were able to reduce proteasome activity and induce apoptosis in patients. At the same time, they would help determine how well proteasome inhibitor treatments were able to penetrate these solid tumours based on the localisation of apoptotic cells within these tumours.

4.1.5 Cell cycle analysis and drug cooperation

Proteasome inhibitors were able to induce G2 cell cycle arrest in Ewing sarcoma cells 24 hours post treatment (Figure 10). Although the changes in DNA content were not major, which could be related to the fact that low concentrations of drug were used (below the 24 h IC_{50}), to minimise cell death during this assay, they were significant enough to identify cell cycle arrest through increases in DNA in the G2/M phase compared to untreated cells. Bortezomib was previously reported to stimulate G2 cell cycle arrest in other Ewing sarcoma cell lines (Lu et al., 2008). In contrast, melanoma (Beaumont et al., 2016) and mesothelioma (Gordon et al., 2008) cells experienced cell cycle arrest in both G1 and G2 phases following bortezomib treatment. Proteasome inhibitors are thought to impact on the cell cycle by upregulating cyclin dependent kinase inhibitors p21 and p27 (Hideshima & Anderson, 2012). The protein p21 has demonstrated to promote cell cycle arrest, resulting in the inhibition of DNA synthesis and cell proliferation (Abbas & Dutta, 2009). Also, proteasome inhibition has also demonstrated to lead to an accumulation of the tumour

suppressor p53, that is involved in G1 and G2 cell cycle arrest, as a result of mdm2 ligase which tags p53 for proteasomal degradation and is upregulated in cancer cells (Marine & Lozano, 2010; Rastogi & Mishra, 2012). The purpose of this cell cycle analysis was to assess possible drug antagonism with combination therapies involving proteasome inhibitors and chemotherapies as most chemotherapy drugs only function at particular stages of the cell cycle. Therefore, they require a fully functional cell cycle to elicit their optimal response.

Interpretation of any cooperation between current chemotherapy drugs along with proteasome inhibitors would provide an important insight into potential clinical applications of combination therapies. The proteasome inhibitors bortezomib and ixazomib used in combination with doxorubicin (Figure 11) and cisplatin (Figure 12) demonstrated overall additive to slight antagonistic effects on Ewing sarcoma cells. Synergistic effects between bortezomib and cisplatin have been published in human ovarian cancer cell lines (Al-Eisawi et al., 2011). However, antagonism between chemotherapy drugs and proteasome inhibitors has also been noted previously in other contexts. For example, *in vitro*, doxorubicin could activate 20S proteasome peptidases in purified 20S proteasomes in a test tube which are inhibited by proteasome inhibitor therapies, thereby causing drug antagonism (Liu et al., 2008). The combination of bortezomib and cisplatin was able to cause drug antagonism at low concentrations and synergism at higher concentrations in malignant pleural mesothelioma cells (Gordon et al., 2008). The ability of proteasome inhibitors to induce cell cycle arrest conflicts with the mode of action of cisplatin (Fuertes et al., 2003) and doxorubicin (Thorn et al., 2011) which require and are specific to causing DNA damage in proliferating cancer cells. Studies indicated that cells are most sensitive to doxorubicin when in the S phase of the cell cycle (El-Far et al., 2020; Wahl et al., 2001), whilst cells are most sensitive to cisplatin treatment when in the G1 phase (Donaldson et al., 1994). This is a possible reason as to why drug antagonism was seen especially in

cases where a proteasome inhibitor was added in combination with a chemotherapy drug for an entire 48 hours i.e. (B+D) (Figure 11,12). As the proteasome inhibitors would have tended to cause cells to accumulate in G2, fewer would be in the G1 or S phases where they are maximally sensitive to cisplatin and doxorubicin respectively. Likewise, based on the cell cycle plots in figure 10, the apparent overcoming of cell cycle arrest after 24 hours (as the DNA content begins to return to untreated levels by then) was the reason why the drugs were also added at 24 hour intervals to avoid this arrest. Interestingly, the addition of a chemotherapeutic followed by a proteasome inhibitor i.e. (D>B) yielded the lowest combination index values, indicating that these were the most synergistic combinations. Also, in most cases the staggered addition of the proteasome inhibitor followed by the chemotherapeutic i.e. (B>D), induced a more synergistic effect than the two drugs applied simultaneously (B+D), although not as favourable as the staggered combination in the opposite order (D>B). Proteasome inhibitors induced cell cycle arrest and therefore some of the cells may still have been arrested 24-hours post treatment, which might explain why the staggered treatments with proteasome inhibitor applied first were not more effective. Interestingly, in CHLA-10 and SK-PN-DW cells concurrent bortezomib and cisplatin (B+C) induced a more synergistic response than the staggered drug combinations. Cell cycle analysis was not undertaken on these cell lines, but it is possible that their cell cycle arrest was less pronounced or more rapidly overcome, allowing for greater periods of drug synergism. Future experiments could involve treating the cells for 36 or 48 hours staggered per drug at a low enough concentration that not all cells died but high enough to observe any effects on the cell cycle. It would also be meaningful to establish the impact that proteasome inhibitors have on the cell cycle of SK-PN-DW and CHLA-10 cells, to determine a more efficient timepoint of drug addition to potentially overcome drug antagonism. These data highlighted the importance of understanding and overcoming drug antagonism in order to develop effective drug combination regimens for *in vivo* use.

4.2 Primary Ewing Sarcoma mouse model

4.2.1 Generation of virally-transduced luciferase cells

The Ewing sarcoma cell line A673 was chosen for *in vivo* experimentation due to its sensitivity to both bortezomib and new class inhibitors ixazomib and carfilzomib as well as being previously published to be tumourigenic in BALB/c nude mice (Rouleau et al., 2015). In previous studies, A673 cells have been successfully virally-transduced to express luciferase in order to generate and image metastatic tumour xenografts (Minas et al., 2017). The infection of A673 cells with a virus encoding luciferase and mCherry (pMSC-mcherry-luc-IRES plasmid) was initially deemed to be successful via the flow cytometry (Figure 13). By comparing differences in mCherry expression in transduced versus parental A673 cells, monoclonal populations were only cultured from mCherry positive cells which had undergone a successful infection. After expansion, however, the clones did not express significant mCherry fluorescence (Appendix 2) or luciferase enzyme activity (Figure 14C), yet contained the luciferase gene (Figure 15, 16).

A number of mechanisms could account for this frustrating absence of reporter gene expression, despite successful genomic integration. Gene expression can be dampened by DNA methylation, in which methyl groups are added to CpG islands to prevent promoter access by transcriptional machinery (Smith & Meissner, 2013). Another possible reason for the loss of gene expression involves histone modifications such as histone deacetylation (HDAC) which condenses the chromosome and causes a reduction of gene expression (Bannister & Kouzarides, 2011). Gene silencing is also believed to provide a protective mechanism to cells by preventing the invasion of foreign DNA (Mok & Lever, 2007) . It is therefore possible that the virally-derived sequences within the integrated DNA triggered transcriptional silencing. The reactivation of retrovirally repressed GFP genes has been

reported in HeLa cells after treatment with HDAC inhibitors (Katz et al., 2007). As a result, treatments with demethylating agents or HDAC inhibitors could have revealed the mechanism of silencing and provided ways of reversing it, but this would not render the cell line useful for *in vivo* imaging or determining tumour burden after culling. All clones exhibited approximately similar sensitivity towards the proteasome inhibitors. The clone which was most similar in sensitivity to parental cells, A673 Luc-4, was chosen for the generation of the primary Ewing sarcoma nude mouse model.

Other possible biomarkers were studied for detecting A673 Luc-4 in a mouse model. CD44 was overexpressed in some Ewing sarcoma patients with enhanced tumour invasiveness (Paulis et al., 2015), though minimal levels of this biomarker were detected in the A673 cells used for tumour implantation (Appendix 6). Hence it could not be used for post-mortem determination of tumour burden. Another biomarker which could be explored to detect Ewing sarcoma cells *in vivo* is CD99, a membrane glycoprotein that is highly expressed in tumour cells from Ewing sarcoma patients (Kovar et al., 1990; Rocchi et al., 2010). The presence of the reporter genes (notwithstanding the lack of their protein products) presumably could have facilitated detection of tumour cells in mouse organs after culling through qPCR, but neither this or CD99 expression could be explored in the A673 Luc-4 mouse model in this project due to time constraints. As the viral origin of the reporter genes may have led to their silencing (Bannister & Kouzarides, 2011; Mok & Lever, 2007; Smith & Meissner, 2013), a non-viral method of enforcing reporter gene expression was subsequently used in A673 cells. This was successful (section 4.3.1), lending credence to the hypothesis that viral silencing was the problem with the initial approach. But before this approach was pursued, the virally transduced A673 cells were used, and calliper measurements, to explore proteasome inhibitor efficacy *in vivo* against primary Ewing sarcoma.

4.2.2 Ewing sarcoma primary mouse model

A BALB/c nu/nu mouse model was established by implanting 50,000 (A673 Luc-4) Ewing sarcoma cells intramuscularly into the *tibialis anterior* of nude mice (Figure 17). All five mice implanted with the cells developed detectable tumours in the muscle by day 14. An advantage of this model over other Ewing mouse models such as subcutaneous implantation is that cells were implanted in an orthotopically relevant site, as A673 cells were resected from a Ewing muscle tumour (Giard et al., 1973). Relatively few cells were required in this model, making it more efficient compared to other models that require one to three-million A673 cells injected subcutaneously to reliably generate a primary tumour (Rouleau et al., 2015). This is the first intramuscular Ewing sarcoma mouse model to be established. It also provides a platform for testing the proteasome inhibitors and other drugs against primary Ewing sarcoma *in vivo*. Although the cells did not generate any detectable luciferase activity, they were deemed appropriate for this study as primary tumour growth could be detected via calliper measurements.

4.2.3 Efficacy of proteasome inhibitors against primary Ewing Sarcoma

A reliable Ewing sarcoma nude mouse model, in which all implanted mice developed tumours, enabled evaluation of the efficacy of proteasome inhibitors *in vivo*. The proteasome inhibitors bortezomib and ixazomib significantly increased the lifespan of Ewing sarcoma implanted mice compared to the saline treatment group (Figure 19). Furthermore, bortezomib delayed the growth of the primary tumour on average compared to saline treated mice, but no significant differences were seen in the ixazomib treatment group (Figure 19). These data established that bortezomib (administered at 1 mg/kg, twice weekly) was more effective at reducing primary tumour growth than ixazomib at (given at 5 mg/kg, twice weekly). Nevertheless, the effects of ixazomib were not pronounced

enough for clinical relevance. This echoed bortezomib's ineffectiveness against solid tumours in clinical trials, although Ewing sarcoma cells have previously been shown in this study to be very sensitive to proteasome inhibition *in vitro*.

Overall, clinical trial data has demonstrated that bortezomib is generally ineffective against solid tumours (Huang et al., 2014) also seen with Ewing sarcoma patients (Maki et al., 2005; Muscal et al., 2013). This was evident in a phase II clinical trial against recurrent and metastatic sarcomas, which involved Ewing, rhabdomyosarcomas as well as other soft tissue sarcomas (leiomyosarcoma) (Maki et al., 2005). Bortezomib was classified as ineffective against these sarcomas in all patients except for a single patient with leiomyosarcoma (Maki et al., 2005). Although this was established the authors recommended future studies using bortezomib along with agents with preclinical synergy rather than recommending to no longer use this treatment (Maki et al., 2005). The rarity of sarcomas meant that only very few Ewing sarcoma patients were included in these trials, so it is difficult to draw conclusions as to the impact bortezomib had on Ewing sarcoma. At the same time, animal experiments have suggested that newer proteasome inhibitors such as ixazomib may be more effective than bortezomib against solid tumours *in vivo* (Kupperman et al., 2010), hence why ixazomib was chosen for further research in this project against Ewing sarcoma. Disappointingly, although it was published *in vivo* that ixazomib had better solid tumour penetrance than bortezomib (Kupperman et al., 2010), major improvements in efficacy compared to bortezomib were not identified in this intramuscular Ewing sarcoma model.

Other preclinical data suggested that well vascularised solid tumours improved bortezomib's preclinical efficacy against prostate cancer mouse models (Williamson et al., 2009). This suggested that limited tumour penetration related to poor tumour vascularisation may explain its lack of efficacy in clinical trials against solid tumours and

in this study against Ewing sarcoma. Perhaps if the tumour cells could experience similar concentrations *in vivo* to those applied *in vitro*, then improvements could be seen with bortezomib against solid tumours in the clinic. The ability to determine vascularisation of solid tumours which did not respond to Ewing sarcoma therapies would be an important experiment which could be undertaken in this field. It could be achieved via MicroCT vascular casting of a mouse after its endpoint through which casts of the vasculature could be prepared and MicroCT imaging done to maintain and observe tumour vasculature (Williamson et al., 2009). If there were certain mice which did not respond as well to treatments it could be determined through this method if it was because of lack of tumour vascularisation. Also, attempts have been made to encapsulate bortezomib in a liposome to improve its tumour penetrance and efficacy (Deshantri et al., 2019; Zuccari et al., 2015). Bortezomib was formulated within a liposome that is specifically targeted for the tumour vasculature, but early issues in its synthesis were related to the drug's non-polar nature that caused it to freely leak across the bilayer before reaching the tumour vasculature (Zuccari et al., 2015). This was overcome by forming a boronic ester with bortezomib which improved its entrapment within the liposome (Zuccari et al., 2015). Preclinically, bortezomib did not exhibit any anti-tumour effects against a neuroblastoma mouse model, whist the encapsulated bortezomib demonstrated enhanced anti-tumour activity against neuroblastoma with reduced side effects (Zuccari et al., 2015). In another similar study, bortezomib was encapsulated into a hollow mesoporous silica nanosphere particle, which was able to reduce the growth of subcutaneously implanted human non-small lung cancer carcinoma cells in nude mice by greater than 50% compared to bortezomib (Shen et al., 2014). Although encapsulated bortezomib treatments have yet to be tested in the clinic, they provide hope to overcome bortezomib's poor solid tumour penetrance with greater preclinical success against the solid tumour types neuroblastoma and non-small lung cancer carcinoma.

Potential tumour drug resistance was examined via *ex vivo* drug sensitivity analysis of the primary Ewing sarcoma nude mice tumours (Figure 20). This experiment was undertaken to assess whether acquired drug resistance was the reason why proteasome inhibitors were effective *in vitro* but not *in vivo*. This is relevant in a clinical setting as bortezomib drug resistance has been observed in multiple myeloma patients (Bai & Su, 2021; Zaal et al., 2017). In this experiment Mouse number 606 in the bortezomib treatment group had the most significant response to treatment, with no tumour detected from days 20 to 25. The cells from this tumour did not show any resistance to bortezomib in *ex vivo* analysis compared to the *in vitro*-cultured A673 Luc-4 cells (Figure 20). Tumour drug resistance was identified but did not seem to be related to prior *in vivo* treatments (cells were cultured to ensure no muscle cells were included in the assays). The most significant resistance was identified in mice in the saline treatment group. Six out of seven tumours became more resistant to ixazomib during the *in vivo* growth in that group. Some Ewing tumours became more resistant to proteasome inhibitors *in vivo* seemingly because of the changes in tumour microenvironment compared to 2D cell culture rather than any treatments. This *ex vivo* data provided a possible explanation as to why there were differences seen between the sensitivity of Ewing sarcoma cells *in vivo* compared to *in vitro*. One recent hypothesis involving cancer stem-like cells, describes a small number of cells within tumours which are responsible for metastasis and drug resistance (Fujiwara & Ozaki, 2016). These cells have been identified using a CD133 marker and reported in osteosarcoma (Fujii et al., 2009; Gibbs et al., 2005) and Ewing sarcoma (Suvà et al., 2009). Ewing sarcoma cells lacking this marker failed to grow in NOD/SCID mice but as few as 2,500 $CD133^+$ cells were required for tumour formation (Suvà et al., 2009). These stem cells when present in higher quantities were able to demonstrate and enhance drug resistance in Ewing and osteosarcoma cells (Fujii et al., 2009). It would be informative to apply this technique to compare proteasome inhibitor sensitivity of CD133 positive and negative Ewing sarcoma

cells. It could also be used to identify whether tumours generated in this mouse model that were resistant to therapies contained higher quantities of $CD133^+$ cells. Another possible hypothesis as to why the treatments were not as effective *in vivo* as *in vitro* was due to the fact that cells from solid tumours proliferate slower *in vivo* than *in vitro* as seen in a 2D versus 3D Ewing sarcoma model (Fong et al., 2013). So, they may not rely as much on proteasome activity and this could also render proteasome inhibitors less effective. This theory could be tested by developing 3D models for Ewing sarcoma and observing their growth rates and proteasome activity compared to their 2D counterparts.

Better efficacy may have been observed in the primary setting if treatments were commenced earlier or if less cells were implanted in the mice due to their fast growth rate. However, the model used is more clinically relevant, as patients present to the clinic once the tumour has been physically detected, rather than at earlier pre-symptomatic stages. It would be interesting to repeat this experiment in the future with luciferase tagged A673 cells to monitor metastasis. Such an experimental design could reveal whether proteasome inhibitors like ixazomib could delay the formation of Ewing sarcoma metastases, as was seen in an osteosarcoma study (Harris et al., 2020b). The authors found that bortezomib and ixazomib (at 5 mg/kg) had minimal impact on the growth of primary osteosarcomas but ixazomib was able slow the progression and growth of pulmonary and abdominal osteosarcoma metastases (Harris et al., 2020b). It would be therefore informative to observe whether these drugs were able to disrupt the growth and spread of metastatic Ewing sarcoma, which is more life-threatening than the localised form of the disease. The differences between *in vivo* and *in vitro* sensitivity profiles for Ewing sarcoma was somewhat mirrored in the differences in sensitivity between adhered (at site of solid tumour) and non-adhered (in the blood stream) Ewing sarcoma cells (Figure 5,6). The non-adhered cells were shown to be more sensitive to treatments as discussed in 4.1.3. So if this finding was translated into an *in vivo* setting there is a possibility that a similar finding

may have been observed as the study by Harris et al. (2020b) between circulating and non-circulating sarcoma cells.

No studies have been published on the efficacy of ixazomib to primary and metastatic Ewing sarcoma tumours, hence the data yielded by this study was novel. Although ixazomib was not more successful than bortezomib in this study, whilst being effective *in vitro* suggested that acquired drug resistance, poor tumour penetrance because of poor tumour visualisation and cell-adhesion drug resistance may have all played a role in this disappointing finding. Patients are not usually treated with single agent therapies; it would therefore be beneficial to observe whether ixazomib along with current therapies vincristine and cyclophosphamide were synergistic and apply this to attempt to improve primary Ewing sarcoma efficacy.

4.3 Metastatic Ewing sarcoma mouse model

H & E staining revealed that nude mice developed lung tumours when A673 cells were implanted in the *tibialis anterior* which has not been previously shown from this site (Figure 22). One way to quantify the metastasis in these mice would involve removing the lungs and determining tumour burden via quantitative PCR (qPCR) for the luciferase gene which was determined to be present in the A673 Luc-4 cell line (Figure 15,16). This is an important aspect to study as the 5-year survival rates for patients with metastatic Ewing sarcoma is 30% (Hamilton et al., 2017) compared to 70% for patients with localised disease (Womer et al., 2012). Whilst lung metastasis was detected, extraskeletal Ewing sarcoma has been shown to spread to many different sites in patients (Huh et al., 2015). Because A673 cells were able to grow in sites outside of the primary leg muscle, this implied that it may be plausible to develop a metastatic Ewing sarcoma mouse model using these cells.

4.3.1 Stable transfection of A673 cells

The A673 Luc-4 cells contained inadequate levels of luciferase activity so were unable to be used for quantification of tumour growth and metastasis *in vivo*. Consequently, A673 cells underwent a stable transfection (with the pcDNA3.1(+)/Luc2=tdT plasmid) and sorted to generate luciferase tagged A673 cells (Figure 23). The expectation was this transfection would be more successful than the virally-transduced experiment discussed in 4.2.1, as this method would avoid any potential viral silencing that may have occurred in the A673 Luc-4 cells. The flow cytometry single cell sorting of the stable-transfected cells was not successful due to a defect in the FACSAria Accudrop function. Hence the polyclonal population A673 luc-polyclonal-2 (Appendix 8) which was sorted by the defective FACSAria and composed of a large quantity of tomato positive cells was used to generate A673 luciferase expressing clones via limiting dilution (Fuller et al., 2001; Gross et al., 2015), with the nomenclature A673 Luc1L, A673 Luc2L. Other clones were generated via the G418 antibiotic selection of clones post stable transfection, denoted A673 Luc1G, A673 Luc2G.

The clones were considered based on their clonicity, luciferase activity (Figure 24) as well as sensitivity to the proteasome inhibitors (Figure 25). Previous studies by the lab into generating metastatic osteosarcoma mouse models in which the metastatic spread was monitored via IVIS imaging used the KRIB Luc-20 cell line (Harris et al., 2020b; Harris et al., 2020c) (Figure 24A). Consequently, a clone with similar or higher levels of luciferase activity was sought. Based on these data, all clones generated via limiting dilution were appropriate. A673 Luc3L was selected as it contained intermediate luciferase activity, comparable to KRIB Luc-20. A673 Luc1G was the only clone amongst the G418 resistant clones (A673 Luc1G-6G) which contained appropriate luciferase activity. The reason for this was not determined although it could be related to the dampening of gene expression

as discussed in section 4.2.1 as a result of DNA methylation (Smith & Meissner, 2013), histone modifications (Bannister & Kouzarides, 2011) or as a protective mechanism against foreign DNA (Mok & Lever, 2007). It could not be determined for sure without further experimentation, which was deemed unnecessary for this project as an appropriate clone was selected.

4.3.2 A673 Ewing sarcoma metastatic nude mouse model

The current ineffectiveness of chemotherapies against metastatic Ewing sarcoma has led to minimal improvements in survival over recent times, with current 5-year survival rates of below 30% (Hamilton et al., 2017). Due its severity it was deemed important to generate a metastatic mouse model in this project to better understand the metastatic growth and spread of Ewing sarcoma. Extraskeletal Ewing sarcoma presents with the localised disease in soft tissues most commonly surrounding the pelvis and thorax, with common occurrences of metastasis to the lymph nodes or bones (Huh et al., 2015). Other less common sites of detectable metastasis were the lungs, abdominal organs, peritoneum and the brain (Huh et al., 2015; Murthy et al., 2020). On the other hand, skeletal Ewing sarcoma presents in the axial and non-axial skeleton most frequently in long tubular bones and flat bones (ribs, pelvis and vertebrae)(Murthy et al., 2020), with metastasis commonly to the lungs or bones (Worch et al., 2018). A673 cells are of extraskeletal origin due to being resected from a primary Ewing sarcoma muscle tumour (Giard et al., 1973).

The metastatic mouse model in this project was established via administering the nude mice with an anti-asialo-GM1 (NK depletion) antibody prior to intravenous A673 Luc3L cell inoculation, which has previously been shown to be effective using osteosarcoma cells in nude mice (Harris et al., 2020c). This method has not previously been attempted using Ewing sarcoma cells. Natural killer cells (NK cells) are cells of the innate immune system

which recognise foreign molecules in the body mainly via the interaction with the self-major histocompatibility complex (MHC)-I (Abel et al., 2018). MHC class I receptors are expressed on the surface of healthy cells which prevent their destruction by NK cells, whilst virus invaded cells or cancer cells lose their MHC class I expression (Abel et al., 2018). As a result these foreign or infected cells are recognised by NK cells and destroyed by the activation of death receptors by TNFα and IFN-γ secretion as well as the release of cytolytic molecules (Abel et al., 2018). In a clinical setting NK cells play a major role in the rate and severity of metastasis, with higher circulating NK cells correlating with reduced metastasis and with greater clinical outcomes in gastrointestinal sarcomas (Delahaye et al., 2011) and prostate cancer patients (Gannon et al., 2009). Whilst it has not been reported for Ewing sarcoma patients, in a murine setting treating Ewing sarcoma xenograft mice with NK cells expanded *ex vivo* significantly limited pulmonary metastasis, with little effect on the primary disease (Tong et al., 2017). Consequently, it would be useful to transiently deplete NK cells in a mouse as a means of enhancing metastatic spread to successfully develop a Ewing sarcoma metastatic mouse model.

The nude mice in this project were either administered saline or NK depletion prior to intravenous inoculation with either 150,000 (Figure 26) or 500,000 (Figure 27) A673 Luc3L cells. When inoculated with 150,000 A673 Luc3L cells only two mice (both in the NK depletion group) had detectable *in vivo* metastasis. This was insufficient for the model to be used in drug efficacy studies. Via endpoint *ex vivo* analysis bioluminescence was detected in numerous mouse organs including the lungs, brain, liver, kidneys, stomach, muscle, and adipose tissue (Figure 26). Smaller tumours were detected *ex vivo* in the saline treated mice highlighting the importance of the NK depletion to generate a metastatic mouse model. While this was the case, weak widespread signals were detected *in vivo* on day 28 in the NK depletion mice 767-770 in the lower body which may have been liver metastasis which was detected *ex vivo*. These small widespread signals were not counted

as detectable *in vivo* metastasis as they were only present in a single imaging session without a distinct hotspot site of tumour growth. This demonstrated that in this model in particular NK cells were able to discourage growth and rate of growth of Ewing sarcoma metastasis. The murine metastatic model was attempted again, this time successfully by increasing the cell dosage to 500,000 A673 Luc3L cells per nude mouse (Figure 27). Four out of five NK depletion mice had detectable metastasis *in vivo* in the legs, rib cage and lungs. On further analysis, metastatic disease was also detected *ex vivo* in the lungs, brain, liver, kidneys, heart, muscles, and bones. This is consistent with metastatic spread in extraskeletal Ewing sarcoma patients. At the same time, all five saline treated mice had no detectable *in vivo* or *ex vivo* metastasis at any time during this study, further highlighting the importance and novelty of using NK depletion in this model. In the metastatic mouse model generated in this project, no mice were required to be culled because of cancer related symptoms at the endpoint of day 28. It would be useful to repeat this experiment and monitor metastatic spread in the mice until the onset of symptoms rather than a set endpoint. This would allow for further detection of metastasis as well as demonstrating whether the saline mice with 500,000 A673 Luc3L cells were ever able to develop any detectable metastasis or whether circulating NK cells were preventing this from occurring.

Previously published models used 1-2 million A673 cells which were intravenously inoculated into nude mice, with only lung metastasis reported (Garcia-Monclús et al., 2018; Lagares-Tena et al., 2016; Sáinz-Jaspeado et al., 2010). Although the authors were able to generate metastasis without NK depletion, it seemed as if these protocols were inefficient with small tumours detected 45 to 60 days post cell inoculation even though up to four times as many cells were administered in those mice compared to this study (Garcia-Monclús et al., 2018; Lagares-Tena et al., 2016; Sáinz-Jaspeado et al., 2010). The only recorded metastatic sites in these models were the lungs with no metastatic disease reported at other sites. There is a possibility that other sites were not analysed by the authors or their

models were far less effective at generating widespread metastasis as seen in the clinic compared to the model generated in this project.

Interestingly the only mouse model showing widespread metastatic spread with A673 cells were in NOD/SCID mice (Chaturvedi et al., 2014). In that model metastatic spread was detected in the lungs, tibia, rib cage and spine following injection of A673 cells into the tibia (Chaturvedi et al., 2014). A major difference between NOD/SCID mice compared to the nude mice used in this study is that NOD/SCID mice lack NK cells (Shultz et al., 1995). This may explain why the authors were able to detect A673 metastasis without NK depletion. At the same time, this process was quite invasive on the mice as it required predrilling the tibia of the mice prior to cell inoculation, compared to intravenous injections used here. A flaw with the model developed by Chaturvedi et al. (2014) was that they initiated primary tumour growth in the tibia which was not the orthotopically relevant site of A673 cells which were resected from a muscle tumour. Other disadvantages of the NOD/SCID published metastatic model (Chaturvedi et al., 2014) were that although it identified as a metastatic Ewing sarcoma mouse model the mice still contained a primary Ewing sarcoma tumour, which was not the case in the model developed in this study. The impacts of the primary tibial tumour on the mice may require them to be culled early as a result of reported osteolysis (Chaturvedi et al., 2014) which would hinder the ability to use that model for efficacy in a longer experiment against metastatic Ewing sarcoma.

Future sarcoma nude mouse experiments could be undertaken by transfecting SK-PN-DW and CHLA-10 cells with a luciferase containing plasmid as a means of comparing the metastatic spread in a skeletal versus an extraskeletal cell line. SK-PN-DW cells were derived from the lower spine in the presacral mass (Potluri et al., 1987), so it would be informative to compare how sites of metastasis differed with Ewing cells from different primary origins, as seen in the clinic (Huh et al., 2015). Both SK-PN-DW (Hingorani et

al., 2011) and CHLA-10 (El-Naggar et al., 2019) cells have been previously published to grow in the flanks or renal capsules of immunodeficient mice, with no description of any metastasis. Since it has been highlighted in this project how important depleting NK cells were for the growth of Ewing sarcoma tumours it would be interesting to compare the levels of NK cells in organs of favourable tumour growth versus those less favourable. A previous publication has identified that without NK depletion, 10% of circulating cells in nude mice are NK cells (Harris et al., 2020c) which was evidently enough to prevent the formation of Ewing sarcoma metastases in mice 771-775 (Figure 27). One day post NK depletion, circulating NK levels dropped to 0.6% (Harris et al., 2020c), which provided a favourable outcome for A673 tumour formation, returning to normal NK levels one week later (Harris et al., 2020c). The role of NK cells inhibiting tumour metastasis in nude mice has been previously reported in hepatocellular carcinoma (Hong et al., 2016). The authors established a protocol where NK cells were stained with a fluorescent dye cleaved via the cell's cytoplasm, and implanted in nude mice to observe the localisation and impact of NK cells in a hepatocellular carcinoma model (Hong et al., 2016). They only reported NK cell localisation to the liver, as it was their site of interest, but this experiment would be beneficial to observe the localisation of NK cells in the metastatic Ewing sarcoma mouse model generated in this project. NK cells have been implicated in impeding metastasis in clinical contexts too: patients with high levels of NK cells in the blood stream show fewer and less severe metastasis in gastrointestinal sarcoma (Delahaye et al., 2011) and prostate cancer (Gannon et al., 2009). This has been exploited in patients via the use of CAR-NK cell therapies. These involved isolating NK cells from cancer patients and transducing them using a viral vector to express CAR, a chimeric antigen receptor, as a result the NK cells are able to be specifically targeted for particular antigens of interest such as those on cancer cells (Basar et al., 2020). This technique of cellular immunotherapy has been shown to be safe in patients (Tang et al., 2018), with many current studies attempting to target

metastatic solid tumours to improve tumour selectivity by targeting antigens commonly upregulated in solid tumours such as HER2 and MUC1 (Xie et al., 2020). Although CAR-NK cell therapies have yet to be tested for Ewing sarcoma, the inability of proteasome inhibitors to penetrate solid tumours along with the effectiveness of NK cells to assist in reducing metastatic disease in various patients would make it a viable option for future experimentation.

4.4 Evaluation of primary and metastatic A673 nude mouse models

Whilst the primary Ewing sarcoma nude mouse model required 50,000 A673 Luc-4 cells to develop large detectable tumours, the successful metastatic mouse model required the intravenous inoculation of 500,000 A673 Luc3L cells after NK depletion. Benefits of the A673 primary model were that the cells grew consistently in all mice implanted in the *tibialis anterior* in both the tumourigenicity and efficacy experiments. This consistency meant that an efficacy experiment could be undertaken using the proteasome inhibitors and any differences identified in tumour growth could be attributed to the treatments rather than any potential variability in the models. On the other hand, disadvantages of the primary model with the A673 Luc-4 cells were as previously discussed that the cells did not contain luciferase activity to observe any metastatic spread. Also, as efficacy experiments could only commence once the tumours were palpable, the delay in starting treatments may have impacted any potential drug efficacy. This could have been overcome with luciferase expressing cells as tumour growth would have been detected at earlier stages of the experiment. Alternatively, a beneficial aspect of the metastatic mouse model was that tumour growth rates were consistent, with luminescence readings doubling every few days, whilst the large number of metastatic sites mimicked what is seen in the clinic for extraskeletal metastasis. Whilst this was the case, variability in metastatic sites would complicate the design of experiments aimed at evaluating the efficacy of drugs against

metastases in particular anatomical sites. Although bioluminescence provides information about the location of metastases, it is not precise. This was illustrated in the 500,000 A673 Luc3L model, in which mice 777 and 778 had similar luminescence readings detected in their right legs. It was only determined through *ex vivo* analysis at the endpoint that mouse 777 had metastatic spread to both the muscles and femur whereas mouse 778 had a larger metastasis in the muscle only with no bone involvement. These potential drawbacks of the A673 Luc3L metastatic model along with the variability in the site of metastasis detected would require much larger mouse numbers to determine any significance in treatments tested. Although the mouse models generated in this project have both advantages and drawbacks, and may be useful for identifying potentially useful therapies, it is important to apply these results into more clinically relevant settings. This could be achieved by applying findings of this project as to why tumours grew at certain sites or why treatments were not more effective *in vivo* to improve drug efficacy against primary and metastatic Ewing sarcoma in the clinic.

4.5 A673 tumours and the immune system

Tumours from the A673 metastatic mouse model contained relatively few immune cells (Figure 28A). The frequencies of immune cells in these tumours were evaluated to observe whether immune involvement was playing a role in the growth of these tumours and consequently if immunotherapies could be potentially tested against Ewing sarcoma. In the two tumours analysed from mouse 776, the descending aorta tumour contained a slightly greater proportion of immune cells, including macrophages and neutrophils than the lung sample. NK cells accounted for <3% of cells in both tumours. As stated above, the relatively low levels of NK cells in these tumours compared to previously published NK cell levels in the bloodstream of nude mice (10%) (Harris et al., 2020c) provided a potential insight into why these two sites were favourable for A673 tumour growth. At the

same time these experiments only stained for neutrophils, macrophages, and NK cells so the remaining 20-30% of each of the tumours denoted 'other' could potentially be other immune cells present in these tumours. These Ewing tumours were generated in athymic nude mice, so was expected that they would be composed of fewer immune cells than in a clinical setting, as they lack a thymus so are unable to produce mature functional T cells as well as containing significantly lower circulating lymphocytes compared to mice with a functional thymus (Pantelouris, 1968). In a study analysing the immune tumour microenvironment for Ewing sarcoma via computational analysis of gene expression microarrays, it was identified that macrophages were the most common leukocyte in Ewing sarcoma tumours (Stahl et al., 2019). The second most common cell type were T-cells, where neutrophils and NK cells made up 3 and 6% of all leukocytes in these tumours (Stahl et al., 2019). Other studies have identified that Ewing sarcoma tumours did not have major immune involvement compared to osteosarcomas which were enriched in T and B cells (Dyson et al., 2019). These studies confirmed that whilst Ewing sarcoma tumours were composed of minimal immune filtration that the most common immune cells identified were macrophages, as seen in the Ewing sarcoma tumours from mouse 776 in this study. The authors were able to identify that low levels of neutrophils, high levels of active NK cells and high levels of T cells in Ewing sarcoma tumours correlated with significantly improved overall survival rates (Stahl et al., 2019). To further confirm these findings more immunophenotyping experiments could be undertaken on A673 metastatic tumours in other sites such as the muscle, liver, and brain. The purpose of understanding immune filtration in these Ewing sarcoma tumours was to evaluate whether immunotherapies would be worth pursuing against Ewing sarcoma, as these therapies are more effective in immune rich tumours (Bonaventura et al., 2019). Although little immune infiltration was identified in these tumours, the study only analysed a very small number of tumours and the tumours grew in nude mice who lack an entire immune system. Therefore, to better understand the

composition of immune cells in Ewing sarcoma tumours it would be ideal to use patient's biopsies in the future rather than from nude mice. It would also be advantageous to use a larger panel of immune cell recognition antibodies for dendritic cells, osteoclasts, and granulocytes for greater understanding of the remaining tumour composition of these A673 tumours denoted 'other'.

H & E staining of the A673 metastatic tissue confirmed that the tumour growth at these sites were not embolisms (Figure 28B). Embolisms are intravascular deposits of tumour cells which grow like regular tumours and cause thrombus and blockages of blood vessels (Roberts et al., 2003). Staining various tissue samples of the leg muscle, lungs, and liver, identified that the A673 tumours were growing within the tissue rather than within blood vessels. Although they are a rare phenomenon, pulmonary embolisms have been identified in solid tumours in the clinic in adenocarcinoma (Masoud et al., 2017) and myxofibrosarcoma (Latchana et al., 2017) patients. At the same time, pulmonary embolisms have also been identified clinically in a few occasions in Ewing sarcoma patients (Chang et al., 1996; Villa & Knowling, 2010). No embolisms detected in this metastatic mouse model indicated that the model faithfully represented the extravasation and colonisation steps of metastasis (Fares et al., 2020). Consequently, this model could be used in the future to test drug efficacy against Ewing sarcoma metastases without embolisms in various anatomical sites in nude mice. The advantage of developing a metastatic mouse model which lacks a primary tumour was that the efficacy of drug treatments could be observed directly without impacts from the primary tumour.

4.6 Conclusions and future directions

A673 human Ewing sarcoma cells were able to grow and metastasise in BALB/c nude mice following implantation into the *tibialis anterior*. Experimental metastases could also be

achieved via intravenous inoculation of A673 cells. In a primary tumour setting, both bortezomib and ixazomib both significantly increased the lifespan of mice bearing intramuscular Ewing sarcomas compared to the saline treatment group. On average, bortezomib was able to reduce tumour progression to a greater extent than ixazomib. However only slight reductions in tumour growth rates were observed. A673 cells were also able to successfully form tumours in an experimental metastatic model of extraskeletal Ewing sarcoma, exhibiting spread to many sites such as the lungs, brain, liver, kidneys, and muscle, as seen in patients. The model generated in this project was novel as it achieved Ewing sarcoma metastasis in organs other than the lungs. Consequently, this project was able to generate two A673 nude mouse models to further understand the growth and metastasis of extraskeletal Ewing sarcoma.

In future it would be important to analyse why the proteasome inhibitors showed limited efficacy to primary (intramuscular) Ewing sarcoma, despite the cells that formed those tumours being very sensitive *in vitro*. This finding is a general observation for all solid tumours which have undergone unsuccessful clinical trials with bortezomib (Huang et al., 2014; Maki et al., 2005; Muscal et al., 2013). Therefore, if it was possible to overcome the *in vivo* resistance, proteasome inhibitors may be broadly useful for many cancer types. One reason for this being the inability of the drugs to penetrate the Ewing tumour tissue, as previous studies have demonstrated the importance of a well vascularised solid tumour for improved drug effectiveness of bortezomib (Williamson et al., 2009). This could be tested by culling intramuscular implanted mice when the tumours were smaller and undertaking proteasome and caspase activity assays. These experiments would allow for the evaluation of drug penetration in proteasome inhibitor treated tumours via examining whether cells in the centre of the tumour were affected as much as those on the outer. Other potential reasons for differences between *in vitro* and *in vivo* sensitivity of Ewing sarcoma to proteasome inhibitors were related to differences in proliferation rates in Ewing cells. As

in a 3D model Ewing cells proliferate at slower rates than 2D culture so they may not rely as much on proteasome activity for survival (Fong et al., 2013). If, as expected protein synthesis rates are lower when the cells proliferate slower in tissue than when cultured in suspension or adhered to plastic, the cells may not rely as much on proteasome activity for survival rendering proteasome inhibitors less effective.

Future directions in this project could also involve establishing other primary and metastatic Ewing sarcoma mouse models with luciferase tagged Ewing sarcoma cells, like SK-PN-DW which had similar sensitivity *in vitro* to bortezomib and carfilzomib (Figure 5,6). Other longer-term goals could be to further study synergy *in vitro* between the proteasome inhibitors and other current treatments for Ewing sarcoma such as vincristine and cyclophosphamide, and/or to investigate ways to overcome drug antagonism with cisplatin and doxorubicin. If any synergy was present these treatments could be tested against the primary and metastatic disease in the models developed in this project. Even though metastasis was detected in a variety of sites in A673 intravenous model, consistent growth in the leg and chest regions would make this experiment feasible, although relatively large numbers of mice would be needed given the heterogeneity in metastasis sites. These Ewing mouse models could also evaluate the *in vivo* efficacy of BH3 mimetics such as navitoclax, which was the second most effective agent at reducing cell viability of A673 cells *in vitro* (Figure 3).

Other goals for this project would be to test the effectiveness of proteasome inhibitors towards Ewing sarcoma tumour patient samples cultured *ex vivo* from various sites of origin. This would enable an ability to compare the effectiveness of these therapies in heterogenous patient samples previously treated with chemotherapies which could also alter the drug effectiveness of proteasome inhibitors. Ultimately, the goals for this project would be to find a combination treatment possibly involving a proteasome inhibitor and

current chemotherapy agent to provide a second line of treatment for Ewing sarcoma patients.

References

Abbas T, Dutta A (2009) p21 in cancer: intricate networks and multiple activities. *Nature reviews Cancer* 9: 400-14

Abdi J, Chen G, Chang H (2013) Drug resistance in multiple myeloma: latest findings and new concepts on molecular mechanisms. *Oncotarget* 4: 2186-207

Abel AM, Yang C, Thakar MS, Malarkannan S (2018) Natural Killer Cells: Development, Maturation, and Clinical Utilization. *Frontiers in immunology* 9: 1869

Agaram NP, Zhang L, LeLoarer F, Silk T, Sung YS, Scott SN, Kuk D, Qin LX, Berger MF, Antonescu CR, Singer S (2016) Targeted exome sequencing profiles genetic alterations in leiomyosarcoma. *Genes, chromosomes & cancer* 55: 124-30

Al-Eisawi Z, Beale P, Chan C, Yu JQ, Huq F (2011) Modulation of cisplatin cytotoxicity due to its combination with bortezomib and the nature of its administration. *Anticancer research* 31: 2757-62

Allen MM, Douds JJ, Liang SX, Desouki MM, Parkash V, Fadare O (2015) An immunohistochemical analysis of stathmin 1 expression in uterine smooth muscle tumors: differential expression in leiomyosarcomas and leiomyomas. *International journal of clinical and experimental pathology* 8: 2795-801

Altun M, Galardy PJ, Shringarpure R, Hideshima T, LeBlanc R, Anderson KC, Ploegh HL, Kessler BM (2005) Effects of PS-341 on the activity and composition of proteasomes in multiple myeloma cells. *Cancer Res* 65: 7896-901

Amaravadi RK, Schilder RJ, Martin LP, Levin M, Graham MA, Weng DE, Adjei AA (2015) A Phase I Study of the SMAC-Mimetic Birinapant in Adults with Refractory Solid Tumors or Lymphoma. *Molecular cancer therapeutics* 14: 2569-75

Ambati SR, Lopes EC, Kosugi K, Mony U, Zehir A, Shah SK, Taldone T, Moreira AL, Meyers PA, Chiosis G, Moore MA (2014) Pre-clinical efficacy of PU-H71, a novel HSP90 inhibitor, alone and in combination with bortezomib in Ewing sarcoma. *Molecular oncology* 8: 323-36

Applebaum MA, Worch J, Matthay KK, Goldsby R, Neuhaus J, West DC, Dubois SG (2011) Clinical features and outcomes in patients with extraskeletal Ewing sarcoma. *Cancer* 117: 3027-32

Augello G, Modica M, Azzolina A, Puleio R, Cassata G, Emma MR, Di Sano C, Cusimano A, Montalto G, Cervello M (2018) Preclinical evaluation of antitumor activity of the proteasome inhibitor MLN2238 (ixazomib) in hepatocellular carcinoma cells. *Cell Death & Disease* 9: 28

Bai Y, Su X (2021) Updates to the drug-resistant mechanism of proteasome inhibitors in multiple myeloma. *Asia-Pacific Journal of Clinical Oncology* 17: 29-35

Bailly RA, Bosselut R, Zucman J, Cormier F, Delattre O, Roussel M, Thomas G, Ghysdael J (1994) DNA-binding and transcriptional activation properties of the EWS-FLI-1 fusion protein resulting from the t(11;22) translocation in Ewing sarcoma. *Molecular and cellular biology* 14: 3230-41

Baklaushev VP, Kilpeläinen A, Petkov S, Abakumov MA, Grinenko NF, Yusubalieva GM, Latanova AA, Gubskiy IL, Zabozlaev FG, Starodubova ES, Abakumova TO, Isaguliants MG, Chekhonin VP (2017) Luciferase Expression Allows Bioluminescence Imaging But

Imposes Limitations on the Orthotopic Mouse (4T1) Model of Breast Cancer. *Scientific reports* 7: 7715

Banfalvi G (2017) Methods to detect apoptotic cell death. *Apoptosis : an international journal on programmed cell death* 22: 306-323

Bannister AJ, Kouzarides T (2011) Regulation of chromatin by histone modifications. *Cell research* 21: 381-95

Bao X, Ren T, Huang Y, Ren C, Yang K, Zhang H, Guo W (2017) Bortezomib induces apoptosis and suppresses cell growth and metastasis by inactivation of Stat3 signaling in chondrosarcoma. *International journal of oncology* 50: 477-486

Barker LM, Pendergrass TW, Sanders JE, Hawkins DS (2005) Survival after recurrence of Ewing's sarcoma family of tumors. *Journal of clinical oncology : official journal of the American Society of Clinical Oncology* 23: 4354-62

Barr FG, Galili N, Holick J, Biegel JA, Rovera G, Emanuel BS (1993) Rearrangement of the PAX3 paired box gene in the paediatric solid tumour alveolar rhabdomyosarcoma. *Nature genetics* 3: 113-7

Basar R, Daher M, Rezvani K (2020) Next-generation cell therapies: the emerging role of CAR-NK cells. *Blood Advances* 4: 5868-5876

Batra S, Reynolds CP, Maurer BJ (2004) Fenretinide cytotoxicity for Ewing's sarcoma and primitive neuroectodermal tumor cell lines is decreased by hypoxia and synergistically enhanced by ceramide modulators. *Cancer Res* 64: 5415-24

Beaumont KA, Hill DS, Daignault SM, Lui GYL, Sharp DM, Gabrielli B, Weninger W, Haass NK (2016) Cell Cycle Phase-Specific Drug Resistance as an Escape Mechanism of Melanoma Cells. *Journal of Investigative Dermatology* 136: 1479-1489

Berkers CR, Leestemaker Y, Schuurman KG, Ruggeri B, Jones-Bolin S, Williams M, Ovaa H (2012) Probing the specificity and activity profiles of the proteasome inhibitors bortezomib and delanzomib. *Molecular pharmaceutics* 9: 1126-35

Berman SD, Calo E, Landman AS, Danielian PS, Miller ES, West JC, Fonhoue BD, Caron A, Bronson R, Bouxsein ML, Mukherjee S, Lees JA (2008) Metastatic osteosarcoma induced by inactivation of Rb and p53 in the osteoblast lineage. *Proceedings of the National Academy of Sciences* 105: 11851

Bersani F, Taulli R, Accornero P, Morotti A, Miretti S, Crepaldi T, Ponzetto C (2008) Bortezomib-mediated proteasome inhibition as a potential strategy for the treatment of rhabdomyosarcoma. *European journal of cancer (Oxford, England : 1990)* 44: 876-84

Bianchi G, Oliva L, Cascio P, Pengo N, Fontana F, Cerruti F, Orsi A, Pasqualetto E, Mezghrani A, Calbi V, Palladini G, Giuliani N, Anderson KC, Sitia R, Cenci S (2009) The proteasome load versus capacity balance determines apoptotic sensitivity of multiple myeloma cells to proteasome inhibition. *Blood* 113: 3040-9

Bloomer DT, Kitevska-Ilioski T, Pantaki-Eimany D, Ji Y, Miles MA, Heras B, Hawkins CJ (2019) CrmA orthologs from diverse poxviruses potently inhibit caspases-1 and -8, yet cleavage site mutagenesis frequently produces caspase-1-specific variants. *The Biochemical journal* 476: 1335-1357

Bonaventura P, Shekarian T, Alcazer V, Valladeau-Guilemond J, Valsesia-Wittmann S, Amigorena S, Caux C, Depil S (2019) Cold Tumors: A Therapeutic Challenge for Immunotherapy. *Frontiers in immunology* 10: 168

Brada M, Judson I, Beale P, Moore S, Reidenberg P, Statkevich P, Dugan M, Batra V, Cutler D (1999) Phase I dose-escalation and pharmacokinetic study of temozolomide (SCH 52365) for refractory or relapsing malignancies. *British journal of cancer* 81: 1022-30

Bridge J, Hogendoorn P, DM C, Bridge JA, CW P, Fletcher CD (2013) *WHO classification of tumours of soft tissue and bone*. International Agency for Research on Cancer,

Budenholzer L, Cheng CL, Li Y, Hochstrasser M (2017) Proteasome Structure and Assembly. *Journal of molecular biology* 429: 3500-3524

Cardiff RD, Miller CH, Munn RJ (2014) Manual hematoxylin and eosin staining of mouse tissue sections. *Cold Spring Harbor protocols* 2014: 655-8

Caserta TM, Smith AN, Gultice AD, Reedy MA, Brown TL (2003) Q-VD-OPh, a broad spectrum caspase inhibitor with potent antiapoptotic properties. *Apoptosis : an international journal on programmed cell death* 8: 345-52

Cenci S, Oliva L, Cerruti F, Milan E, Bianchi G, Raule M, Mezghrani A, Pasqualetto E, Sitia R, Cascio P (2012) Pivotal Advance: Protein synthesis modulates responsiveness of differentiating and malignant plasma cells to proteasome inhibitors. *Journal of leukocyte biology* 92: 921-31

Chang SK, Wang TL, Teh M (1996) Extraskeletal Ewing's sarcoma presenting with pulmonary embolism. *Australasian radiology* 40: 175-8

Chaturvedi A, Hoffman LM, Jensen CC, Lin YC, Grossmann AH, Randall RL, Lessnick SL, Welm AL, Beckerle MC (2014) Molecular dissection of the mechanism by which EWS/FLI expression compromises actin cytoskeletal integrity and cell adhesion in Ewing sarcoma. *Molecular biology of the cell* 25: 2695-709

Chen C, Borker R, Ewing J, Tseng WY, Hackshaw MD, Saravanan S, Dhanda R, Nadler E (2014) Epidemiology, treatment patterns, and outcomes of metastatic soft tissue sarcoma in a community-based oncology network. *Sarcoma* 2014: 145764

Chen L, Madura K (2005) Increased proteasome activity, ubiquitin-conjugating enzymes, and eEF1A translation factor detected in breast cancer tissue. *Cancer Res* 65: 5599-606

Chen MB, Whisler JA, Jeon JS, Kamm RD (2013) Mechanisms of tumor cell extravasation in an in vitro microvascular network platform. *Integrative biology : quantitative biosciences from nano to macro* 5: 1262-71

Chou TC (2010) Drug combination studies and their synergy quantification using the Chou-Talalay method. *Cancer Res* 70: 440-6

Cotterill SJ, Ahrens S, Paulussen M, Jürgens HF, Voûte PA, Gadner H, Craft AW (2000) Prognostic Factors in Ewing's Tumor of Bone: Analysis of 975 Patients From the European Intergroup Cooperative Ewing's Sarcoma Study Group. *Journal of Clinical Oncology* 18: 3108-3114

Coupland LA, Chong BH, Parish CR (2013) Beware of NK cells in pre-clinical metastasis models. *Clinical & Experimental Metastasis* 30: 945-947

Crist WM, Garnsey L, Beltangady MS, Gehan E, Ruymann F, Webber B, Hays DM, Wharam M, Maurer HM (1990) Prognosis in children with rhabdomyosarcoma: a report of the intergroup rhabdomyosarcoma studies I and II. Intergroup Rhabdomyosarcoma Committee. *Journal of clinical oncology : official journal of the American Society of Clinical Oncology* 8: 443-52

Crose LE, Galindo KA, Kephart JG, Chen C, Fitamant J, Bardeesy N, Bentley RC, Galindo RL, Chi JT, Linardic CM (2014) Alveolar rhabdomyosarcoma-associated PAX3-FOXO1

promotes tumorigenesis via Hippo pathway suppression. *The Journal of clinical investigation* 124: 285-96

Dai H, Meng XW, Kaufmann SH (2016) Mitochondrial apoptosis and BH3 mimetics. *F1000Research* 5: 2804

Damiano JS, Cress AE, Hazlehurst LA, Shtil AA, Dalton WS (1999) Cell adhesion mediated drug resistance (CAM-DR): role of integrins and resistance to apoptosis in human myeloma cell lines. *Blood* 93: 1658-67

Damiano JS, Hazlehurst LA, Dalton WS (2001) Cell adhesion-mediated drug resistance (CAM-DR) protects the K562 chronic myelogenous leukemia cell line from apoptosis induced by BCR/ABL inhibition, cytotoxic drugs, and gamma-irradiation. *Leukemia* 15: 1232-9

Delahaye NF, Rusakiewicz S, Martins I, Ménard C, Roux S, Lyonnet L, Paul P, Sarabi M, Chaput N, Semeraro M, Minard-Colin V, Poirier-Colame V, Chaba K, Flament C, Baud V, Authier H, Kerdine-Römer S, Pallardy M, Cremer I, Peaudecerf L et al. (2011) Alternatively spliced NKp30 isoforms affect the prognosis of gastrointestinal stromal tumors. *Nature Medicine* 17: 700-707

Demicco EG, Boland GM, Brewer Savannah KJ, Lusby K, Young ED, Ingram D, Watson KL, Bailey M, Guo X, Hornick JL, van de Rijn M, Wang WL, Torres KE, Lev D, Lazar AJ (2015) Progressive loss of myogenic differentiation in leiomyosarcoma has prognostic value. *Histopathology* 66: 627-38

Demo SD, Kirk CJ, Aujay MA, Buchholz TJ, Dajee M, Ho MN, Jiang J, Laidig GJ, Lewis ER, Parlati F, Shenk KD, Smyth MS, Sun CM, Vallone MK, Woo TM, Molineaux CJ, Bennett MK (2007) Antitumor activity of PR-171, a novel irreversible inhibitor of the proteasome. *Cancer Res* 67: 6383-91

Deshantri AK, Metselaar JM, Zagkou S, Storm G, Mandhane SN, Fens MHAM, Schiffelers RM (2019) Development and characterization of liposomal formulation of bortezomib. *International Journal of Pharmaceutics: X* 1: 100011

Dimopoulos M, Siegel D, White DJ, Boccia R, Iskander KS, Yang Z, Kimball AS, Mezzi K, Ludwig H, Niesvizky R (2019) Carfilzomib vs bortezomib in patients with multiple myeloma and renal failure: a subgroup analysis of ENDEAVOR. *Blood* 133: 147-155

Donaldson KL, Goolsby GL, Wahl AF (1994) Cytotoxicity of the anticancer agents cisplatin and taxol during cell proliferation and the cell cycle. *Int J Cancer* 57: 847-55

Dou QP, Smith DM, Daniel KG, Kazi A (2003) Interruption of tumor cell cycle progression through proteasome inhibition: implications for cancer therapy. *Progress in cell cycle research* 5: 441-6

Du C, Fang M, Li Y, Li L, Wang X (2000) Smac, a mitochondrial protein that promotes cytochrome c-dependent caspase activation by eliminating IAP inhibition. *Cell* 102: 33-42

Duan Z, Gao Y, Shen J, Choy E, Cote G, Harmon D, Bernstein K, Lozano-Calderon S, Mankin H, Hornicek FJ (2017) miR-15b modulates multidrug resistance in human osteosarcoma in vitro and in vivo. *Molecular oncology* 11: 151-166

Duman BB, Gunaldi M, Ercolak V, Afsar CU, Sahin B, Erkisi IM, Kara O, Paydas S, Gönlüsen G, Sertdemir Y (2012) Retrospective analysis of 498 primary soft tissue sarcomas in a single Turkish centre. *Asian Pacific journal of cancer prevention : APJCP* 13: 4125-8

Dyson KA, Stover BD, Grippin A, Mendez-Gomez HR, Lagmay J, Mitchell DA, Sayour EJ (2019) Emerging trends in immunotherapy for pediatric sarcomas. *Journal of Hematology & Oncology* 12: 78

Eckelman BP, Salvesen GS (2006) The human anti-apoptotic proteins cIAP1 and cIAP2 bind but do not inhibit caspases. *The Journal of biological chemistry* 281: 3254-60

Edrissi B, Taghizadeh K, Dedon PC (2013) Quantitative analysis of histone modifications: formaldehyde is a source of pathological n(6)-formyllysine that is refractory to histone deacetylases. *PLoS genetics* 9: e1003328

El-Far AH, Darwish NHE, Mousa SA (2020) Senescent Colon and Breast Cancer Cells Induced by Doxorubicin Exhibit Enhanced Sensitivity to Curcumin, Caffeine, and Thymoquinone. *Integrative cancer therapies* 19: 1534735419901160

El-Naggar AM, Somasekharan SP, Wang Y, Cheng H, Negri GL, Pan M, Wang XQ, Delaidelli A, Rafn B, Cran J, Zhang F, Zhang H, Colborne S, Gleave M, Mandinova A, Kedersha N, Hughes CS, Surdez D, Delattre O, Wang Y et al. (2019) Class I HDAC inhibitors enhance YB-1 acetylation and oxidative stress to block sarcoma metastasis. *EMBO reports* 20: e48375

Ewing J (1972) Diffuse endothelioma of bone. *CA: A Cancer Journal for Clinicians* 22: 95-98

Fares J, Fares MY, Khachfe HH, Salhab HA, Fares Y (2020) Molecular principles of metastasis: a hallmark of cancer revisited. *Signal Transduction and Targeted Therapy* 5: 28

Faria M, Matos P, Pereira T, Cabrera R, Cardoso BA, Bugalho MJ, Silva AL (2017) RAC1b overexpression stimulates proliferation and NF-kB-mediated anti-apoptotic signaling in thyroid cancer cells. *PloS one* 12: e0172689

Fletcher C, Bridge J, Hogendoorn P, Mertens F (2013) World Health Organization Classification of Tumours (2013) Pathology and genetics of tumours of soft tissue and bone. In WHO Press, Lyon

Fletcher CD, Bridge JA, Hogendoorn PC, Mertens F (2003) WHO Classification of tumours of soft tissue and bone. 2013. *Lyon: IARC*: 305-310

Foley OW, Rauh-Hain JA, Clemmer J, Clark RM, Hall T, Diver EJ, Schorge JO, del Carmen MG (2015) Trends in the treatment of uterine leiomyosarcoma in the Medicare population. *International journal of gynecological cancer : official journal of the International Gynecological Cancer Society* 25: 453-8

Fong EL, Lamhamedi-Cherradi SE, Burdett E, Ramamoorthy V, Lazar AJ, Kasper FK, Farach-Carson MC, Vishwamitra D, Demicco EG, Menegaz BA, Amin HM, Mikos AG, Ludwig JA (2013) Modeling Ewing sarcoma tumors in vitro with 3D scaffolds. *Proceedings of the National Academy of Sciences of the United States of America* 110: 6500-5

Fuertes MA, Castilla J, Alonso C, Pérez JM (2003) Cisplatin biochemical mechanism of action: from cytotoxicity to induction of cell death through interconnections between apoptotic and necrotic pathways. *Current medicinal chemistry* 10: 257-66

Fujii H, Honoki K, Tsujiuchi T, Kido A, Yoshitani K, Takakura Y (2009) Sphere-forming stem-like cell populations with drug resistance in human sarcoma cell lines. *International journal of oncology* 34: 1381-6

Fujiwara T, Ozaki T (2016) Overcoming Therapeutic Resistance of Bone Sarcomas: Overview of the Molecular Mechanisms and Therapeutic Targets for Bone Sarcoma Stem Cells. *Stem cells international* 2016: 2603092

Fulda S (2017) Chapter Four - Smac Mimetics to Therapeutically Target IAP Proteins in Cancer. In *International Review of Cell and Molecular Biology*, Galluzzi L (ed) pp 157-169. Academic Press

Fuller SA, Takahashi M, Hurrell JG (2001) Cloning of hybridoma cell lines by limiting dilution. *Current protocols in molecular biology* Chapter 11: Unit11.8

Gallerani E, Zucchetti M, Brunelli D, Marangon E, Noberasco C, Hess D, Delmonte A, Martinelli G, Böhm S, Driessen C, De Braud F, Marsoni S, Cereda R, Sala F, D'Incalci M, Sessa C (2013) A first in human phase I study of the proteasome inhibitor CEP-18770 in patients with advanced solid tumours and multiple myeloma. *European journal of cancer (Oxford, England : 1990)* 49: 290-6

Gandhi L, Camidge DR, Ribeiro de Oliveira M, Bonomi P, Gandara D, Khaira D, Hann CL, McKeegan EM, Litvinovich E, Hemken PM, Dive C, Enschede SH, Nolan C, Chiu YL, Busman T, Xiong H, Krivoshik AP, Humerickhouse R, Shapiro GI, Rudin CM (2011) Phase I study of Navitoclax (ABT-263), a novel Bcl-2 family inhibitor, in patients with small-cell lung cancer and other solid tumors. *Journal of clinical oncology : official journal of the American Society of Clinical Oncology* 29: 909-16

Gandolfi S, Laubach JP, Hideshima T, Chauhan D, Anderson KC, Richardson PG (2017) The proteasome and proteasome inhibitors in multiple myeloma. *Cancer metastasis reviews* 36: 561-584

Gannon PO, Poisson AO, Delvoye N, Lapointe R, Mes-Masson A-M, Saad F (2009) Characterization of the intra-prostatic immune cell infiltration in androgen-deprived prostate cancer patients. *Journal of immunological methods* 348: 9-17

Garcia-Monclús S, López-Alemany R, Almacellas-Rabaiget O, Herrero-Martín D, Huertas-Martinez J, Lagares-Tena L, Alba-Pavón P, Hontecillas-Prieto L, Mora J, de Álava E, Rello-Varona S, Giangrande PH, Tirado OM (2018) EphA2 receptor is a key player in the metastatic onset of Ewing sarcoma. *Int J Cancer* 143: 1188-1201

Ghobrial IM, Vij R, Siegel D, Badros A, Kaufman J, Raje N, Jakubowiak A, Savona MR, Obreja M, Berdeja JG (2019) A Phase Ib/II Study of Oprozomib in Patients with Advanced Multiple Myeloma and Waldenström Macroglobulinemia. *Clinical cancer research : an official journal of the American Association for Cancer Research* 25: 4907-4916

Giard DJ, Aaronson SA, Todaro GJ, Arnstein P, Kersey JH, Dosik H, Parks WP (1973) In Vitro Cultivation of Human Tumors: Establishment of Cell Lines Derived From a Series of Solid Tumors2. *JNCI: Journal of the National Cancer Institute* 51: 1417-1423

Gibbs CP, Kukekov VG, Reith JD, Tchigrinova O, Suslov ON, Scott EW, Ghivizzani SC, Ignatova TN, Steindler DA (2005) Stem-like cells in bone sarcomas: implications for tumorigenesis. *Neoplasia (New York, NY)* 7: 967-76

Gierisch ME, Pedot G, Walser F, Lopez-Garcia LA, Jaaks P, Niggli FK, Schäfer BW (2019) USP19 deubiquitinates EWS-FLI1 to regulate Ewing sarcoma growth. *Scientific reports* 9: 951

Gladdy RA, Qin LX, Moraco N, Agaram NP, Brennan MF, Singer S (2013) Predictors of survival and recurrence in primary leiomyosarcoma. *Annals of surgical oncology* 20: 1851-7

Gonzalez H, Hagerling C, Werb Z (2018) Roles of the immune system in cancer: from tumor initiation to metastatic progression. *Genes & development* 32: 1267-1284

Gordon GJ, Mani M, Maulik G, Mukhopadhyay L, Yeap BY, Kindler HL, Salgia R, Sugarbaker DJ, Bueno R (2008) Preclinical studies of the proteasome inhibitor bortezomib in malignant pleural mesothelioma. *Cancer chemotherapy and pharmacology* 61: 549-58

Groll M, Ditzel L, Lowe J, Stock D, Bochtler M, Bartunik HD, Huber R (1997) Structure of 20S proteasome from yeast at 2.4 A resolution. *Nature* 386: 463-71

Gross A, Schoendube J, Zimmermann S, Steeb M, Zengerle R, Koltay P (2015) Technologies for Single-Cell Isolation. *International journal of molecular sciences* 16: 16897-919

Guo KY, Han L, Li X, Yang AV, Lu J, Guan S, Li H, Yu Y, Zhao Y, Yang J, Zhang H (2017) Novel proteasome inhibitor delanzomib sensitizes cervical cancer cells to doxorubicin-induced apoptosis via stabilizing tumor suppressor proteins in the p53 pathway. *Oncotarget* 8: 114123-114135

Gupta N, Hanley MJ, Venkatakrishnan K, Perez R, Norris RE, Nemunaitis J, Yang H, Qian MG, Falchook G, Labotka R, Fu S (2016) Pharmacokinetics of ixazomib, an oral proteasome inhibitor, in solid tumour patients with moderate or severe hepatic impairment. *British journal of clinical pharmacology* 82: 728-38

Hamaguchi T, Doi T, Eguchi-Nakajima T, Kato K, Yamada Y, Shimada Y, Fuse N, Ohtsu A, Matsumoto S, Takanashi M, Matsumura Y (2010) Phase I study of NK012, a novel SN-38-incorporating micellar nanoparticle, in adult patients with solid tumors. *Clinical cancer research : an official journal of the American Association for Cancer Research* 16: 5058-66

Hamilton SN, Carlson R, Hasan H, Rassekh SR, Goddard K (2017) Long-term Outcomes and Complications in Pediatric Ewing Sarcoma. *American journal of clinical oncology* 40: 423-428

Hari P, Paba-Prada CE, Voorhees PM, Frye J, Chang YL, Moreau P, Zonder J, Boccia R, Shain KH (2019) Efficacy and safety results from a phase 1b/2, multicenter, open-label study of oprozomib and dexamethasone in patients with relapsed and/or refractory multiple myeloma. *Leukemia research* 83: 106172

Harris MA, Hawkins CJ, Miles MA (2020a) Tetrazolium reduction assays under-report cell death provoked by clinically relevant concentrations of proteasome inhibitors. *Molecular biology reports* 47: 4849-4856

Harris MA, Miles MA, Shekhar TM, Cerra C, Georgy SR, Ryan SD, Cannon CM, Hawkins CJ (2020b) The Proteasome Inhibitor Ixazomib Inhibits the Formation and Growth of Pulmonary and Abdominal Osteosarcoma Metastases in Mice. *Cancers* 12

Harris MA, Shekhar TM, Coupland LA, Miles MA, Hawkins CJ (2020c) Transient NK Cell Depletion Facilitates Pulmonary Osteosarcoma Metastases After Intravenous Inoculation in Athymic Mice. *J Adolesc Young Adult Oncol*

Hawkins CJ, Uren AG, Häcker G, Medcalf RL, Vaux DL (1996) Inhibition of interleukin 1 beta-converting enzyme-mediated apoptosis of mammalian cells by baculovirus IAP. *Proceedings of the National Academy of Sciences of the United States of America* 93: 13786-90

Hazlehurst LA, Dalton WS (2001) Mechanisms associated with cell adhesion mediated drug resistance (CAM-DR) in hematopoietic malignancies. *Cancer metastasis reviews* 20: 43-50

Heinemann M, Ranft A, Langer T, Jürgens H, Kreyer J, Vieth V, Schäfers M, Weckesser M, Simon T, Hassenpflug W, Corbacioglu S, Bielack S, Mayer-Steinacker R, Kühne T,

van den Berg H, Gelderblom H, Bauer S, Stegger L, Dirksen U (2018) Recurrence of Ewing sarcoma: Is detection by imaging follow-up protocol associated with survival advantage? *Pediatric blood & cancer* 65: e27011

Herndon TM, Deisseroth A, Kaminskas E, Kane RC, Koti KM, Rothmann MD, Habtemariam B, Bullock J, Bray JD, Hawes J, Palmby TR, Jee J, Adams W, Mahayni H, Brown J, Dorantes A, Sridhara R, Farrell AT, Pazdur R (2013) U.S. Food and Drug Administration Approval: Carfilzomib for the Treatment of Multiple Myeloma. 19: 4559-4563

Hideshima T, Anderson KC (2012) Biologic impact of proteasome inhibition in multiple myeloma cells--from the aspects of preclinical studies. *Seminars in hematology* 49: 223-7

Hideshima T, Richardson P, Chauhan D, Palombella VJ, Elliott PJ, Adams J, Anderson KC (2001) The proteasome inhibitor PS-341 inhibits growth, induces apoptosis, and overcomes drug resistance in human multiple myeloma cells. *Cancer Res* 61: 3071-6

Hingorani P, Maas ML, Gustafson MP, Dickman P, Adams RH, Watanabe M, Eshun F, Williams J, Seidel MJ, Dietz AB (2015) Increased CTLA-4(+) T cells and an increased ratio of monocytes with loss of class II (CD14(+) HLA-DR(lo/neg)) found in aggressive pediatric sarcoma patients. *Journal for immunotherapy of cancer* 3: 35

Hingorani P, Zhang W, Lin J, Liu L, Guha C, Kolb EA (2011) Systemic administration of reovirus (Reolysin) inhibits growth of human sarcoma xenografts. *Cancer* 117: 1764-74

Hong SH, Tilan JU, Galli S, Izycka-Swieszewska E, Polk T, Horton M, Mahajan A, Christian D, Jenkins S, Acree R, Connors K, Ledo P, Lu C, Lee YC, Rodriguez O, Toretsky JA, Albanese C, Kitlinska J (2015) High neuropeptide Y release associates with Ewing sarcoma bone dissemination - in vivo model of site-specific metastases. *Oncotarget* 6: 7151-65

Hong YS, Hong SW, Kim SM, Jin DH, Shin JS, Yoon DH, Kim KP, Lee JL, Heo DS, Lee JS, Kim TW (2012) Bortezomib induces G2-M arrest in human colon cancer cells through ROS-inducible phosphorylation of ATM-CHK1. *International journal of oncology* 41: 76-82

Hong ZF, Zhao WX, Yin ZY, Xie CR, Xu YP, Chi XQ, Zhang S, Wang XM (2016) Natural killer cells inhibit pulmonary metastasis of hepatocellular carcinoma in nude mice. *Oncology letters* 11: 2019-2026

Houghton PJ, Morton CL, Kolb EA, Lock R, Carol H, Reynolds CP, Keshelava N, Maris JM, Keir ST, Wu J, Smith MA (2008) Initial testing (stage 1) of the proteasome inhibitor bortezomib by the pediatric preclinical testing program. *Pediatric blood & cancer* 50: 37-45

Hua J, Mutch DG, Herzog TJ (2005) Stable suppression of MDR-1 gene using siRNA expression vector to reverse drug resistance in a human uterine sarcoma cell line. *Gynecol Oncol* 98: 31-8

Huang H, Ding Y, Sun XS, Nguyen TA (2013) Peptide hydrogelation and cell encapsulation for 3D culture of MCF-7 breast cancer cells. *PloS one* 8: e59482

Huang H, Liu N, Zhao K, Zhu C, Lu X, Li S, Lian W, Zhou P, Dong X, Zhao C, Guo H, Zhang C, Yang C, Wen G, Lu L, Li X, Guan L, Liu C, Wang X, Dou QP et al. (2011) Sanggenon C decreases tumor cell viability associated with proteasome inhibition. *Frontiers in bioscience (Elite edition)* 3: 1315-25

Huang HL, Hsing HW, Lai TC, Chen YW, Lee TR, Chan HT, Lyu PC, Wu CL, Lu YC, Lin ST, Lin CW, Lai CH, Chang HT, Chou HC, Chan HL (2010) Trypsin-induced

proteome alteration during cell subculture in mammalian cells. *Journal of biomedical science* 17: 36

Huang Y, Huang X, Cheng C, Xu X, Liu H, Yang X, Yao L, Ding Z, Tang J, He S, Wang Y (2019) Elucidating the expression and function of Numbl during cell adhesion-mediated drug resistance (CAM-DR) in multiple myeloma (MM). *BMC cancer* 19: 1269

Huang Z, Wu Y, Zhou X, Xu J, Zhu W, Shu Y, Liu P (2014) Efficacy of therapy with bortezomib in solid tumors: a review based on 32 clinical trials. *Future oncology (London, England)* 10: 1795-807

Huh J, Kim KW, Park SJ, Kim HJ, Lee JS, Ha HK, Tirumani SH, Ramaiya NH (2015) Imaging Features of Primary Tumors and Metastatic Patterns of the Extraskeletal Ewing Sarcoma Family of Tumors in Adults: A 17-Year Experience at a Single Institution. *Korean journal of radiology* 16: 783-90

Hummel TR, Wagner L, Ahern C, Fouladi M, Reid JM, McGovern RM, Ames MM, Gilbertson RJ, Horton T, Ingle AM, Weigel B, Blaney SM (2013) A pediatric phase 1 trial of vorinostat and temozolomide in relapsed or refractory primary brain or spinal cord tumors: a Children's Oncology Group phase 1 consortium study. *Pediatric blood & cancer* 60: 1452-7

Hung TH, Chen CM, Tseng CP, Shen CJ, Wang HL, Choo KB, Chong KY (2014) FZD1 activates protein kinase C delta-mediated drug-resistance in multidrug-resistant MES-SA/Dx5 cancer cells. *The international journal of biochemistry & cell biology* 53: 55-65

Infante JR, Dees EC, Olszanski AJ, Dhuria SV, Sen S, Cameron S, Cohen RB (2014) Phase I dose-escalation study of LCL161, an oral inhibitor of apoptosis proteins inhibitor, in patients with advanced solid tumors. *Journal of clinical oncology : official journal of the American Society of Clinical Oncology* 32: 3103-10

Infante JR, Mendelson DS, Burris HA, 3rd, Bendell JC, Tolcher AW, Gordon MS, Gillenwater HH, Arastu-Kapur S, Wong HL, Papadopoulos KP (2016) A first-in-human dose-escalation study of the oral proteasome inhibitor oprozomib in patients with advanced solid tumors. *Investigational new drugs* 34: 216-24

Ingley KM, Cohen-Gogo S, Gupta AA (2020) Systemic therapy in pediatric-type soft-tissue sarcoma. *Current oncology (Toronto, Ont)* 27: 6-16

Irvin WJ, Jr., Orlowski RZ, Chiu WK, Carey LA, Collichio FA, Bernard PS, Stijleman IJ, Perou C, Ivanova A, Dees EC (2010) Phase II study of bortezomib and pegylated liposomal doxorubicin in the treatment of metastatic breast cancer. *Clinical breast cancer* 10: 465-70

Israels ED, Israels LG (2001) The Cell Cycle. *STEM CELLS* 19: 88-91

Jacques C, Lamoureux F, Baud'huin M, Rodriguez Calleja L, Quillard T, Amiaud J, Tirode F, Rédini F, Bradner JE, Heymann D, Ory B (2016) Targeting the epigenetic readers in Ewing sarcoma inhibits the oncogenic transcription factor EWS/Fli1. *Oncotarget* 7: 24125-40

Juhasz-Böss I, Gabriel L, Bohle RM, Horn LC, Solomayer EF, Breitbach GP (2018) Uterine Leiomyosarcoma. *Oncology Research and Treatment* 41: 680-686

Kambhampati S, Wiita AP (2020) Lessons Learned from Proteasome Inhibitors, the Paradigm for Targeting Protein Homeostasis in Cancer. In *HSF1 and Molecular Chaperones in Biology and Cancer*, Mendillo ML, Pincus D, Scherz-Shouval R (eds) pp 147-162. Cham: Springer International Publishing

Karski EE, McIlvaine E, Segal MR, Krailo M, Grier HE, Granowetter L, Womer RB, Meyers PA, Felgenhauer J, Marina N, DuBois SG (2016) Identification of Discrete Prognostic Groups in Ewing Sarcoma. *Pediatric blood & cancer* 63: 47-53

Katz RA, Jack-Scott E, Narezkina A, Palagin I, Boimel P, Kulkosky J, Nicolas E, Greger JG, Skalka AM (2007) High-frequency epigenetic repression and silencing of retroviruses can be antagonized by histone deacetylase inhibitors and transcriptional activators, but uniform reactivation in cell clones is restricted by additional mechanisms. *Journal of virology* 81: 2592-604

Khanna N, Pandey A, Bajpai J (2017) Metastatic Ewing's Sarcoma: Revisiting the "Evidence on the Fence". *Indian journal of medical and paediatric oncology : official journal of Indian Society of Medical & Paediatric Oncology* 38: 173-181

Kim JR, Yoon HM, Koh KN, Jung AY, Cho YA, Lee JS (2017) Rhabdomyosarcoma in Children and Adolescents: Patterns and Risk Factors of Distant Metastasis. *AJR American journal of roentgenology* 209: 409-416

Kisselev AF, Callard A, Goldberg AL (2006) Importance of the different proteolytic sites of the proteasome and the efficacy of inhibitors varies with the protein substrate. *The Journal of biological chemistry* 281: 8582-90

Kisselev AF, Goldberg AL (2005) Monitoring activity and inhibition of 26S proteasomes with fluorogenic peptide substrates. *Methods in enzymology* 398: 364-78

Kohsaka S, Shukla N, Ameur N, Ito T, Ng CK, Wang L, Lim D, Marchetti A, Viale A, Pirun M, Socci ND, Qin LX, Sciot R, Bridge J, Singer S, Meyers P, Wexler LH, Barr FG, Dogan S, Fletcher JA et al. (2014) A recurrent neomorphic mutation in MYOD1 defines a clinically aggressive subset of embryonal rhabdomyosarcoma associated with PI3K-AKT pathway mutations. *Nature genetics* 46: 595-600

Kovar H, Dworzak M, Strehl S, Schnell E, Ambros IM, Ambros PF, Gadner H (1990) Overexpression of the pseudoautosomal gene MIC2 in Ewing's sarcoma and peripheral primitive neuroectodermal tumor. *Oncogene* 5: 1067-70

Kuhn DJ, Chen Q, Voorhees PM, Strader JS, Shenk KD, Sun CM, Demo SD, Bennett MK, van Leeuwen FW, Chanan-Khan AA, Orlowski RZ (2007) Potent activity of carfilzomib, a novel, irreversible inhibitor of the ubiquitin-proteasome pathway, against preclinical models of multiple myeloma. *Blood* 110: 3281-90

Kumar SK, Jacobus SJ, Cohen AD, Weiss M, Callander N, Singh AK, Parker TL, Menter A, Yang X, Parsons B, Kumar P, Kapoor P, Rosenberg A, Zonder JA, Faber E, Jr., Lonial S, Anderson KC, Richardson PG, Orlowski RZ, Wagner LI et al. (2020) Carfilzomib or bortezomib in combination with lenalidomide and dexamethasone for patients with newly diagnosed multiple myeloma without intention for immediate autologous stem-cell transplantation (ENDURANCE): a multicentre, open-label, phase 3, randomised, controlled trial. *The Lancet Oncology* 21: 1317-1330

Kupperman E, Lee EC, Cao Y, Bannerman B, Fitzgerald M, Berger A, Yu J, Yang Y, Hales P, Bruzzese F, Liu J, Blank J, Garcia K, Tsu C, Dick L, Fleming P, Yu L, Manfredi M, Rolfe M, Bolen J (2010) Evaluation of the Proteasome Inhibitor MLN9708 in Preclinical Models of Human Cancer. 70: 1970-1980

Lagares-Tena L, Garcia-Monclus S, Lopez-Alemany R, Almacellas-Rabaiget O, Huertas-Martinez J, Sainz-Jaspeado M, Mateo-Lozano S, Rodriguez-Galindo C, Rello-Varona S, Herrero-Martin D, Tirado OM (2016) Caveolin-1 promotes Ewing sarcoma metastasis regulating MMP-9 expression through MAPK/ERK pathway. *Oncotarget* 7: 56889-56903

Laporte AN, Poulin NM, Barrott JJ, Wang XQ, Lorzadeh A, Vander Werff R, Jones KB, Underhill TM, Nielsen TO (2017) Death by HDAC Inhibition in Synovial Sarcoma Cells. *Molecular cancer therapeutics* 16: 2656-2667

Latchana N, Daniel VC, Gould RW, Pollock RE (2017) Pulmonary tumor embolism secondary to soft tissue and bone sarcomas: a case report and literature review. *World Journal of Surgical Oncology* 15: 168

Lau A, Arundine M, Sun HS, Jones M, Tymianski M (2006) Inhibition of caspase-mediated apoptosis by peroxynitrite in traumatic brain injury. *The Journal of neuroscience : the official journal of the Society for Neuroscience* 26: 11540-53

Leavey PJ, Mascarenhas L, Marina N, Chen Z, Krailo M, Miser J, Brown K, Tarbell N, Bernstein ML, Granowetter L, Gebhardt M, Grier HE (2008) Prognostic factors for patients with Ewing sarcoma (EWS) at first recurrence following multi-modality therapy: A report from the Children's Oncology Group. *Pediatric blood & cancer* 51: 334-8

Li G, Zheng YH, Xu L, Feng J, Tang HL, Luo C, Song YP, Chen XQ (2020) BRD4 inhibitor nitroxoline enhances the sensitivity of multiple myeloma cells to bortezomib in vitro and in vivo by promoting mitochondrial pathway-mediated cell apoptosis. *Therapeutic advances in hematology* 11: 2040620720932686

Ling YH, Liebes L, Jiang JD, Holland JF, Elliott PJ, Adams J, Muggia FM, Perez-Soler R (2003) Mechanisms of proteasome inhibitor PS-341-induced G(2)-M-phase arrest and apoptosis in human non-small cell lung cancer cell lines. *Clinical cancer research : an official journal of the American Association for Cancer Research* 9: 1145-54

Liu GT, Huang YL, Tzeng HE, Tsai CH, Wang SW, Tang CH (2015) CCL5 promotes vascular endothelial growth factor expression and induces angiogenesis by down-regulating miR-199a in human chondrosarcoma cells. *Cancer Lett* 357: 476-87

Liu J, Zheng H, Tang M, Ryu YC, Wang X (2008) A therapeutic dose of doxorubicin activates ubiquitin-proteasome system-mediated proteolysis by acting on both the ubiquitination apparatus and proteasome. *American journal of physiology Heart and circulatory physiology* 295: H2541-50

Liu R, Fu C, Sun J, Wang X, Geng S, Wang X, Zou J, Bi Z, Yang C (2017) A New Perspective for Osteosarcoma Therapy: Proteasome Inhibition by MLN9708/2238 Successfully Induces Apoptosis and Cell Cycle Arrest and Attenuates the Invasion Ability of Osteosarcoma Cells *in Vitro*. *Cellular Physiology and Biochemistry* 41: 451-465

Lohberger B, Steinecker-Frohnwieser B, Stuendl N, Kaltenegger H, Leithner A, Rinner B (2016) The Proteasome Inhibitor Bortezomib Affects Chondrosarcoma Cells via the Mitochondria-Caspase Dependent Pathway and Enhances Death Receptor Expression and Autophagy. *PloS one* 11: e0168193

Lu G, Punj V, Chaudhary PM (2008) Proteasome inhibitor Bortezomib induces cell-cycle arrest and apoptosis in cell lines derived from Ewing's sarcoma family of tumors and synergizes with TRAIL. *Cancer Biology & Therapy* 7: 603-608

Ma MH, Yang HH, Parker K, Manyak S, Friedman JM, Altamirano C, Wu ZQ, Borad MJ, Frantzen M, Roussos E, Neeser J, Mikail A, Adams J, Sjak-Shie N, Vescio RA, Berenson JR (2003) The proteasome inhibitor PS-341 markedly enhances sensitivity of multiple myeloma tumor cells to chemotherapeutic agents. *Clinical cancer research : an official journal of the American Association for Cancer Research* 9: 1136-44

Maki RG, Kraft AS, Scheu K, Yamada J, Wadler S, Antonescu CR, Wright JJ, Schwartz GK (2005) A multicenter Phase II study of bortezomib in recurrent or metastatic sarcomas. *Cancer* 103: 1431-1438

Mann BS, Johnson JR, Cohen MH, Justice R, Pazdur R (2007) FDA approval summary: vorinostat for treatment of advanced primary cutaneous T-cell lymphoma. *The oncologist* 12: 1247-52

Marine JC, Lozano G (2010) Mdm2-mediated ubiquitylation: p53 and beyond. *Cell Death & Differentiation* 17: 93-102

Masoud SR, Koegelenberg CF, van Wyk AC, Allwood BW (2017) Fatal tumour pulmonary embolism. *Respirology case reports* 5: e00209

Matyskiela ME, Lander GC, Martin A (2013) Conformational switching of the 26S proteasome enables substrate degradation. *Nature structural & molecular biology* 20: 781-8

McStay GP (2016) In Vitro Use of Peptide Based Substrates and Inhibitors of Apoptotic Caspases. *Methods in molecular biology (Clifton, NJ)* 1419: 57-67

Merino D, Kelly GL, Lessene G, Wei AH, Roberts AW, Strasser A (2018) BH3-Mimetic Drugs: Blazing the Trail for New Cancer Medicines. *Cancer Cell* 34: 879-891

Mills CC, Kolb EA, Sampson VB (2018) Development of Chemotherapy with Cell-Cycle Inhibitors for Adult and Pediatric Cancer Therapy. *Cancer Res* 78: 320-325

Minas TZ, Surdez D, Javaheri T, Tanaka M, Howarth M, Kang HJ, Han J, Han ZY, Sax B, Kream BE, Hong SH, Çelik H, Tirode F, Tuckermann J, Toretsky JA, Kenner L, Kovar H, Lee S, Sweet-Cordero EA, Nakamura T et al. (2017) Combined experience of six independent laboratories attempting to create an Ewing sarcoma mouse model. *Oncotarget* 8: 34141-34163

Mitchell SY, Lingard EA, Kesteven P, McCaskie AW, Gerrand CH (2007) Venous thromboembolism in patients with primary bone or soft-tissue sarcomas. *The Journal of bone and joint surgery American volume* 89: 2433-9

Mlynarczuk-Bialy I, Doeppner TR, Golab J, Nowis D, Wilczynski GM, Parobczak K, Wigand ME, Hajdamowicz M, Biały ŁP, Aniolek O, Henklein P, Bähr M, Schmidt B, Kuckelkorn U, Kloetzel P-M (2014) Biodistribution and Efficacy Studies of the Proteasome Inhibitor BSc2118 in a Mouse Melanoma Model. *Translational Oncology* 7: 570-579

Mok HP, Lever AM (2007) Chromatin, gene silencing and HIV latency. *Genome Biol* 8: 228

Moore D (2016) Panobinostat (Farydak): A Novel Option for the Treatment of Relapsed Or Relapsed and Refractory Multiple Myeloma. *P & T : a peer-reviewed journal for formulary management* 41: 296-300

Moreau P, Karamanesht, II, Domnikova N, Kyselyova MY, Vilchevska KV, Doronin VA, Schmidt A, Hulin C, Leleu X, Esseltine DL, Venkatakrishnan K, Skee D, Feng H, Girgis S, Cakana A, van de Velde H, Deraedt W, Facon T (2012) Pharmacokinetic, pharmacodynamic and covariate analysis of subcutaneous versus intravenous administration of bortezomib in patients with relapsed multiple myeloma. *Clinical pharmacokinetics* 51: 823-9

Moreau P, Masszi T, Grzasko N, Bahlis NJ, Hansson M, Pour L, Sandhu I, Ganly P, Baker BW, Jackson SR, Stoppa A-M, Simpson DR, Gimsing P, Palumbo A, Garderet L, Cavo M, Kumar S, Touzeau C, Buadi FK, Laubach JP et al. (2016) Oral Ixazomib, Lenalidomide, and Dexamethasone for Multiple Myeloma. 374: 1621-1634

Moreau P, Pylypenko H, Grosicki S, Karamanesht I, Leleu X, Grishunina M, Rekhtman G, Masliak Z, Robak T, Shubina A, Arnulf B, Kropff M, Cavet J, Esseltine DL, Feng H, Girgis

S, van de Velde H, Deraedt W, Harousseau JL (2011) Subcutaneous versus intravenous administration of bortezomib in patients with relapsed multiple myeloma: a randomised, phase 3, non-inferiority study. *The Lancet Oncology* 12: 431-40

Murad R, Bakkar R, Sukkar R, Mahmoud F, Al-Dairy A (2019) A Case of Ewing Sarcoma Presenting With Cardiac Metastasis. *World journal for pediatric & congenital heart surgery* 10: 632-634

Murthy SS, Challa S, Raju K, Rajappa SJ, Fonseca D, Gundimeda SD, Rao BV, Ahmed F, Kodandapani S, Nambaru L, Mundada MC, Sharma R, Mallavarapu KM, Koppula VC, Rao TS (2020) Ewing Sarcoma With Emphasis on Extra-skeletal Ewing Sarcoma: A Decade's Experience From a Single Centre in India. *Clinical pathology (Thousand Oaks, Ventura County, Calif)* 13: 2632010x20970210

Muscal JA, Thompson PA, Horton TM, Ingle AM, Ahern CH, McGovern RM, Reid JM, Ames MM, Espinoza-Delgado I, Weigel BJ, Blaney SM (2013) A phase I trial of vorinostat and bortezomib in children with refractory or recurrent solid tumors: a Children's Oncology Group phase I consortium study (ADVL0916). *Pediatric blood & cancer* 60: 390-5

Mutsaers AJ, Ng AJM, Baker EK, Russell MR, Chalk AM, Wall M, Liddicoat BJJ, Ho PWM, Slavin JL, Goradia A, Martin TJ, Purton LE, Dickins RA, Walkley CR (2013) Modeling distinct osteosarcoma subtypes in vivo using Cre:lox and lineage-restricted transgenic shRNA. *Bone* 55: 166-178

Nakamura T, Tanaka K, Matsunobu T, Okada T, Nakatani F, Sakimura R, Hanada M, Iwamoto Y (2007) The mechanism of cross-resistance to proteasome inhibitor bortezomib and overcoming resistance in Ewing's family tumor cells. *International journal of oncology* 31: 803-11

Nesbit ME (1976) Ewing's sarcoma. *CA: A Cancer Journal for Clinicians* 26: 174-180

Nicoletti I, Migliorati G, Pagliacci MC, Grignani F, Riccardi C (1991) A rapid and simple method for measuring thymocyte apoptosis by propidium iodide staining and flow cytometry. *Journal of immunological methods* 139: 271-279

Noborio-Hatano K, Kikuchi J, Takatoku M, Shimizu R, Wada T, Ueda M, Nobuyoshi M, Oh I, Sato K, Suzuki T, Ozaki K, Mori M, Nagai T, Muroi K, Kano Y, Furukawa Y, Ozawa K (2009) Bortezomib overcomes cell-adhesion-mediated drug resistance through downregulation of VLA-4 expression in multiple myeloma. *Oncogene* 28: 231-42

O'Connor OA, Stewart AK, Vallone M, Molineaux CJ, Kunkel LA, Gerecitano JF, Orlowski RZ (2009) A phase 1 dose escalation study of the safety and pharmacokinetics of the novel proteasome inhibitor carfilzomib (PR-171) in patients with hematologic malignancies. *Clinical cancer research : an official journal of the American Association for Cancer Research* 15: 7085-91

Odri GA, Dumoucel S, Picarda G, Battaglia S, Lamoureux F, Corradini N, Rousseau J, Tirode F, Laud K, Delattre O, Gouin F, Heymann D, Redini F (2010) Zoledronic Acid as a New Adjuvant Therapeutic Strategy for Ewings Sarcoma Patients. *Cancer Research* 70: 7610

Offidani M, Corvatta L, Caraffa P, Gentili S, Maracci L, Leoni P (2014) An evidence-based review of ixazomib citrate and its potential in the treatment of newly diagnosed multiple myeloma. *OncoTargets and therapy* 7: 1793-800

Ognjanovic S, Linabery AM, Charbonneau B, Ross JA (2009) Trends in childhood rhabdomyosarcoma incidence and survival in the United States, 1975-2005. *Cancer* 115: 4218-26

Ordóñez JL, Amaral AT, Carcaboso AM, Herrero-Martín D, del Carmen García-Macías M, Sevillano V, Alonso D, Pascual-Pasto G, San-Segundo L, Vila-Ubach M, Rodrigues T, Fraile S, Teodosio C, Mayo-Iscar A, Aracil M, Galmarini CM, Tirado OM, Mora J, de Álava E (2015) The PARP inhibitor olaparib enhances the sensitivity of Ewing sarcoma to trabectedin. *Oncotarget* 6: 18875-90

Orlowski RZ, Stinchcombe TE, Mitchell BS, Shea TC, Baldwin AS, Stahl S, Adams J, Esseltine DL, Elliott PJ, Pien CS, Guerciolini R, Anderson JK, Depcik-Smith ND, Bhagat R, Lehman MJ, Novick SC, O'Connor OA, Soignet SL (2002) Phase I trial of the proteasome inhibitor PS-341 in patients with refractory hematologic malignancies. *Journal of clinical oncology : official journal of the American Society of Clinical Oncology* 20: 4420-7

Pachmayr E, Treese C, Stein U (2017) Underlying Mechanisms for Distant Metastasis - Molecular Biology. *Visceral Medicine* 33: 11-20

Pantelouris EM (1968) Absence of Thymus in a Mouse Mutant. *Nature* 217: 370-371

Parbin S, Kar S, Shilpi A, Sengupta D, Deb M, Rath SK, Patra SK (2014) Histone deacetylases: a saga of perturbed acetylation homeostasis in cancer. *The journal of histochemistry and cytochemistry : official journal of the Histochemistry Society* 62: 11-33

Patatsos K, Shekhar TM, Hawkins CJ (2018) Pre-clinical evaluation of proteasome inhibitors for canine and human osteosarcoma. *Veterinary and comparative oncology* 16: 544-553

Paulis YW, Huijbers EJ, van der Schaft DW, Soetekouw PM, Pauwels P, Tjan-Heijnen VC, Griffioen AW (2015) CD44 enhances tumor aggressiveness by promoting tumor cell plasticity. *Oncotarget* 6: 19634-46

Paulussen M, Bielack S, Jürgens H, Casali PG, Group ObotEGW (2009) Ewing's sarcoma of the bone: ESMO Clinical Recommendations for diagnosis, treatment and follow-up. *Annals of Oncology* 20: iv140-iv142

Peng KA, Grogan T, Wang MB (2014) Head and neck sarcomas: analysis of the SEER database. *Otolaryngology--head and neck surgery : official journal of American Academy of Otolaryngology-Head and Neck Surgery* 151: 627-33

Perez M, Peinado-Serrano J, Garcia-Heredia JM, Felipe-Abrio I, Tous C, Ferrer I, Martin-Broto J, Saez C, Carnero A (2016) Efficacy of bortezomib in sarcomas with high levels of MAP17 (PDZK1IP1). *Oncotarget* 7: 67033-67046

Petitprez F, de Reyniès A, Keung EZ, Chen TW-W, Sun C-M, Calderaro J, Jeng Y-M, Hsiao L-P, Lacroix L, Bougoüin A, Moreira M, Lacroix G, Natario I, Adam J, Lucchesi C, Laizet Yh, Toulmonde M, Burgess MA, Bolejack V, Reinke D et al. (2020) B cells are associated with survival and immunotherapy response in sarcoma. *Nature* 577: 556-560

Petrovic M, Zhao B, Thangam M, Loyalka P, Buja LM, Kar B, Gregoric ID (2016) Ewing Sarcoma in the Right Ventricle. *Texas Heart Institute Journal* 43: 458-460

Potluri VR, Gilbert F, Helsen C, Helson L (1987) Primitive neuroectodermal tumor cell lines: Chromosomal analysis of five cases. *Cancer Genetics and Cytogenetics* 24: 75-86

Präbst K, Engelhardt H, Ringgeler S, Hübner H (2017) Basic Colorimetric Proliferation Assays: MTT, WST, and Resazurin. In *Cell Viability Assays: Methods and Protocols*, Gilbert DF, Friedrich O (eds) pp 1-17. New York, NY: Springer New York

Quach H, White D, Spencer A, Ho PJ, Bhutani D, White M, Inamdar S, Morris C, Ou Y, Gyger M (2017) Pharmacokinetics and safety of carfilzomib in patients with relapsed

multiple myeloma and end-stage renal disease (ESRD): an open-label, single-arm, phase I study. *Cancer Chemother Pharmacol* 79: 1067-1076

Rastogi N, Mishra DP (2012) Therapeutic targeting of cancer cell cycle using proteasome inhibitors. *Cell division* 7: 26

Rautela J, Baschuk N, Slaney CY, Jayatilleke KM, Xiao K, Bidwell BN, Lucas EC, Hawkins ED, Lock P, Wong CS, Chen W, Anderson RL, Hertzog PJ, Andrews DM, Moller A, Parker BS (2015) Loss of Host Type-I IFN Signaling Accelerates Metastasis and Impairs NK-cell Antitumor Function in Multiple Models of Breast Cancer. *Cancer immunology research* 3: 1207-17

Reece DE, Sullivan D, Lonial S, Mohrbacher AF, Chatta G, Shustik C, Burris H, 3rd, Venkatakrishnan K, Neuwirth R, Riordan WJ, Karol M, von Moltke LL, Acharya M, Zannikos P, Keith Stewart A (2011) Pharmacokinetic and pharmacodynamic study of two doses of bortezomib in patients with relapsed multiple myeloma. *Cancer Chemother Pharmacol* 67: 57-67

Rello-Varona S, Fuentes-Guirado M, López-Alemany R, Contreras-Pérez A, Mulet-Margalef N, García-Monclús S, Tirado OM, García Del Muro X (2019) Bcl-x(L) inhibition enhances Dinaciclib-induced cell death in soft-tissue sarcomas. *Scientific reports* 9: 3816

Ricci S, Stone RL, Fader AN (2017) Uterine leiomyosarcoma: Epidemiology, contemporary treatment strategies and the impact of uterine morcellation. *Gynecologic Oncology* 145: 208-216

Richardson PG, Baz R, Wang M, Jakubowiak AJ, Laubach JP, Harvey RD, Talpaz M, Berg D, Liu G, Yu J, Gupta N, Di Bacco A, Hui AM, Lonial S (2014) Phase 1 study of twice-weekly ixazomib, an oral proteasome inhibitor, in relapsed/refractory multiple myeloma patients. *Blood* 124: 1038-46

Richter GH, Plehm S, Fasan A, Rössler S, Unland R, Bennani-Baiti IM, Hotfilder M, Löwel D, von Luettichau I, Mossbrugger I, Quintanilla-Martinez L, Kovar H, Staege MS, Müller-Tidow C, Burdach S (2009) EZH2 is a mediator of EWS/FLI1 driven tumor growth and metastasis blocking endothelial and neuro-ectodermal differentiation. *Proceedings of the National Academy of Sciences of the United States of America* 106: 5324-9

Riley RS, June CH, Langer R, Mitchell MJ (2019) Delivery technologies for cancer immunotherapy. *Nature reviews Drug discovery* 18: 175-196

Roberts KE, Hamele-Bena D, Saqi A, Stein CA, Cole RP (2003) Pulmonary tumor embolism: a review of the literature. *The American Journal of Medicine* 115: 228-232

Rocchi A, Manara MC, Sciandra M, Zambelli D, Nardi F, Nicoletti G, Garofalo C, Meschini S, Astolfi A, Colombo MP, Lessnick SL, Picci P, Scotlandi K (2010) CD99 inhibits neural differentiation of human Ewing sarcoma cells and thereby contributes to oncogenesis. *The Journal of clinical investigation* 120: 668-80

Rodríguez-Galindo C, Navid F, Liu T, Billups CA, Rao BN, Krasin MJ (2007) Prognostic factors for local and distant control in Ewing sarcoma family of tumors. *Annals of Oncology* 19: 814-820

Rouleau C, Gianolio DA, Smale R, Roth SD, Krumbholz R, Harper J, Munroe KJ, Green TL, Horten BC, Schmid SM, Teicher BA (2015) Anti-Endosialin Antibody-Drug Conjugate: Potential in Sarcoma and Other Malignancies. *Molecular cancer therapeutics* 14: 2081-9

Rudin CM, Hann CL, Garon EB, Ribeiro de Oliveira M, Bonomi PD, Camidge DR, Chu Q, Giaccone G, Khaira D, Ramalingam SS, Ranson MR, Dive C, McKeegan EM, Chyla

BJ, Dowell BL, Chakravartty A, Nolan CE, Rudersdorf N, Busman TA, Mabry MH et al. (2012) Phase II study of single-agent navitoclax (ABT-263) and biomarker correlates in patients with relapsed small cell lung cancer. *Clinical cancer research : an official journal of the American Association for Cancer Research* 18: 3163-9

Rushing DA, Piscitelli SC, Rodvold KA, Tewksbury DA (1993) The disposition of doxorubicin on repeated dosing. *Journal of clinical pharmacology* 33: 698-702

Sáinz-Jaspeado M, Lagares-Tena L, Lasheras J, Navid F, Rodriguez-Galindo C, Mateo-Lozano S, Notario V, Sanjuan X, Garcia Del Muro X, Fabra A, Tirado OM (2010) Caveolin-1 modulates the ability of Ewing's sarcoma to metastasize. *Mol Cancer Res* 8: 1489-1500

Sankar S, Bell R, Stephens B, Zhuo R, Sharma S, Bearss DJ, Lessnick SL (2013a) Mechanism and relevance of EWS/FLI-mediated transcriptional repression in Ewing sarcoma. *Oncogene* 32: 5089-5100

Sankar S, Tanner JM, Bell R, Chaturvedi A, Randall RL, Beckerle MC, Lessnick SL (2013b) A novel role for keratin 17 in coordinating oncogenic transformation and cellular adhesion in Ewing sarcoma. *Molecular and cellular biology* 33: 4448-60

Schmidmaier R, Mörsdorf K, Baumann P, Emmerich B, Meinhardt G (2006) Evidence for cell adhesion-mediated drug resistance of multiple myeloma cells in vivo. *The International journal of biological markers* 21: 218-22

Schweitzer A, Aufderheide A, Rudack T, Beck F, Pfeifer G, Plitzko JM, Sakata E, Schulten K, Förster F, Baumeister W (2016) Structure of the human 26S proteasome at a resolution of 3.9 Å. *Proceedings of the National Academy of Sciences of the United States of America* 113: 7816-21

Seddon B, Strauss SJ, Whelan J, Leahy M, Woll PJ, Cowie F, Rothermundt C, Wood Z, Benson C, Ali N, Marples M, Veal GJ, Jamieson D, Küver K, Tirabosco R, Forsyth S, Nash S, Dehbi H-M, Beare S (2017) Gemcitabine and docetaxel versus doxorubicin as first-line treatment in previously untreated advanced unresectable or metastatic soft-tissue sarcomas (GeDDiS): a randomised controlled phase 3 trial. *The Lancet Oncology* 18: 1397-1410

Shah NN, Merchant MS, Cole DE, Jayaprakash N, Bernstein D, Delbrook C, Richards K, Widemann BC, Wayne AS (2016) Vincristine Sulfate Liposomes Injection (VSLI, Marqibo®): Results From a Phase I Study in Children, Adolescents, and Young Adults With Refractory Solid Tumors or Leukemias. *Pediatric blood & cancer* 63: 997-1005

Shain KH, Dalton WS (2001) Cell adhesion is a key determinant in de novo multidrug resistance (MDR): new targets for the prevention of acquired MDR. *Molecular cancer therapeutics* 1: 69-78

Shekhar TM, Burvenich IJG, Harris MA, Rigopoulos A, Zanker D, Spurling A, Parker BS, Walkley CR, Scott AM, Hawkins CJ (2019) Smac mimetics LCL161 and GDC-0152 inhibit osteosarcoma growth and metastasis in mice. *BMC cancer* 19: 924

Shen J, Song G, An M, Li X, Wu N, Ruan K, Hu J, Hu R (2014) The use of hollow mesoporous silica nanospheres to encapsulate bortezomib and improve efficacy for non-small cell lung cancer therapy. *Biomaterials* 35: 316-326

Shern JF, Chen L, Chmielecki J, Wei JS, Patidar R, Rosenberg M, Ambrogio L, Auclair D, Wang J, Song YK, Tolman C, Hurd L, Liao H, Zhang S, Bogen D, Brohl AS, Sindiri S, Catchpoole D, Badgett T, Getz G et al. (2014) Comprehensive genomic analysis of rhabdomyosarcoma reveals a landscape of alterations affecting a common genetic axis in fusion-positive and fusion-negative tumors. *Cancer discovery* 4: 216-31

Shi J, Yang J, Ma X, Wang X (2020) Risk factors for metastasis and poor prognosis of Ewing sarcoma: a population based study. *Journal of orthopaedic surgery and research* 15: 88

Shukla N, Somwar R, Smith RS, Ambati S, Munoz S, Merchant M, D'Arcy P, Wang X, Kobos R, Antczak C, Bhinder B, Shum D, Radu C, Yang G, Taylor BS, Ng CK, Weigelt B, Khodos I, de Stanchina E, Reis-Filho JS et al. (2016) Proteasome Addiction Defined in Ewing Sarcoma Is Effectively Targeted by a Novel Class of 19S Proteasome Inhibitors. *Cancer Res* 76: 4525-34

Shultz LD, Schweitzer PA, Christianson SW, Gott B, Schweitzer IB, Tennent B, McKenna S, Mobraaten L, Rajan TV, Greiner DL, et al. (1995) Multiple defects in innate and adaptive immunologic function in NOD/LtSz-scid mice. *Journal of immunology (Baltimore, Md : 1950)* 154: 180-91

Silke J, Meier P (2013) Inhibitor of apoptosis (IAP) proteins-modulators of cell death and inflammation. *Cold Spring Harbor perspectives in biology* 5

Skapek SX, Anderson J, Barr FG, Bridge JA, Gastier-Foster JM, Parham DM, Rudzinski ER, Triche T, Hawkins DS (2013) PAX-FOXO1 fusion status drives unfavorable outcome for children with rhabdomyosarcoma: a children's oncology group report. *Pediatric blood & cancer* 60: 1411-7

Skorstad M, Kent A, Lieng M (2016) Preoperative evaluation in women with uterine leiomyosarcoma. A nationwide cohort study. *Acta Obstetricia et Gynecologica Scandinavica* 95: 1228-1234

Smith DC, Kalebic T, Infante JR, Siu LL, Sullivan D, Vlahovic G, Kauh JS, Gao F, Berger AJ, Tirrell S, Gupta N, Di Bacco A, Berg D, Liu G, Lin J, Hui AM, Thompson JA (2015) Phase 1 study of ixazomib, an investigational proteasome inhibitor, in advanced non-hematologic malignancies. *Investigational new drugs* 33: 652-63

Smith ZD, Meissner A (2013) DNA methylation: roles in mammalian development. *Nature Reviews Genetics* 14: 204-220

Soave CL, Guerin T, Liu J, Dou QP (2017) Targeting the ubiquitin-proteasome system for cancer treatment: discovering novel inhibitors from nature and drug repurposing. *Cancer metastasis reviews* 36: 717-736

Soriano FX, Chawla S, Skehel P, Hardingham GE (2013) SMRT-mediated co-shuttling enables export of class IIa HDACs independent of their CaM kinase phosphorylation sites. *Journal of neurochemistry* 124: 26-35

Stahl D, Gentles AJ, Thiele R, Gütgemann I (2019) Prognostic profiling of the immune cell microenvironment in Ewing´s Sarcoma Family of Tumors. *OncoImmunology* 8: e1674113

Stahl M, Ranft A, Paulussen M, Bölling T, Vieth V, Bielack S, Görtitz I, Braun-Munzinger G, Hardes J, Jürgens H, Dirksen U (2011) Risk of recurrence and survival after relapse in patients with Ewing sarcoma. *Pediatric blood & cancer* 57: 549-53

Staib P, Tiehen J, Strunk T, Schinköthe T (2005) Determination of caspase-3 activation fails to predict chemosensitivity in primary acute myeloid leukemia blasts. *BMC cancer* 5: 60

Stilgenbauer S, Eichhorst B, Schetelig J, Coutre S, Seymour JF, Munir T, Puvvada SD, Wendtner CM, Roberts AW, Jurczak W, Mulligan SP, Bottcher S, Mobasher M, Zhu M, Desai M, Chyla B, Verdugo M, Enschede SH, Cerri E, Humerickhouse R et al. (2016) Venetoclax in relapsed or refractory chronic lymphocytic leukaemia with 17p deletion: a multicentre, open-label, phase 2 study. *The Lancet Oncology* 17: 768-778

Stiller CA, Trama A, Serraino D, Rossi S, Navarro C, Chirlaque MD, Casali PG (2013) Descriptive epidemiology of sarcomas in Europe: report from the RARECARE project. *European journal of cancer (Oxford, England : 1990)* 49: 684-95

Stolte B, Iniguez AB, Dharia NV, Robichaud AL, Conway AS, Morgan AM, Alexe G, Schauer NJ, Liu X, Bird GH, Tsherniak A, Vazquez F, Buhrlage SJ, Walensky LD, Stegmaier K (2018) Genome-scale CRISPR-Cas9 screen identifies druggable dependencies in TP53 wild-type Ewing sarcoma. *The Journal of experimental medicine* 215: 2137-2155

Suvà ML, Riggi N, Stehle JC, Baumer K, Tercier S, Joseph JM, Suvà D, Clément V, Provero P, Cironi L, Osterheld MC, Guillou L, Stamenkovic I (2009) Identification of cancer stem cells in Ewing's sarcoma. *Cancer Res* 69: 1776-81

Szuhai K, de Jong D, Leung WY, Fletcher CD, Hogendoorn PC (2014) Transactivating mutation of the MYOD1 gene is a frequent event in adult spindle cell rhabdomyosarcoma. *The Journal of Pathology* 232: 300-307

Tada H, Shiho O, Kuroshima K, Koyama M, Tsukamoto K (1986) An improved colorimetric assay for interleukin 2. *J Immunol Methods* 93: 157-65

Tang X, Yang L, Li Z, Nalin AP, Dai H, Xu T, Yin J, You F, Zhu M, Shen W, Chen G, Zhu X, Wu D, Yu J (2018) First-in-man clinical trial of CAR NK-92 cells: safety test of CD33-CAR NK-92 cells in patients with relapsed and refractory acute myeloid leukemia. *American journal of cancer research* 8: 1083-1089

Teng H, Xue L, Wang Y, Ding X, Li J (2020) Nuclear factor kappaB -inducing kinase is a diagnostic marker of gastric cancer. *Medicine* 99: e18864

Thibaudeau TA, Smith DM (2019) A Practical Review of Proteasome Pharmacology. *Pharmacological reviews* 71: 170-197

Thorn CF, Oshiro C, Marsh S, Hernandez-Boussard T, McLeod H, Klein TE, Altman RB (2011) Doxorubicin pathways: pharmacodynamics and adverse effects. *Pharmacogenetics and genomics* 21: 440-6

Tirumani SH, Deaver P, Shinagare AB, Tirumani H, Hornick JL, George S, Ramaiya NH (2014) Metastatic pattern of uterine leiomyosarcoma: retrospective analysis of the predictors and outcome in 113 patients. *Journal of gynecologic oncology* 25: 306-12

Tong AA, Hashem H, Eid S, Allen F, Kingsley D, Huang AY (2017) Adoptive natural killer cell therapy is effective in reducing pulmonary metastasis of Ewing sarcoma. *Oncoimmunology* 6: e1303586

Toro JR, Travis LB, Wu HJ, Zhu K, Fletcher CDM, Devesa SS (2006) Incidence patterns of soft tissue sarcomas, regardless of primary site, in the surveillance, epidemiology and end results program, 1978–2001: An analysis of 26,758 cases. *International Journal of Cancer* 119: 2922-2930

Trautmann F, Schuler M, Schmitt J (2015) Burden of soft-tissue and bone sarcoma in routine care: Estimation of incidence, prevalence and survival for health services research. *Cancer Epidemiology* 39: 440-446

Tsafou K, Katschnig AM, Radic-Sarikas B, Mutz CN, Iljin K, Schwentner R, Kauer MO, Mühlbacher K, Aryee DNT, Westergaard D, Haapa-Paananen S, Fey V, Superti-Furga G, Toretsky J, Brunak S, Kovar H (2018) Identifying the druggable interactome of EWS-FLI1 reveals MCL-1 dependent differential sensitivities of Ewing sarcoma cells to apoptosis inducers. *Oncotarget* 9: 31018-31031

Tse C, Shoemaker AR, Adickes J, Anderson MG, Chen J, Jin S, Johnson EF, Marsh KC, Mitten MJ, Nimmer P, Roberts L, Tahir SK, Xiao Y, Yang X, Zhang H, Fesik S, Rosenberg

SH, Elmore SW (2008) ABT-263: A Potent and Orally Bioavailable Bcl-2 Family Inhibitor. *Cancer Research* 68: 3421-3428

Tsvetkov P, Adler J, Myers N, Biran A, Reuven N, Shaul Y (2018) Oncogenic addiction to high 26S proteasome level. *Cell Death Dis* 9: 773

van Hennik MB, van der Vijgh WJ, Klein I, Elferink F, Vermorken JB, Winograd B, Pinedo HM (1987) Comparative pharmacokinetics of cisplatin and three analogues in mice and humans. *Cancer Res* 47: 6297-301

van Maldegem AM, Benson C, Rutkowski P, Blay JY, van den Berg H, Placzke J, Rasper M, Judson I, Juergens H, Dirksen U, Gelderblom H (2015) Etoposide and carbo-or cisplatin combination therapy in refractory or relapsed Ewing sarcoma: a large retrospective study. *Pediatric blood & cancer* 62: 40-4

Vaux DL, Cory S, Adams JM (1988) Bcl-2 gene promotes haemopoietic cell survival and cooperates with c-myc to immortalize pre-B cells. *Nature* 335: 440-442

Vaziri SA, Grabowski DR, Hill J, Rybicki LR, Burk R, Bukowski RM, Ganapathi MK, Ganapathi R (2009) Inhibition of proteasome activity by bortezomib in renal cancer cells is p53 dependent and VHL independent. *Anticancer research* 29: 2961-9

Vickers CJ, Gonzalez-Paez GE, Wolan DW (2013) Selective detection of caspase-3 versus caspase-7 using activity-based probes with key unnatural amino acids. *ACS chemical biology* 8: 1558-66

Villa D, Knowling M (2010) Acute Saddle Pulmonary Embolism in Ewing Sarcoma. *Journal of pediatric hematology/oncology* 32: e210-e212

Vince JE, Wong WW, Khan N, Feltham R, Chau D, Ahmed AU, Benetatos CA, Chunduru SK, Condon SM, McKinlay M, Brink R, Leverkus M, Tergaonkar V, Schneider P, Callus BA, Koentgen F, Vaux DL, Silke J (2007) IAP antagonists target cIAP1 to induce TNFalpha-dependent apoptosis. *Cell* 131: 682-93

Vogl DT, Martin TG, Vij R, Hari P, Mikhael JR, Siegel D, Wu KL, Delforge M, Gasparetto C (2017) Phase I/II study of the novel proteasome inhibitor delanzomib (CEP-18770) for relapsed and refractory multiple myeloma. *Leukemia & lymphoma* 58: 1872-1879

Wahl AF, Donaldson KL, Mixan BJ, Trail PA, Siegall CB (2001) Selective tumor sensitization to taxanes with the mAb-drug conjugate cBR96-doxorubicin. *Int J Cancer* 93: 590-600

Walkley CR, Qudsi R, Sankaran VG, Perry JA, Gostissa M, Roth SI, Rodda SJ, Snay E, Dunning P, Fahey FH, Alt FW, McMahon AP, Orkin SH (2008) Conditional mouse osteosarcoma, dependent on p53 loss and potentiated by loss of Rb, mimics the human disease. *Genes & development* 22: 1662-76

Wang M, Liang L, Lu J, Yu Y, Zhao Y, Shi Z, Li H, Xu X, Yan Y, Niu Y, Liu Z, Shen L, Zhang H (2019) Delanzomib, a novel proteasome inhibitor, sensitizes breast cancer cells to doxorubicin-induced apoptosis. *Thoracic cancer* 10: 918-929

Wang Y, Janku F, Piha-Paul S, Hess K, Broaddus R, Liu L, Shi N, Overman M, Kopetz S, Subbiah V, Naing A, Hong D, Tsimberidou AM, Karp D, Yao J, Fu S (2020) Phase I studies of vorinostat with ixazomib or pazopanib imply a role of antiangiogenesis-based therapy for TP53 mutant malignancies. *Scientific reports* 10: 3080

Welch D, Kahen E, Fridley B, Brohl AS, Cubitt CL, Reed DR (2019) Small molecule inhibition of lysine-specific demethylase 1 (LSD1) and histone deacetylase (HDAC) alone and in combination in Ewing sarcoma cell lines. *PloS one* 14: e0222228

Williamson MJ, Silva MD, Terkelsen J, Robertson R, Yu L, Xia C, Hatsis P, Bannerman B, Babcock T, Cao Y, Kupperman E (2009) The relationship among tumor architecture, pharmacokinetics, pharmacodynamics, and efficacy of bortezomib in mouse xenograft models. *Molecular cancer therapeutics* 8: 3234-43

Wilson WH, O'Connor OA, Czuczman MS, LaCasce AS, Gerecitano JF, Leonard JP, Tulpule A, Dunleavy K, Xiong H, Chiu YL, Cui Y, Busman T, Elmore SW, Rosenberg SH, Krivoshik AP, Enschede SH, Humerickhouse RA (2010) Navitoclax, a targeted high-affinity inhibitor of BCL-2, in lymphoid malignancies: a phase 1 dose-escalation study of safety, pharmacokinetics, pharmacodynamics, and antitumour activity. *The Lancet Oncology* 11: 1149-59

Wlodkowic D, Skommer J, Darzynkiewicz Z (2012) Cytometry of apoptosis. Historical perspective and new advances. *Experimental oncology* 34: 255-62

Womer RB, West DC, Krailo MD, Dickman PS, Pawel BR, Grier HE, Marcus K, Sailer S, Healey JH, Dormans JP, Weiss AR (2012) Randomized controlled trial of interval-compressed chemotherapy for the treatment of localized Ewing sarcoma: a report from the Children's Oncology Group. *Journal of clinical oncology : official journal of the American Society of Clinical Oncology* 30: 4148-54

Worch J, Ranft A, DuBois SG, Paulussen M, Juergens H, Dirksen U (2018) Age dependency of primary tumor sites and metastases in patients with Ewing sarcoma. *Pediatric blood & cancer* 65: e27251

Xiao H, Chen L, Luo G, Son H, Prectoni JH, Zheng W (2014) Effect of the cytokine levels in serum on osteosarcoma. *Tumour biology : the journal of the International Society for Oncodevelopmental Biology and Medicine* 35: 1023-8

Xie G, Dong H, Liang Y, Ham JD, Rizwan R, Chen J (2020) CAR-NK cells: A promising cellular immunotherapy for cancer. *EBioMedicine* 59: 102975

Xu J, Xie L, Sun X, Dong S, Tang X, Guo W (2019) Management of recurrent or refractory Ewing sarcoma: A systematic review of phase II clinical trials in the last 15 years. *Oncology letters* 18: 348-358

Yang QH, Du C (2004) Smac/DIABLO selectively reduces the levels of c-IAP1 and c-IAP2 but not that of XIAP and livin in HeLa cells. *The Journal of biological chemistry* 279: 16963-70

Zaal EA, Wu W, Jansen G, Zweegman S, Cloos J, Berkers CR (2017) Bortezomib resistance in multiple myeloma is associated with increased serine synthesis. *Cancer & metabolism* 5: 7

Zhou H-J, Aujay MA, Bennett MK, Dajee M, Demo SD, Fang Y, Ho MN, Jiang J, Kirk CJ, Laidig GJ, Lewis ER, Lu Y, Muchamuel T, Parlati F, Ring E, Shenk KD, Shields J, Shwonek PJ, Stanton T, Sun CM et al. (2009) Design and Synthesis of an Orally Bioavailable and Selective Peptide Epoxyketone Proteasome Inhibitor (PR-047). *Journal of Medicinal Chemistry* 52: 3028-3038

Zhu N, Hou J (2020) Assessing immune infiltration and the tumor microenvironment for the diagnosis and prognosis of sarcoma. *Cancer Cell International* 20: 577

Zivanovic O, Jacks LM, Iasonos A, Leitao MM, Jr., Soslow RA, Veras E, Chi DS, Abu-Rustum NR, Barakat RR, Brennan MF, Hensley ML (2012) A nomogram to predict postresection 5-year overall survival for patients with uterine leiomyosarcoma. *Cancer* 118: 660-9

Zuccari G, Milelli A, Pastorino F, Loi M, Petretto A, Parise A, Marchetti C, Minarini A, Cilli M, Emionite L, Di Paolo D, Brignole C, Piaggio F, Perri P, Tumiatti V, Pistoia V, Pagnan G, Ponzoni M (2015) Tumor vascular targeted liposomal-bortezomib minimizes side effects and increases therapeutic activity in human neuroblastoma. *Journal of controlled release : official journal of the Controlled Release Society* 211: 44-52

Zupkovitz G, Tischler J, Posch M, Sadzak I, Ramsauer K, Egger G, Grausenburger R, Schweifer N, Chiocca S, Decker T, Seiser C (2006) Negative and positive regulation of gene expression by mouse histone deacetylase 1. *Molecular and cellular biology* 26: 7913-28

Appendix

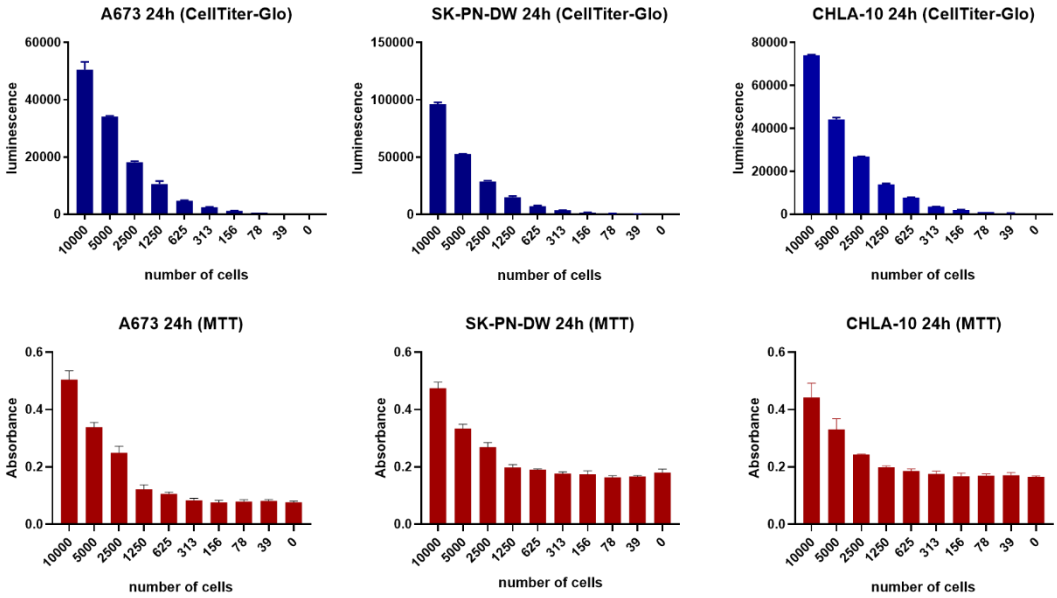

Appendix 1: **CellTiter-Glo provides a more sensitive measure of viable cells than MTT assay**. Three Ewing sarcoma cell lines A673, CHLA-10, SK-PN-DW were seeded at various cell numbers, then underwent either MTT (top graphs) or CellTiter-Glo assays (bottom), n = 3, +/- SEM. The blank was not subtracted to compare differences in cell count.

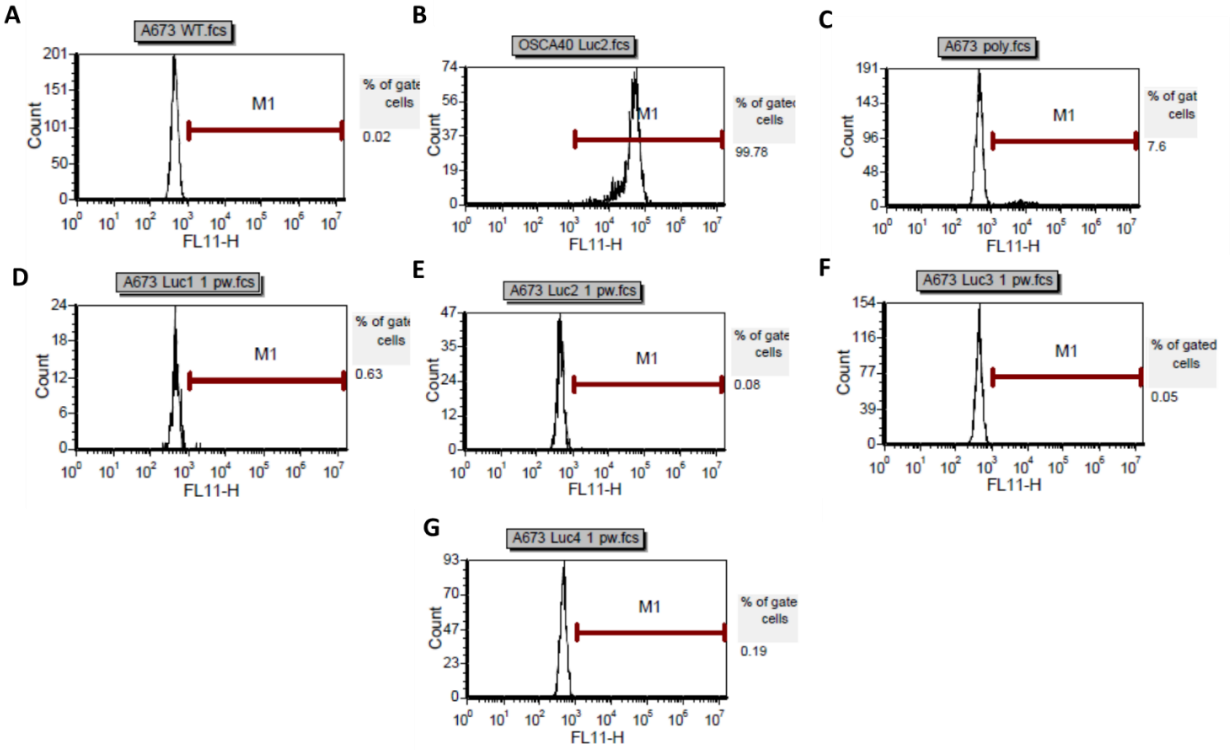

Appendix 2: **Infected A673 clones have low levels of mCherry positive cells.** The A673(WT) (A) along with a positive control (OSCA40 Luc-2) (B), a polyclonal A673 infected population (C) and subclones A673 Luc-1 (D) , 2 (E), 3 (F), 4 (G) were harvested and processed on the FACS Cytoflex using the FL11-H channel for mCherry fluorescence. The percentage of gate cells in the box on the right of each plot demonstrates the percentage of mCherry positive cells in each population.

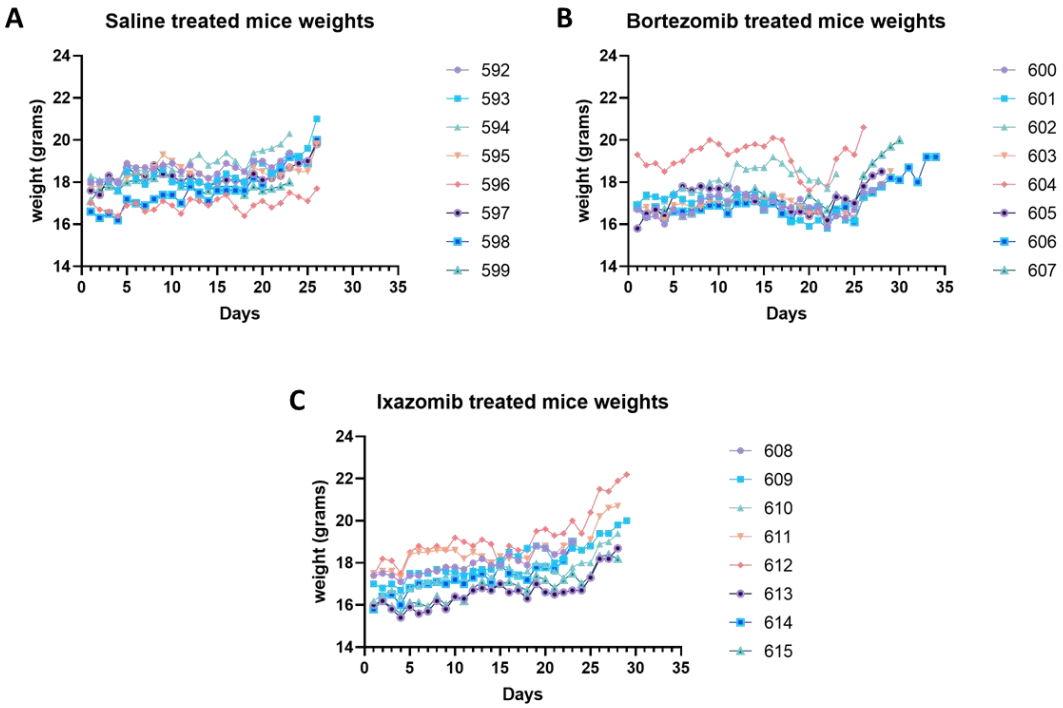

Appendix 3: **Mouse weights of BALB/c nude mice in A673 Luc-4 efficacy experiment.** The daily weights of saline (A), bortezomib (B) and ixazomib (C) treated mice throughout the primary A673 efficacy experiment (n = 8). Note that the day of tumour implantation was treated as day one.

A

Mouse Number	Reason for cull
592	Tumour size
593	Tumour size
594	Tumour size
595	Tumour size
596	Tumour size
597	Tumour size
598	Tumour size
599	Tumour Ulceration
600	Tumour size
601	Tumour size
602	Tumour Ulceration
603	Tumour size
604	Tumour size
605	Tumour size
606	Tumour size
607	Tumour size
608	Tumour Ulceration
609	Tumour size
610	Tumour Ulceration
611	Tumour size
612	Tumour size
613	Tumour size
614	Tumour Ulceration
615	Tumour Ulceration

B

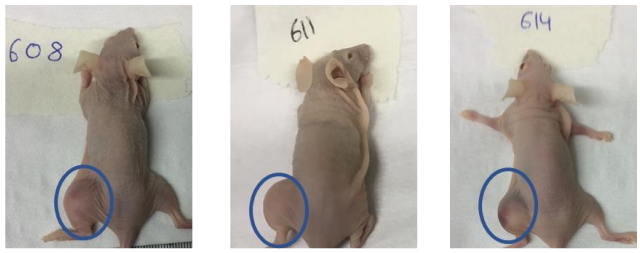

C

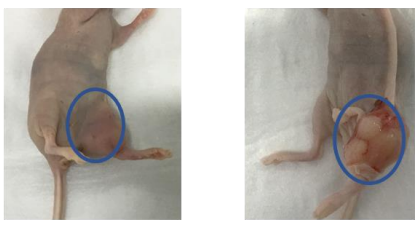

Appendix 4: **A673 Luc-4 implanted mice culled mainly due to endpoint tumour size (Primary efficacy experiment).** (A) During the treatment of A673 intramuscular implanted mice with saline (grey), bortezomib (purple) and ixazomib (blue), the mice were required to be culled due to size or ulceration. (B) Images of mouse 608, 611 culled due to size and 614 culled due to ulceration. (C) Changes in morphology of mouse 606 primary Ewing sarcoma tumour.

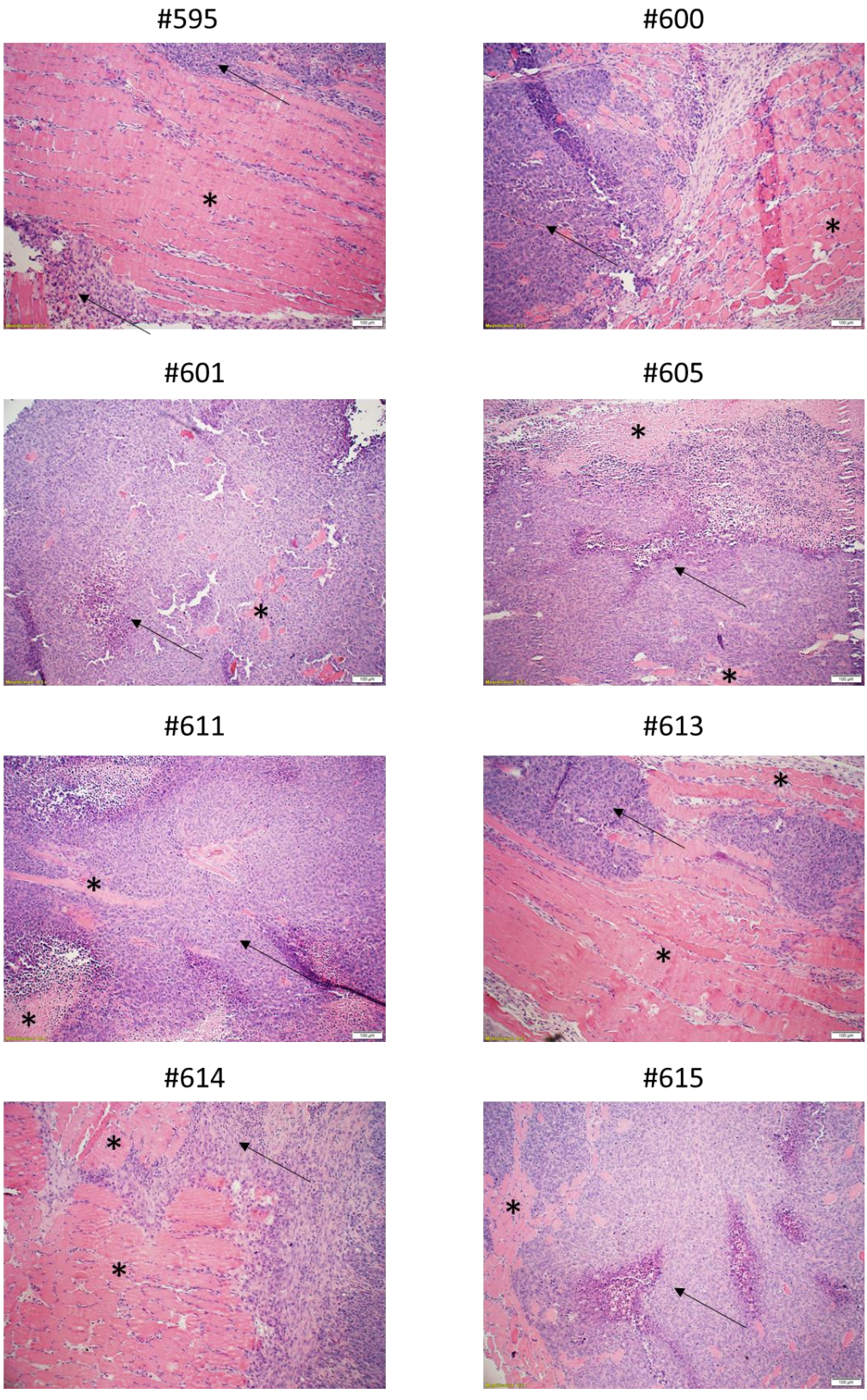

Appendix 5: **A673 tumour invasiveness in smooth muscle (part 2).** A further representation of primary tumour samples from A673 Luc-4 intramuscularly implanted mice stained via H & E. The tumour tissue in purple is identified by an arrow and the muscle tissue in pink is highlighted using an asterisk. (scale = 100 µm). The tissue was sectioned by Michael Harris and photos were taken by Carmelo Cerra.

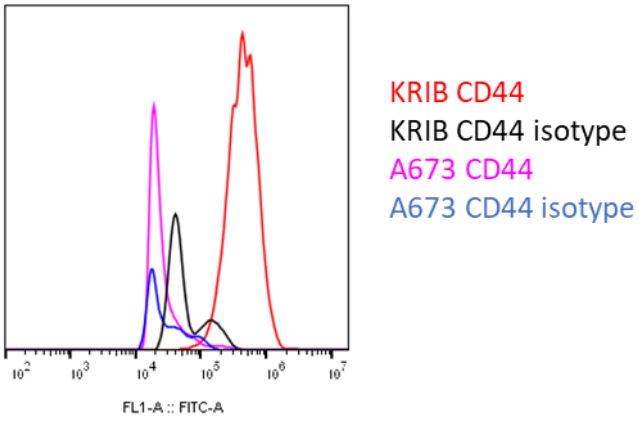

Appendix 6: **A673 cells do not express CD44**. A673 (purple) and KRIB (red) (positive control) were incubated in an antibody for CD44 and an isotype control A673 (blue) and KRIB (black) and analysed on the FACS CytoFLEX.

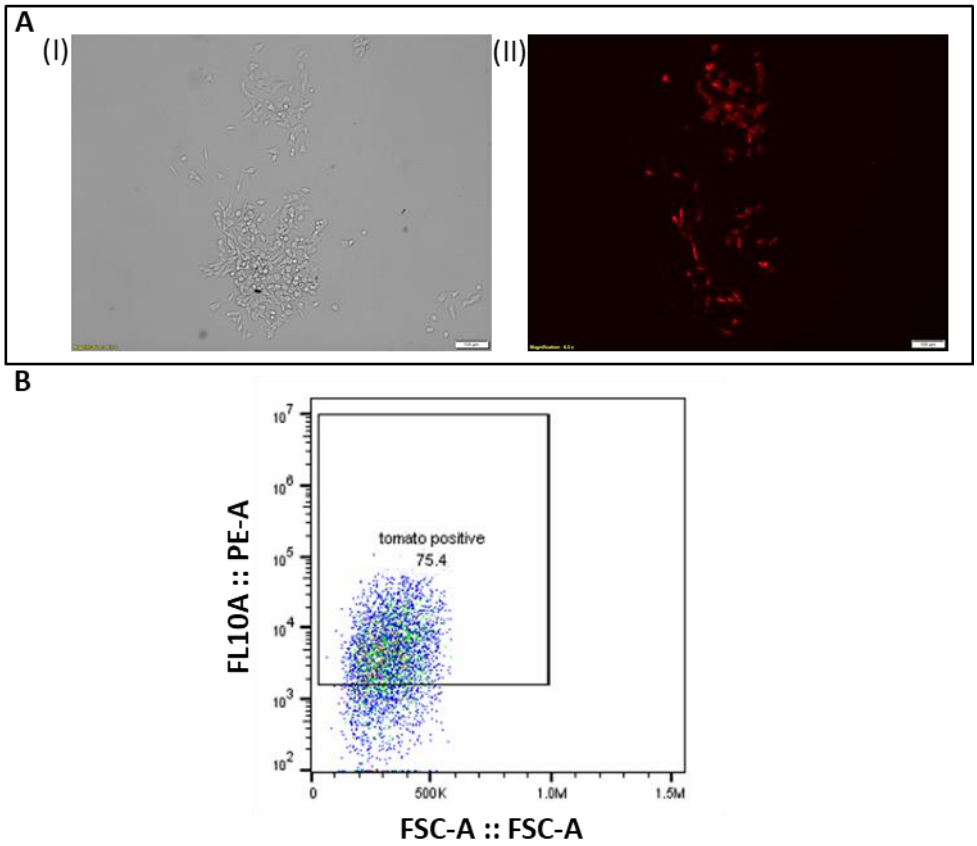

Appendix 7: **A673 stable transfected polyclonal populations contain partially tomato positive cells.** Another polyclonal population (A673 Luc-polyclonal-2) was generated from the initial FACSAria sorting of A673 cells transfected with the tomato/luciferase (pcDNA3.1(+)/Luc2=tdT) plasmid. (A) The cells were analysed via fluorescence microscopy using the bright field (I) and TRITC (II) channels. (B) This population was analysed via flow cytometry for tomato fluorescence using the PE channel on the FACS CytoFLEX.

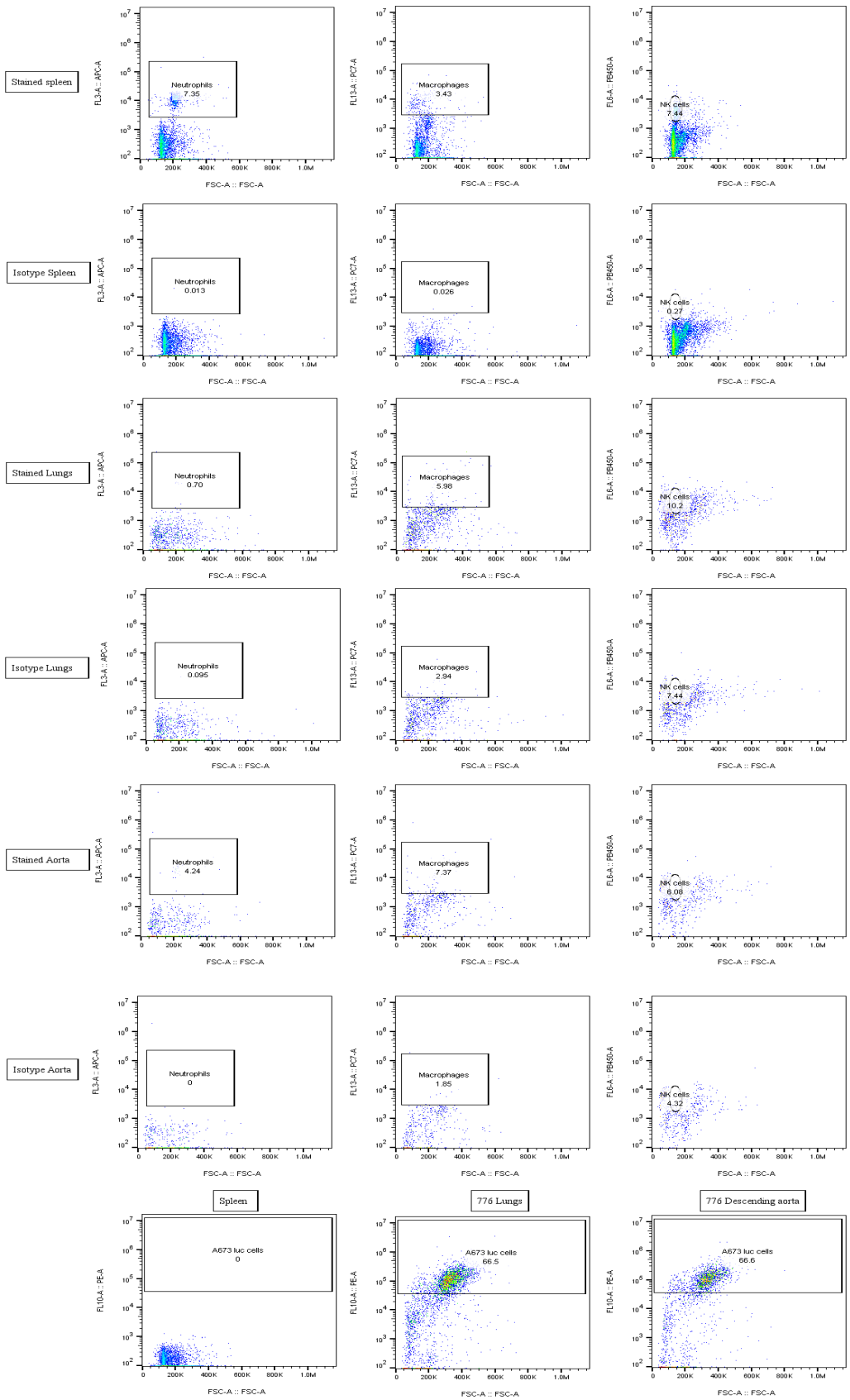

Appendix 8: **A673 metastases are composed of relatively few immune cells.** A mouse spleen, 776 lung metastasis and 776 descending aorta metastases were stained with antibodies F4/80-PE-Cy7 (macrophages), CD335/NKP46-BV421 (NK cells) and Ly-6G-APC (neutrophils) as well as their respective isotype controls. The amounts of immune cells were determined by subtracting the difference between the two for the tumours. The amount of A673 Luc3L cells was also determined for the spleen, lungs, and aorta via flow cytometry analysis for tomato fluorescence.